Waveform-Diverse Stretch Processing

By

Dana Hemmingsen

Submitted to the graduate degree program in Department of Electrical Engineering and Computer Science and the Graduate Faculty of the University of Kansas in partial fulfillment of the requirements for the degree of Master's.

Shannon Blunt, Chairperson

Committee members

James Stiles

Chris Allen

Date defended: March 27, 2019

The Thesis Committee for Dana Hemmingsen certifies
that this is the approved version of the following thesis :

Waveform-Diverse Stretch Processing

Shannon Blunt, Chairperson

Date approved: March 27, 2019

Abstract

Stretch processing with the use of a wideband LFM transmit waveform is a commonly used technique, and its popularity is in large part due to the large time-bandwidth product that provides fine range resolution capabilities for applications that require it. It allows pulse compression of echoes at a much lower sampling bandwidth without sacrificing any range resolution. Previously, this technique has been restrictive in terms of waveform diversity because the literature shows that the LFM is the only type of waveform that will result in a tone after stretch processing. However, there are also many examples in the literature that demonstrate an ability to compensate for distortions from an ideal LFM waveform structure caused by various hardware components in the transmitter and receiver. This idea of compensating for variations is borrowed here, and the use of nonlinear FM (NLFM) waveforms is proposed to facilitate more variety in wideband waveforms that are usable with stretch processing.

A compensation transform that permits the use of these proposed NLFM waveforms replaces the final fast Fourier transform (FFT) stage of the stretch processing configuration, but the rest of the RF receive chain remains the same. This modification to the receive processing structure makes possible the use of waveform diversity for legacy radar systems that already employ stretch processing.

Similarly, using the same concept of compensating for distortions to the LFM structure along with the notion that a Fourier transform is essentially the matched filter bank for an LFM waveform mixed with an LFM reference, a least-squares based mismatched filtering (MMF) scheme is proposed. This MMF could likewise be used to replace the

final FFT stage, and can also facilitate the application of NLFM waveforms to legacy radar systems.

The efficacy of these filtering approaches (compensation transform and least-squares based MMF) are demonstrated in simulation and experimentally using open-air measurements and are applied to different scenarios of NLFM waveform to assess the results and provide a means of comparison between the two techniques.

Acknowledgements

I would like to thank all of my fellow graduate students in the Radar Systems Lab (RSL) for their support, specifically Patrick McCormick and Lu Harnett for their assistance throughout my graduate career. I also would like to express my gratitude to my advisor Dr. Shannon Blunt for the continuous support through my coursework and research. Lastly, I would like to thank my family and close friends for their encouragement throughout my coursework, research, and the writing process.

Contents

List of Figures

Chapter 1

Introduction

Stretch processing is a widely used technique for employing wideband radar systems because it allows for fine range resolution without paying the penalty of high bandwidth requirements on receive processing. Traditionally it has been limiting on the ability to apply waveform diversity because the literature suggests that the only waveform that can produce a tone (and thus realizing the full bandwidth reduction capability) is the linear frequency modulated (LFM) waveform.

With ever increasing dilemma of the congested spectrum it is important that alternate solutions to combat this problem are formulated. One such area of research that has seen a considerable amount of recent growth is waveform diversity due to the advances in digital signal generation and adaptive signal processing [1, 2, 3, 4]. As mentioned, it was previously not useful to apply this idea to stretch processing, but the following chapters outline proposed modifications to the stretch processing receive structure that allows for the use of a more diverse set of waveforms.

The structure of the rest of this document is as follows: the second chapter establishes the necessary background information relating to the topic of stretch processing and the proposed modification, including a brief overview of some of the fundamental concepts of radar that are requisite. The following chapter details the derivation of the required change to the FFT stage of stretch processing and discusses the consequences that result from the modification. It also presents the results of using the new waveform in both simulation and open-air experiments, and compares two variants of NLFM waveform as a way to determine the best way to mediate the advantages and disadvantages of the compensation transform.

A second modification in the form of a least-squares based mismatched filter is derived in the fourth chapter, although its derivation depends on the principles behind the compensation trans-

form. It is first examined in the context of stretch processing as it has been traditionally formulated, but the new NLFM waveforms are later used to examine the results in simulation as well as an open-air experiment. Comparisons are made throughout to continually weigh the advantages and disadvantages that the filtering technique presents, and the baseline is always stretch processing using an LFM and the FFT.

Also included is an Appendix which walks through the mathematical analysis of stretch processing with an expression for the NLFM waveform used in place of an LFM. This analysis follows the steps from transmitting the waveform all the way through the receive processing that are first discussed for standard stretch processing in the third chapter.

Chapter 2

Background

In order to explain the techniques that are presented in the later chapters of this document, it is useful to provide a background in some of the basic principles of radar to establish a foundation. While radar waveforms can be classified as either pulsed or continuous wave (CW), the focus of this work is on pulsed systems.

2.1 Pulsed Radar

As was mentioned, radar waveforms are divided into two classes: continuous wave (CW) and pulsed. Both classes are representative of the process of a waveform being repeatedly modulated onto multiple segments of a transmitted signal. The purpose of this is that the segments can be combined on receive to increase the gain and to enable discrimination in Doppler. The CW waveform is continually being transmitted, which means that the waveform-modulated segments do not take turns with the receive operation. Transmission and receive occur simultaneously in this case. This type of radar is often used in a bistatic configuration in order to maintain isolation between the receiver and the transmitter.

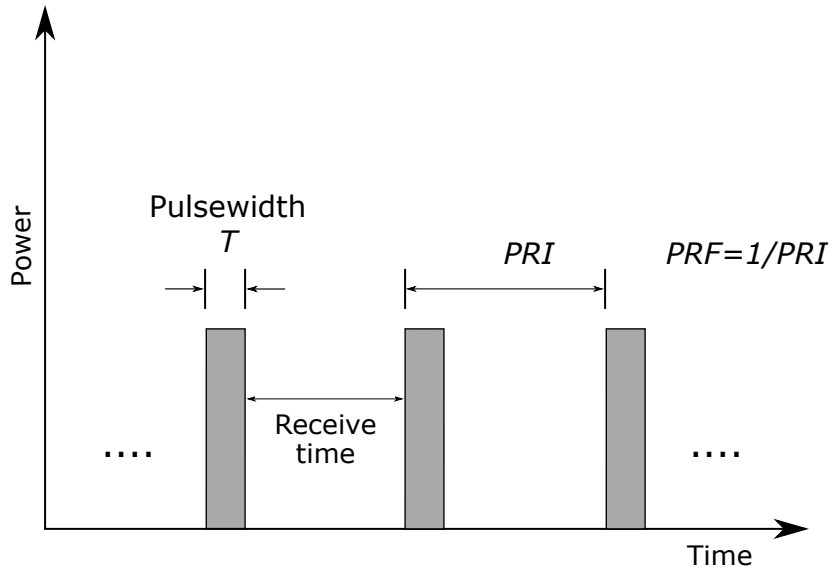

Figure 2.1: Pulsed radar waveform

In contrast, a pulsed radar transmits a waveform over a short period of time, known as the pulsewidth T (generally on the order of microseconds), and then stops transmission for a period of time. The pulsewidth is required to be less than the pulse repetition interval (PRI), denoted T_{PRI}. The duty cycle is determined from the ratio of the pulsewidth and the PRI as

$$d_t = \frac{T}{T_{\text{PRI}}} = T \cdot PRF \tag{2.1}$$

where the inverse of the PRI yields the PRF, the pulse repetition frequency. This implies that CW radar can be considered as a special case of pulsed radar where $d_t = 100\%$. During each pulse repetition interval, the transmitter alternates between transmit and receive intervals so that echoes from objects in the environment can be collected. A plot showing how a pulse of length T is related to the PRI and PRF can be seen in Fig. 2.1

The average power, P_{avg}, of a transmitted waveform is an important factor that affects the strength of a received signal. In general, to detect targets that are at longer ranges, the average power must increase. Average power is the product of the peak transmit power P_{Tx} and the duty

factor

$$P_{avg} = P_{\text{Tx}} \cdot d_t = P_{\text{Tx}} \cdot T \cdot PRF. \tag{2.2}$$

This relationship implies that there can be a tradeoff between peak transmit power and the duration of the pulse, which is visualized in Fig. 2.4

2.2 Range Resolution

An important function of a radar is its ability to resolve targets, and one way of assessing the quality of this type of measurement is through the range resolution. Range resolution is defined to be the ability of the radar to distinguish two or more targets that are closely spaced in range [5]. Range resolution is denoted ΔR, which by definition is the spacing between two targets that is required to be able to resolve them in range. If the targets are spaced by less than ΔR then it is not possible to resolve each target. The quantity ΔR is defined as

$$\Delta R = \frac{c\,T}{2} \tag{2.3}$$

and the concept is demonstrated in Fig. 2.2. The receiver output is portrayed for a single pulse that is reflected off of two point scatterers that are located at a distance ΔR from one another. When ΔR is large enough (as defined by 2.3), the scatterers can be resolved (Figs. 2.2b,d). However, when the scatterers are too close, the returns from the scatterers will overlap causing them to be not resolvable in range (Figs. 2.2c).

It is clear from 2.3 that the range resolution is dependent on the duration of the pulse, hence the shorter the pulse, the finer the range resolution. For example, a pulse that is 1 μs long will have range resolution equivalent to 150 m, which means that in order to resolve separate returns the targets must be separated by a minimum of 150 m in range.

Finally, it is useful to observe the inverse relationship between the pulsewidth and the bandwidth of a signal, $T = \frac{1}{B}$. Therefore, the range resolution has an inverse relationship with the

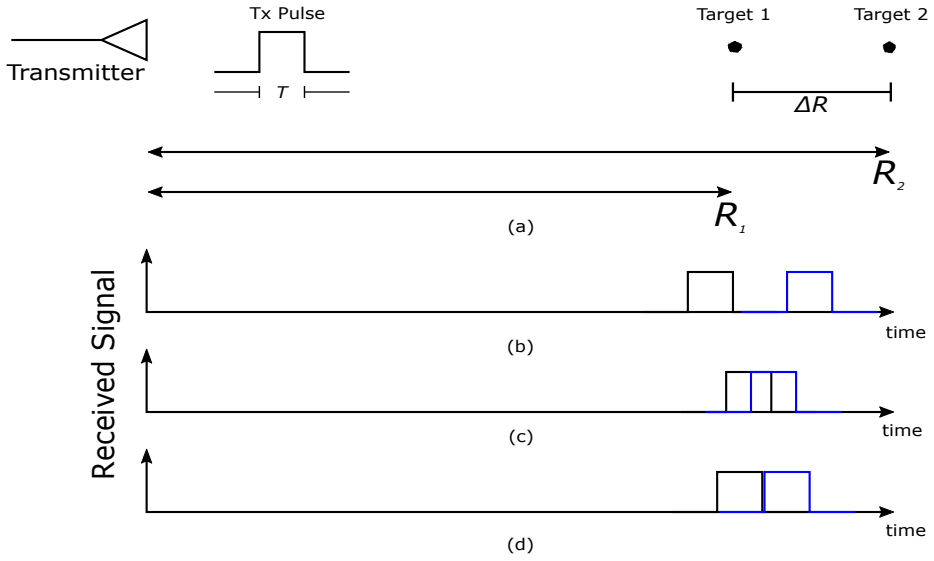

Figure 2.2: Concept of resolution in range (a) Transmit pulse and two point targets. (b) Output of receiver for resolved targets, $\Delta R > \frac{cT}{2}$. (c) Output of receiver for unresolved targets $\Delta R < \frac{cT}{2}$. (d) Output of receiver for definition of range resolution $\Delta R = \frac{cT}{2}$.

bandwidth of the transmit signal $\Delta R = \frac{c}{2B}$.

2.3 Pulse Compression

The technique of pulse compression was developed during the mid-1950's in order to mediate the need to trade off between the contradictory benefits of a short-duration pulse as compared with long-duration pulse [6]. Specifically, since bandwidth of a pulsed, sinusoidal waveform is inversely related to pulse duration, ($T = \frac{1}{B}$, as discussed in Section 2.2) there is an implied advantage for using a short pulse to achieve more fine range resolution. However, received signal strength is proportional to pulse duration, which conversely implies a benefit to using a long pulse, thus ensuring enough energy on target to provide a detectable signal-to-noise ratio (SNR) [6]. Pulse compression is a solution to this dilemma because it employs a longer pulse that has been modulated to yield a bandwidth corresponding to a short-duration pulse. Thus, the range resolution of a wide-bandwidth waveform can be achieved without requiring a high power transmitter because the energy and resolution of a waveform have been decoupled [5]. After appropriate receive process-

ing is applied to the reflected version of a transmsitted waveform (assume for now from a single point scatterer) the response will have a mainlobe with resolution corresponding to that of a short pulse (see Fig. 2.3).

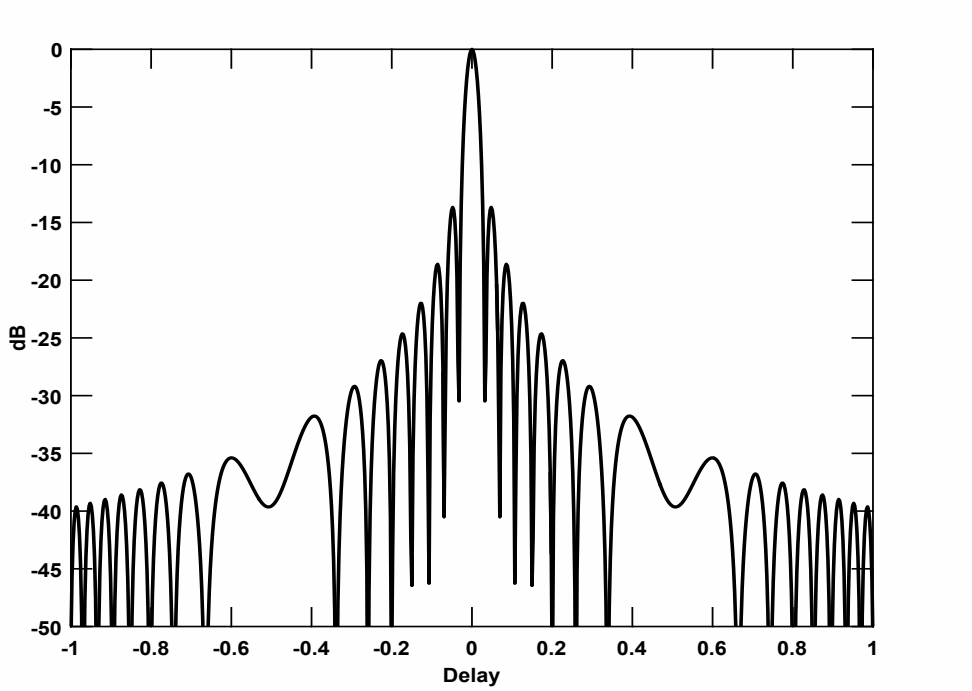

Figure 2.3: Pulse compression response to a stationary point scatterer at delay = 0

There are a variety of types of pulse compression waveforms, but the majority of them fall under two broad categories: frequency modulated waveforms (both intra- and interpulse) and phase-coded waveforms (biphase-coded, polyphase coded, etc.). Most of the work in the radar community thus far focuses on designing waveforms and the receive processing to minimize range sidelobes without degrading range resolution and SNR. In the following sections these principles are discussed in more detail, and includes various simulations of the standard filtering techniques that are applied to pulse compression waveforms in order to establish a baseline for further comparison.

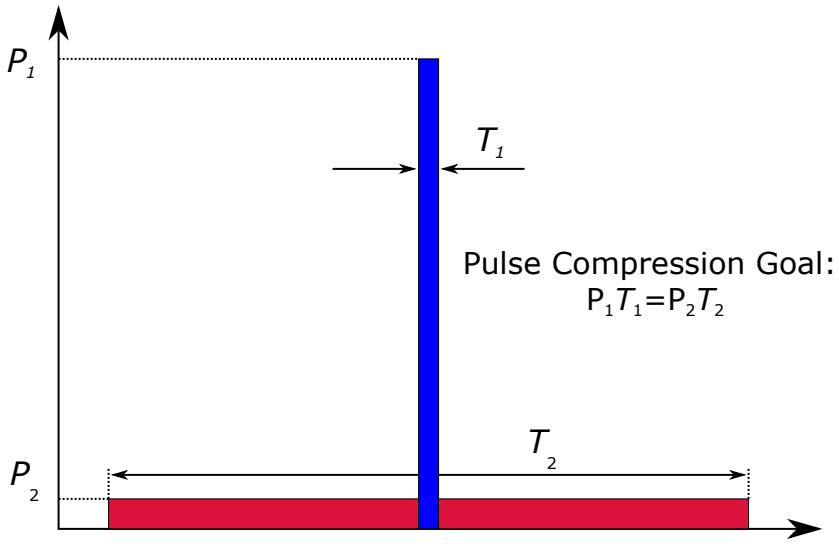

Figure 2.4: Simplified view of pulse compression: the energy content of a low-power but long duration pulse is comparable to that of a high-power pulse of short duration

2.3.1 Pulse Compression Waveforms

While there are numerous types of pulse compression waveforms in existence, they can be generally divided into a few categories. These general categories are frequency modulated (FM) waveforms, phase codes, frequency codes, and random noise waveforms. One of the most commonly used of these categories in actual radar systems are the FM waveforms, and this is one of two classes of waveform that is the subject of the majority of this work. The other waveform type that will be considered on a much smaller scale are phase codes. Sections 2.3.1.1 and 2.3.1.2 describe the details of these two categories of waveforms as they pertain to the nature of this work.

2.3.1.1 Frequency Modulated Waveforms

Within the category of frequency modulated waveforms, the linear frequency modulated (LFM) waveform is arguably one of the most widespread in its use because of its straightforward implementation in hardware. Another attractive feature of this waveform is the ability to apply stretch processing on receive (for more details on this refer to Section 2.6). To derive the expression for the linear FM waveform, it is necessary to start with the complex baseband representation of a

general FM waveform with pulsewidth T (normalized to unit energy)

$$s_{\mathrm{FM}}(t) = \frac{1}{\sqrt{T}}\exp(j\theta(t)) = \cos(\theta(t)) + j\sin(\theta(t)). \tag{2.4}$$

The instantaneous phase is $\theta(t)$ and the instantaneous frequency, $f(t)$, is determined from its derivative

$$f(t) = \frac{1}{2\pi}\frac{d\theta(t)}{dt}. \tag{2.5}$$

In the specific case of an LFM waveform, which is often called a *chirp*, it has a phase function

$$\theta_{\mathrm{LFM}}(t) = \pm\pi\frac{B}{T}t^2 \quad \text{for} \quad 0 \le t \le T, \tag{2.6}$$

with B the approximate 3 dB power bandwidth for the waveform. The selection of either $+$ or $-$ is simply the determination of having either an *up-chirp* (increasing frequency over time) or a *down-chirp* (decreasing frequency over time). Equation 2.6 can now be substituted into 2.5 to determine the instantaneous frequency for the case of an LFM. As can be seen below, it is a linear function of frequency, as the name of the waveform implies,

$$f_{\mathrm{LFM}}(t) = \pm\frac{B}{T}t. \tag{2.7}$$

The *chirp rate*, denoted k, of an LFM waveform is defined as the rate of change of the frequency with respect to time, and is determined by taking another derivative, this time of the instantaneous frequency function. For an LFM, the chirp rate is a constant value, $k = B/T$, which indicates that the waveform sweeps linearly across the bandwidth B during the pulsewidth T (see Fig. 2.5). Inserting 2.7 into 2.4 results in the complex baseband LFM waveform (assuming *up-chirp*)

$$s_{\mathrm{LFM}}(t) = \frac{1}{\sqrt{T}}\exp(j\pi\frac{B}{T}t^2) \quad \text{for} \quad 0 \le t \le T. \tag{2.8}$$

Using the real portion of this signal, a time-domain plot of the signal can be created, as shown in

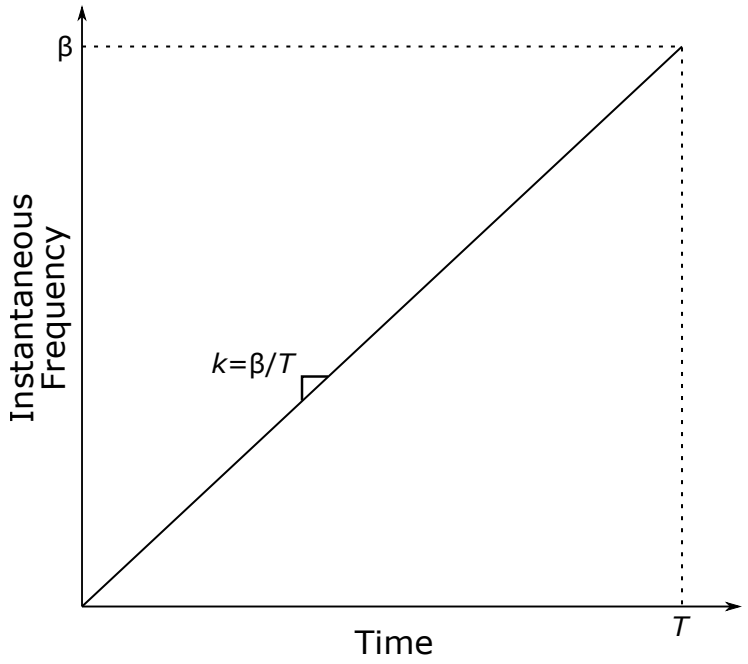

Figure 2.5: Instantaneous frequency versus time for an LFM waveform defined from $0 \leq t \leq T$ with chirp rate k

Fig. 2.6.

For practical application of an LFM waveform, the pulse is centered at a radio frequency (RF), f_{RF} and can be expressed as

$$s_{\mathrm{RF}}(t) = \cos(2\pi f_{\mathrm{RF}} t + \pi \frac{B}{T} t^2) \tag{2.9}$$

It is useful for analysis purposes to represent the frequency domain of the LFM signal, and as with many things, there is a useful approximation that can be applied. There are closed-form expressions that represent the spectrum of an LFM, as in [6] and [7], but it is possible to approximate the spectrum as the following for time-bandwidth products $BT \gg 1$

$$X(f) \approx |X(f)| \exp\left(-j\pi f^2 \frac{T}{B}\right) \exp\left(j\frac{\pi}{4}\right) \tag{2.10}$$

as found in [5], where $|X(f)| \approx 1$ for $-\frac{B}{2} \leq f \leq \frac{B}{2}$. The accuracy of this approximation is dependent on the time-bandwidth product of the waveform, and to illustrate this dependence the spectra of LFM waveforms with two different BT products are compared in Fig. 2.7. The spec-

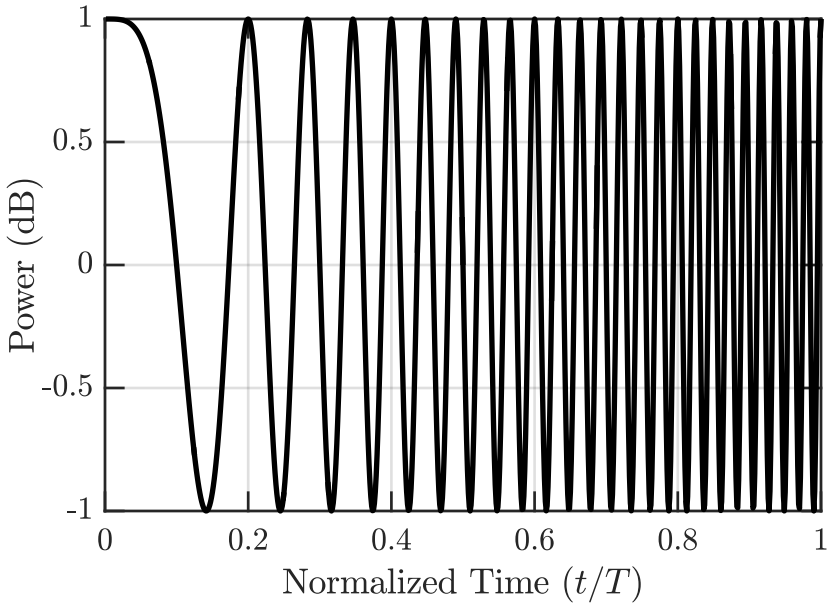

Figure 2.6: Time-domain response of a linear frequency modulated (LFM) waveform with time-bandwidth product equal to 50 from $0 \leq t \leq T$

trum given in 2.10 has a rectangular magnitude response over the swept bandwidth, and will tend to be closer to the ideal rectangular-shaped spectrum as the time-bandwidth product increases. The transition region of the $BT = 200$ spectrum is much sharper, and contains a larger portion of the waveform energy in the nominal frequency range. According to [6], when the time-bandwidth product exceeds 100, then $\approx 98\% - 99\%$ of the waveform energy is contained in the region between $-B/2 \leq f \leq B/2$. It is also useful to note that the presence of a phase term that is quadratic is a distinctive characteristic for the LFM waveform, and it provides some Doppler tolerance.

The biggest limitation of using an LFM are the high range sidelobes that are produced (see Fig. 2.3). In general, the largest range sidelobe is only 13 dB below the peak of the mainlobe, which could easily mask scatterers that are close in range to the mainlobe if they have considerably lower power. There are several methods of suppressing these sidelobes, and one that is sometimes used is to apply an amplitude taper, but this has the trade off of degrading the resolution and incurring a loss in SNR [8]. An alternative to applying a taper is to instead implement a nonlinear Frequency Modulated (NLFM) waveform as the transmit waveform, because they achieve low range side-

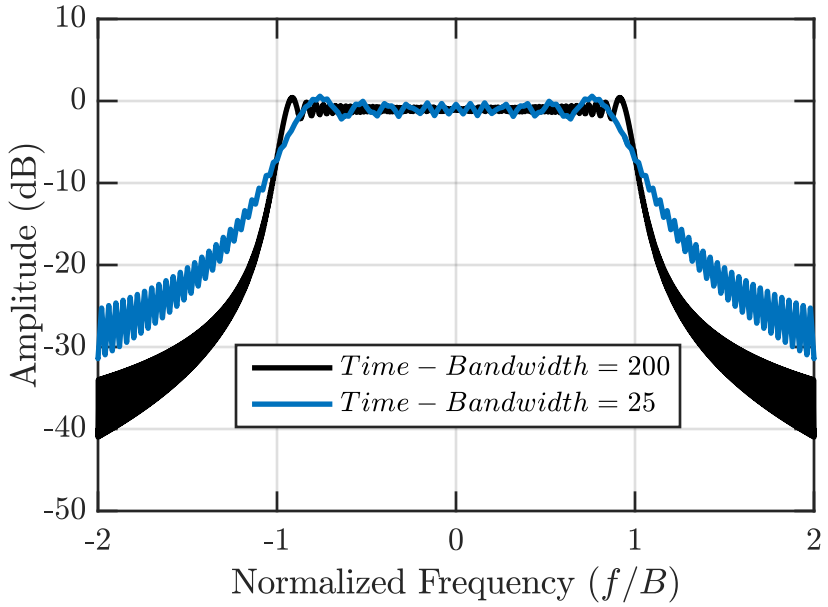

Figure 2.7: Comparison of spectra of LFM waveforms with two different time-bandwidth products

lobes without inducing an SNR loss [9, 10, 11, 12, 13]. The general idea for developing NLFM waveforms is that instead of using amplitude tapering to perform the spectral shaping, it is possible to instead determine a time-varying chirp rate function that spends more time at certain frequencies as opposed to the constant change in frequency of an LFM. In other words, the instantaneous frequency is now a nonlinear function of time (see Fig. 2.8), hence the instantaneous phase is not a quadratic function of time as it was for an LFM. Even using a nonlinear FM waveform there is still some degradation in the resolution that is inherent in the use of any form spectral shaping (see Figs. 2.9 and 2.10). The method for designing and generating NLFM waveforms used in the latter portions of this work is based upon the principle of stationary phase (POSP), which says that the integral of a rapidly oscillating function has no significant value aside from the regions where the phase is "stationary" (i.e. where the derivative of the phase is zero) [10].

The method we will use for designing this type of waveform is described in detail in [10], where the problem is presented as specifying the two moduli functions $u_e(t)$ and $U_m(f)$ (the time envelope and its Fourier transform which is related to the autocorrelation function) by determining

expressions for the phase functions $\varphi(t)$ and $\theta(f)$ in terms of quantities derived from the two modulus functions. Fowle gives a general approximate solution for the phase characteristics $\varphi(t)$ and $\theta(f)$ for independent moduli $u_e(t)$ and $U_m(f)$ defined as

$$u_e(t) = |\int_{-\infty}^{\infty} U(f) e^{j(\theta(f)+2\pi ft)} df| \tag{2.11}$$

and

$$U_m(f) = |\int_{-\infty}^{\infty} u_e(t) e^{j(\varphi(t)-2\pi ft)} dt|. \tag{2.12}$$

The approximate solutions to 2.11 and 2.12 can be found by first applying the concept of stationary phase to determine a stationary point about which a Taylor series expansion can be made. The general process is to then determine the cumulative energy in both the time and frequency domains ($P(t)$ and $Q(t)$ respectively) of the specified moduli, and then to calculate the instantaneous frequency from

$$f(t) \cong Q^{-1}\{P(t)\}. \tag{2.13}$$

Once the instantaneous frequency has been determined, it can be used to calculate the solution for $\varphi(t)$ as

$$\varphi(t) = 2\pi \int Q^{-1}\Big\{P(t)\Big\} dt = 2\pi \int f(t) dt. \tag{2.14}$$

It is this phase function that is used along with the time domain envelope to generate the NLFM waveform as

$$s_{\text{NLFM}}(t) = u_e(t) \exp[j\varphi(t)]. \tag{2.15}$$

2.3.1.2 Phase Codes

Phase-modulated codes are a set of waveforms where the pulsewidth T is subdivided into temporal segments to form a set of constant-amplitude chips. The duration of these chips is define to be $T_c = T/N$, and each chip is modulated by a fixed phase value θ. Phase codes can either be binary codes or polyphase codes, with the latter being the codes of interest to this work. Polyphase codes

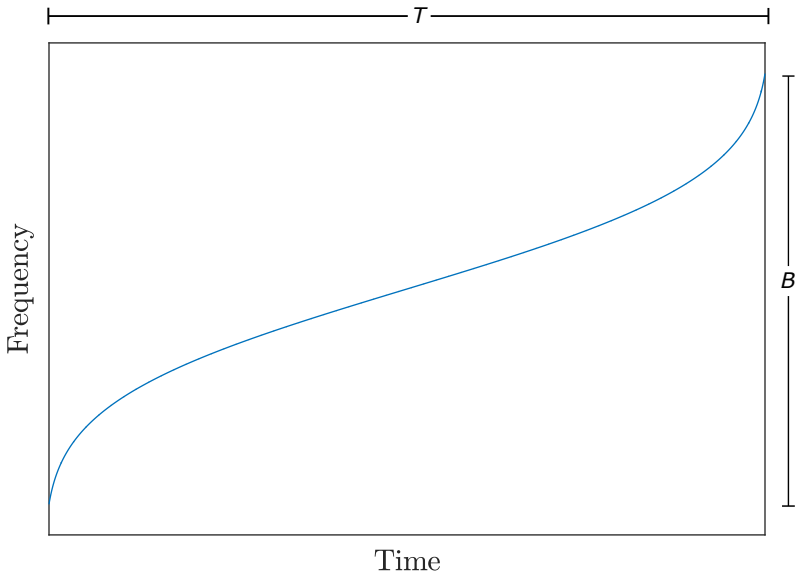

Figure 2.8: Time-frequency relationship for a generic NLFM waveform with bandwidth B and pulse duration T

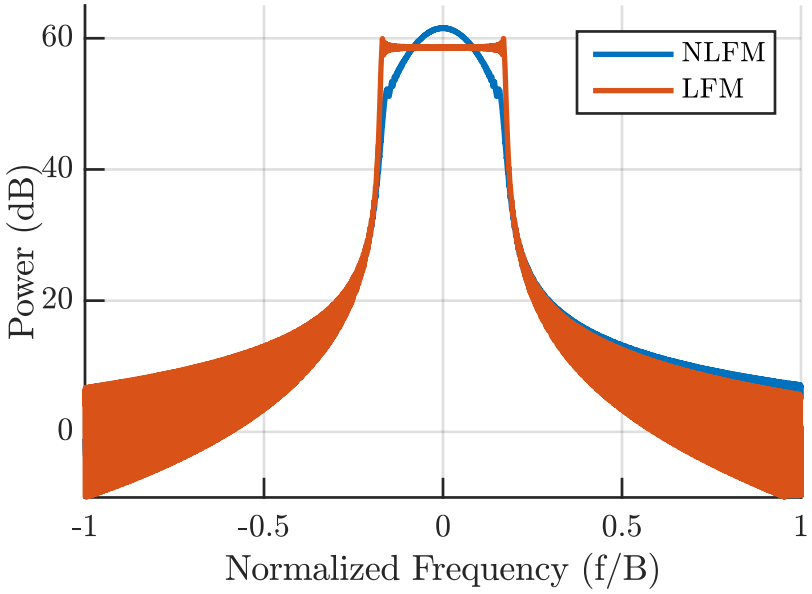

Figure 2.9: Power spectral densities of LFM and NLFM waveforms with identical bandwidths

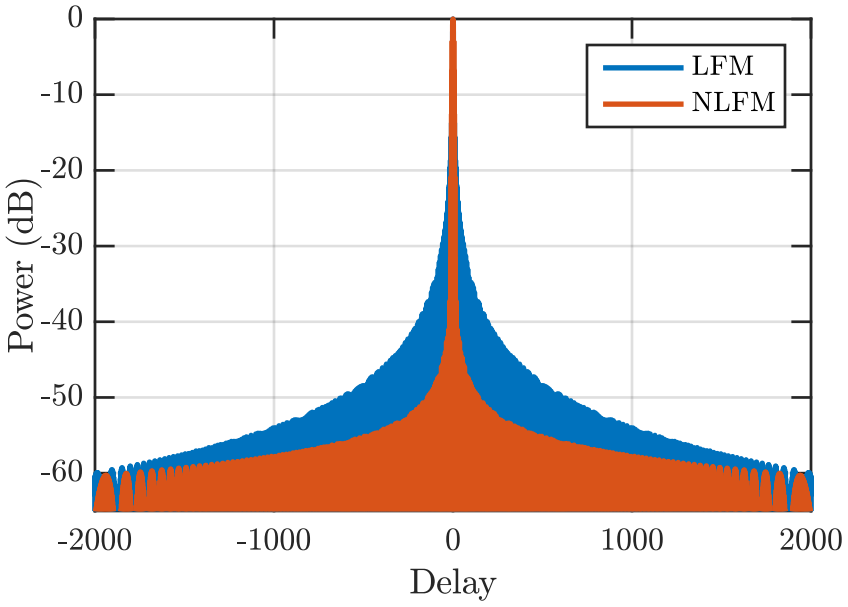

Figure 2.10: Pulse compression responses for LFM and NLFM waveforms

consist of sets of phase values chosen from a constellation that contains phase values between 0° and 360°, limited only by numerical precision. The mathematical expression for a phase-coded waveform is

$$s_{\text{PC}}(t) = \frac{1}{\sqrt{T}} \sum_{n=1}^{N} e^{j\theta_n} \text{rect}\left[\frac{t-(n-1)T_c}{T_c}\right] \quad 0 \le t \le T, \tag{2.16}$$

where the n^{th} chip is modulated by phase θ_n. This waveform has been normalized to unity similarly to what was done with the LFM waveform. There are many different types of polyphase codes (Frank codes, polyphase Barker codes, etc.) [14, 15, 16, 17], although many are not physically realizable without a significant amount of distortion as a result of hardware constraints (i.e. range straddling losses, bandlimiting distortion, intermodulation as a result of nonlinearities from operating a power amplifier in saturation).

Recently a method has been developed that allows arbitrary polyphase codes to be implemented using a modified version of continuous phase modulation (CPM). This waveform, denoted polyphase coded FM (PCFM) consists of a train of N impulses with time separation T_p, meaning that the total time duration is $T = NT_p$. The n^{th} impulse is weighted with values $-\pi \le \alpha_n \le \pi$ representing

the phase change that occurs during time interval T_p between chips of the code. This essentially results in a discretized representation of $\frac{1}{2\pi}\frac{d\theta(t)}{dt}$, the instantaneous frequency. The values of α_n can be determined from

$$\alpha_n = \Psi(\tilde{\alpha}_n) = \begin{cases} \tilde{\alpha}_n & \text{if} \quad |\tilde{\alpha}_n| \leq \pi \\ \tilde{\alpha}_n - 2\pi \text{sgn}(\tilde{\alpha}_n) & quad\text{if} \quad |\tilde{\alpha}_n| > \pi, \end{cases} \tag{2.17}$$

where

$$\tilde{\alpha}_n = \theta_n - \theta_{n-1} \quad \text{for} \quad n = 1, \cdots, N, \tag{2.18}$$

sgn$(\bullet)$ is the signum operation, and θ_n is the phase value of the n^{th} chip for the length $N+1$ polyphase code. With this code of phase changes, $\mathbf{x} = [\alpha_1 \ \alpha_2 \ \cdots \ \alpha_{\text{N}}]^T$ and letting θ_0 be an arbitrary starting phase value the PCFM waveform can be generated as

$$s_{\text{PCFM}}(t;\mathbf{x}) = \exp\left\{ j\Big(\int_0^t g(\tau) * \Big[\sum_{n=1}^{N} \alpha_n \delta(\tau - (n-1)T_p) \Big] d\tau + \theta_0 \Big) \right\} \tag{2.19}$$

where $g(t)$ is a shaping filter that must have time support on $[0, T_p]$ and integrate to unity over the real line (e.g. a rectangular filter), and $(*)$ denotes a convolution. PCFM waveforms can realize peak sidelobe levels (PSL) of 40 dB below the mainlobe according to [1, 18].

2.4 Standard Matched Filtering

The matched filter, which was first developed by [19], maximizes the SNR for a known signal in additive white noise. This filter is derived using knowledge of the transmit waveform. Consider the transmit waveform $s(t)$, a complex, baseband representation of an arbitrary waveform that has pulsewidth T. The matched filter, $h_{\text{MF}}(t)$, for this transmit waveform can be derived to maximize the SNR of s(t) after filtering. This filter has the form $h_{\text{MF}}(t) = As^*(T-t)$ where A is an arbitrary constant, and $(\bullet)^*$ denotes complex conjugation. In order to compare this filter with various other techniques it is useful to define A such that the matched filter is normalized to produce a

unity noise-power gain independent of the waveform. In other words, A should be defined so that $(\int_0^T |h_{\mathrm{MF}}(t)|^2 dt)^{1/2} = 1$ [1].

Assuming, for the moment, that there is no significant Doppler shift, the matched filter response to the given waveform has the following form,

$$h_{\mathrm{MF}}(t) * s(t) = \int_{t=0}^{T} s(t)s^*(t)dt, \tag{2.20}$$

which is also recognizable as the autocorrelation of the transmit waveform. Given a scattering response, $x(t)$, that contains an unknown number of targets, the received signal can be expressed as

$$y(t) = s(t) * x(t) + v(t), \tag{2.21}$$

where $v(t)$ is additive noise and $*$ is the convolution operation. The matched filter response for the received signal after convolution with the environment is

$$\hat{x}_{\mathrm{MF}}(t) = h_{\mathrm{MF}}(t) * y(t) \tag{2.22}$$

where $\hat{x}_{\mathrm{MF}}(t)$ is the matched filter estimate of the actual scattering $x(t)$.

To provide a baseline for comparison for other filtering techniques that will be discussed, refer to Figure 2.11 where a PCFM verson of an LFM waveform has been generated for use in visualizing the matched filter response. The sidelobes are seen at an expected level that is 13 dB below the main lobe.

It is common for the matched filter response from 2.22 to be collected over multiple pulses because it is often useful to further filter the set of responses (e.g. Doppler processing or synthetic aperture radar (SAR) processing). The time interval over which this set of pulses is collected is referred to as the coherent processing interval (CPI).

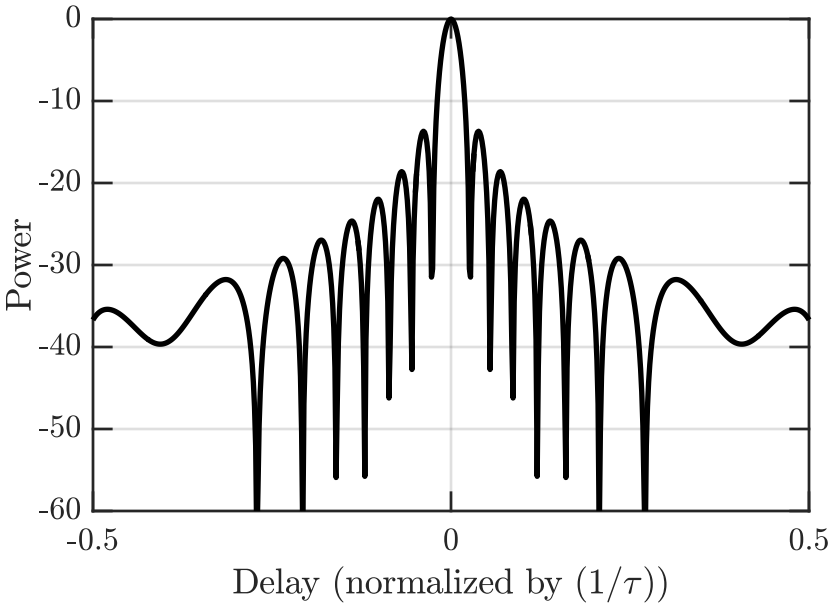

Figure 2.11: Matched filter response for an LFM generated using a PCFM implementation

2.4.1 Discrete Fourier Transform

Generally radar systems are used to collect returns over a range window (defined by some start and end range), which means that the receiver will be turned on at a delay (τ_{near}) that corresponds to the beginning of the range interval (R_{near}). The receiver will then remain on, collecting returns across the entire range swath (corresponding to a delay swath), for a collection time that is equivalent to the sum of the pulse length and the delay swath. The number of samples, N, collected over this range swath is determined from the following

$$N = f_{\text{s}}(T + \Delta\tau), \tag{2.23}$$

where f_{s} is the receiver sampling rate, T is the pulse duration, and $\Delta\tau$ is the notation for the delay swath of the range window.

In order to pulse compress the returns from each range bin, a matrix of matched filters must be generated for each individual range bin (each bin also corresponding to a frequency) contained in

the range interval. This matrix is referred to as the discrete Fourier transform (DFT) matrix, and is often implemented as a fast Fourier transform (FFT). Hence, this matrix can be applied to the discretized receive data vector in order to pulse compress returns from all range bins.

In general the DFT is defined as

$$X_k = \sum_{n=0}^{N-1} x_n \exp\Big(-\frac{j2\pi kn}{N}\Big), \quad k = 0, 1, \cdots, N-1, \tag{2.24}$$

but it is often more useful to formulate it as a complex matrix multiply. To do this, the sampled complex sinusoidal sections s_k can be collected into a matrix $\mathbf{S}_N^*$ which results in

$$\mathbf{S}_N^* = \begin{bmatrix} 1 & 1 & 1 & \cdots & 1 \\ 1 & e^{-j2\pi/N} & e^{-j4\pi/N} & \dots & e^{-j2\pi(N-1)/N} \\ 1 & e^{-j4\pi/N} & e^{-j8\pi/N} & \dots & e^{-j2\pi 2(N-1)/N} \\ \vdots & \vdots & \vdots & \vdots & \vdots \\ 1 & e^{-j2\pi(N-1)/N} & e^{-j2\pi 2(N-1)/N} & \dots & e^{-j2\pi(N-1)(N-1)/N} \end{bmatrix}. \tag{2.25}$$

When the input signal is discretized and represented as a vector, denoted $\mathbf{x}$ the DFT matrix can be applied to it as

$$\mathbf{X} = \mathbf{S}_N^* \mathbf{x}. \tag{2.26}$$

2.5 Ambiguity Function

In the previous section the existence of a Doppler shift was ignored. In order to include the potential for radial motion between the radar and scatterer this Doppler frequency shift must be considered because it imparts a time-varying phase change on the reflected waveform when pulse compression is employed. However, this Doppler shift results in an unwanted mismatch between the received waveform and the matched filter used to pulse compress the response [5]. Ambiguity function are used to examine this distortion by characterizing the response of the matched filter in the presence of Doppler frequencies, and are determined by generalizing the matched filter response to arbitrary

delay τ and Doppler frequency f_D as

$$\chi(\tau, f_D) = \int_{t=0}^{T} e^{j2\pi f_D t} s(t) s^*(t+\tau) dt. \tag{2.27}$$

The ambiguity function is a means of assessing the Doppler tolerance of a waveform, and points to yet another reason for the popularity of the LFM waveform in radar applications. The ambiguity function of an LFM waveform exhibits a ridge, the significance of which is that despite the presence of a considerable Doppler shift there is little loss in SNR relative to the peak of the mainlobe.

2.6 Stretch Processing

In order to discuss the formulation of alternate processing techniques presented in later chapters, it is important to establish a baseline of current techniques here to be able to compare later results against. In the following sections a detailed explanation and mathematical analysis of stretch processing in its current form is presented.

2.6.1 Introduction

Stretch processing [20, 21, 22, 23] is a pulse compression technique that permits transmission of long-duration pulses while still achieving fine range resolution. Wideband radar systems often use stretch processing to take advantage of the inverse relationship between bandwidth and range resolution [24]. One such example of a high-resolution system that commonly applies stretch processing is syntetic aperture radar (SAR). However, it is difficult to design and build hardware that can support extremely wide bandwidths on receive. To mitigate this dilemma, stretch processing is commonly used in conjunction with an LFM waveform. The application of stretch processing reduces the bandwidth required for receive processing prior to converting an analog signal into a digital form, which alleviates the sampling frequency requirements on the analog-to-digital converter (ADC) as they are required to sample at rates of twice the highest frequency (in order to

meet Nyquist criteria). Due to the modulation of an LFM waveform, the transmit bandwidth of a short pulse can still be made wide enough to maintain the fine range resolution required by certain applications.

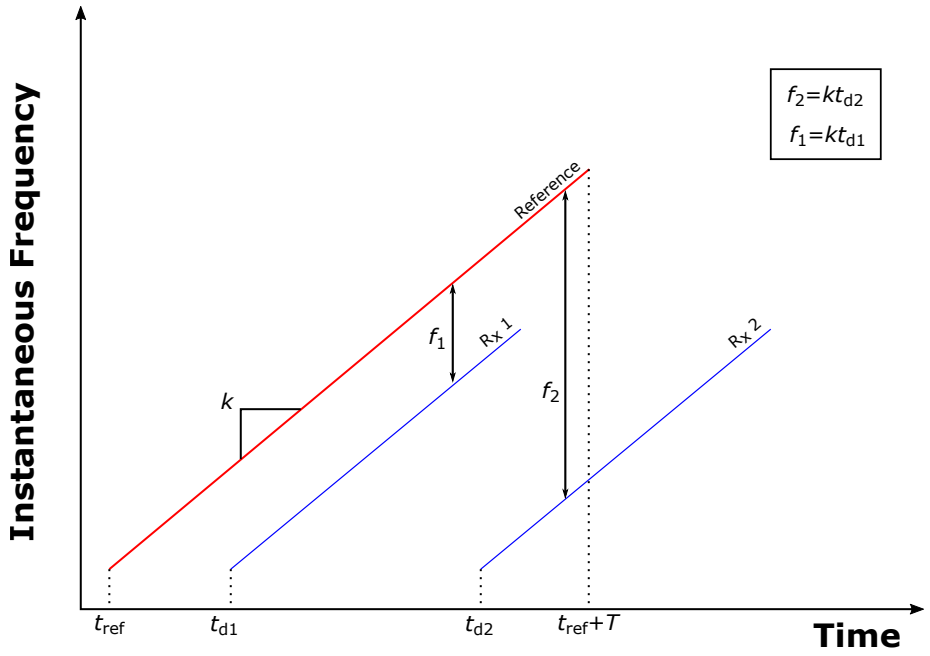

Figure 2.12: The reference waveform is used to mix the two receive waveforms, the result of which are the frequencies f_1 and f_2

The technique of stretch processing was developed by Caputi [20] in the early 1970s, and it serves to convert the bandwidth of an LFM waveform down to a single frequency (see Fig. 2.12 for pictoral description of the process) prior to sampling. This frequency is related to the range at which the target is located relative to the radar. It is important to note that typically the filters used in a stretch processing setup have a passband that is smaller than that of the waveform's bandwidth in order to limit the range of frequencies passed to the ADC. Therefore, the range of observable time delays is also limited, but this constraint is generally acceptable when the distance to the target is known. Stretch processing is commonly used in applications that the distance to the target or area being imaged is known, such as the previously mentioned SAR systems.

Traditionally, stretch processing has been associated with the linear frequency modulated waveform, and while it can be used in both pulsed and continuous wave (CW) setups, the focus in this

work will be on pulsed scenarios. The simulations and analysis that follow in the rest of this work use pulsed waveforms for simplicity.

2.6.2 Signal Model: Receive Chain

Consider a passband representation of a frequency modulated (FM) waveform defined over $0 \leq t \leq T$ as

$$s(t) = \cos(2\pi f(t)t) \tag{2.28}$$

for pulsewidth T and $f(t)$ the instantaneous frequency as a function of time. Specifically for an LFM we can write

$$f(t) = (f_{\text{start}} - f_{\text{end}})\frac{t}{T}, \tag{2.29}$$

where f_{start} and f_{end} are the start and end frequencies.

Let $x(t)$ be the scattering from the illuminated range profile. Ignoring nonlinear effects, the reflected signal captured by the radar is therefore represented by the convolution

$$\tilde{y}(t) = s(t) * x(t) + u(t), \tag{2.30}$$

with $u(t)$ additive noise and $*$ the convolution operation.

The following analysis follows the structure of the system shown in Fig. 2.13, where the receive signal, $\tilde{y}(t)$ is first mixed with reference signal, $s_{\text{ref}}(t)$, which both reduces the bandwidth and down-converts the signal to intermediate frequency f_{IF} where it is bandpass filtered. This intermediate frequency (IF) signal is represented as

$$y_{\text{IF}}(t) = \Phi_{\text{BPF}}\{s_{\text{ref}}(t) \times \tilde{y}(t)\}, \tag{2.31}$$

for $\Phi_{\text{BPF}}\{\bullet\}$ the bandpass filtering operation. The IF signal is then mixed to baseband and IQ

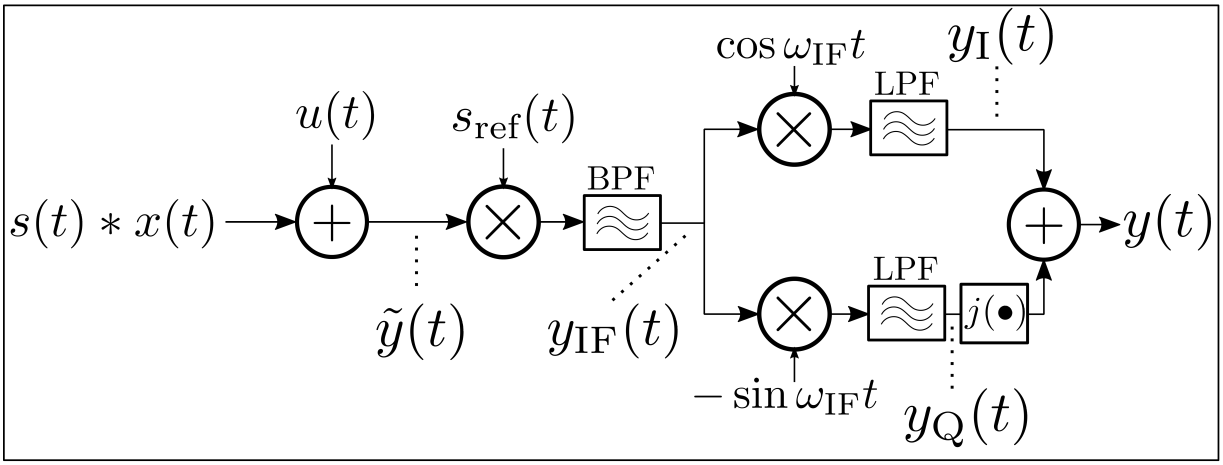

Figure 2.13: Signal model of stretch processing receive chain

demodulated yielding the complex signal

$$y(t) = y_{\mathrm{I}}(t) + j y_{\mathrm{Q}}(t) = \Phi_{\mathrm{LPF}}\{y_{\mathrm{IF}}(t) \times exp(-j2\pi f_{\mathrm{IF}} t)\}, \tag{2.32}$$

where $\Phi_{\mathrm{LPF}}\{\bullet\}$ is a lowpass filtering operation, and $y_{\mathrm{I}}(t)$ and $y_{\mathrm{Q}}(t)$ are the in-phase and quadrature-phase components of the received signal, respectively, that are subsequently sampled.

After passing through the RF receive chain in Fig. 2.13, an LFM waveform reflected from a scatterer at range R would have the complex, baseband response

$$p(t,R) = \Phi_{\mathrm{LPF}}\left\{\Phi_{\mathrm{BPF}}\left\{s_{\mathrm{ref}}(t) \times s\left(t - \frac{2R}{c}\right)\right\} \times \exp(-j2\pi f_{\mathrm{IF}} t)\right\} \tag{2.33}$$

scaled by the amplitude and phase of the particular scatterer, for c the speed of light. For traditional stretch processing, both the transmit signal $s(t)$ and reference signal $s_{\mathrm{ref}}(t)$ are LFM. Therefore $p(t,R)$ is a sinusoid whose frequency depends on the delay at range R. Thus, in general, $y(t)$ from 2.32 is a superposition of sinusoids scaled by the amplitudes/phases of the associated range-dependent scattering for which, after sampling, the fast Fourier transform (FFT) serves as a pulse compression matched filter bank. This baseband response can be sampled to realize the length L

vector

$$\mathbf{p}(R) = \begin{bmatrix} p(\tau_{\text{near}}, R) & \cdots & p(\tau_{\text{near}} + (L-1)T_{\text{s}}, R) \end{bmatrix}^T \tag{2.34}$$

where L is related to the reference chirp duration and the receiver sampling period ($L = T_{\text{ref}}/T_{\text{s}}$). The receive data can be similarly sampled, resulting in the length L discretized response vector

$$\mathbf{y} = \begin{bmatrix} y(\tau_{\text{near}}) & y(\tau_{\text{near}} + T_{\text{s}}) & \cdots & y(\tau_{\text{near}} + (L-1)T_{\text{s}}) \end{bmatrix}^T, \tag{2.35}$$

which, by linearity can be expressed as

$$\mathbf{y} = \Sigma\, x(R)\mathbf{p}(R) + \mathbf{u}. \tag{2.36}$$

In 2.36 $x(R)$ represents the scattering at range R, $\mathbf{p}(R)$ is a complex sinusoid with frequency dependent on R, and $\mathbf{u}$ is the additive complex baseband noise. This representation of the baseband receive signal is traditionally processed using an FFT at this stage in a standard stretch processing model.

For the range swath of interest $\Delta R = R_{\text{far}} - R_{\text{near}}$ with R_{near} and R_{far} the near and far range boundaries respectively, the necessary duration of the reference signal is

$$T_{\text{ref}} = T + \Delta\tau, \tag{2.37}$$

where $\Delta\tau = 2\Delta R/c$ is the delay swath of interest. To capture these ranges, the reference signal $s_{\text{ref}}(t)$ must coincide with time interval $[\tau_{\text{near}}, \tau_{\text{far}} + T]$ for $\tau_{\text{near}} = 2R_{\text{near}}/c$ and $\tau_{\text{far}} = 2R_{\text{far}}/c$, which means the delay swath can likewise be defined as $\Delta\tau = \tau_{\text{far}} - \tau_{\text{near}}$. Further, because the IF signal in 2.31 contains a collection of passband sinusoids that will ultimately become the set of complex baseband sinusoids constituting $y(t)$ in 2.32, the BPF in 2.31 must be sufficiently wide to pass the signals corresponding to the range interval $[R_{\text{near}}, R_{\text{far}}]$. Thus there is a trade-off between the size of the range interval surveilled and the feasible sampling rate of $y(t)$ without aliasing.

2.6.3 Analysis

This section will provide a mathematical baseline of the stretch processing procedure by walking through the implementation in mathematical detail. Refer to Figure 2.14 throughout this section for an understanding of the timing of the relative waveforms, where a homodyne representation of the receive architecture is used for easier illustration.

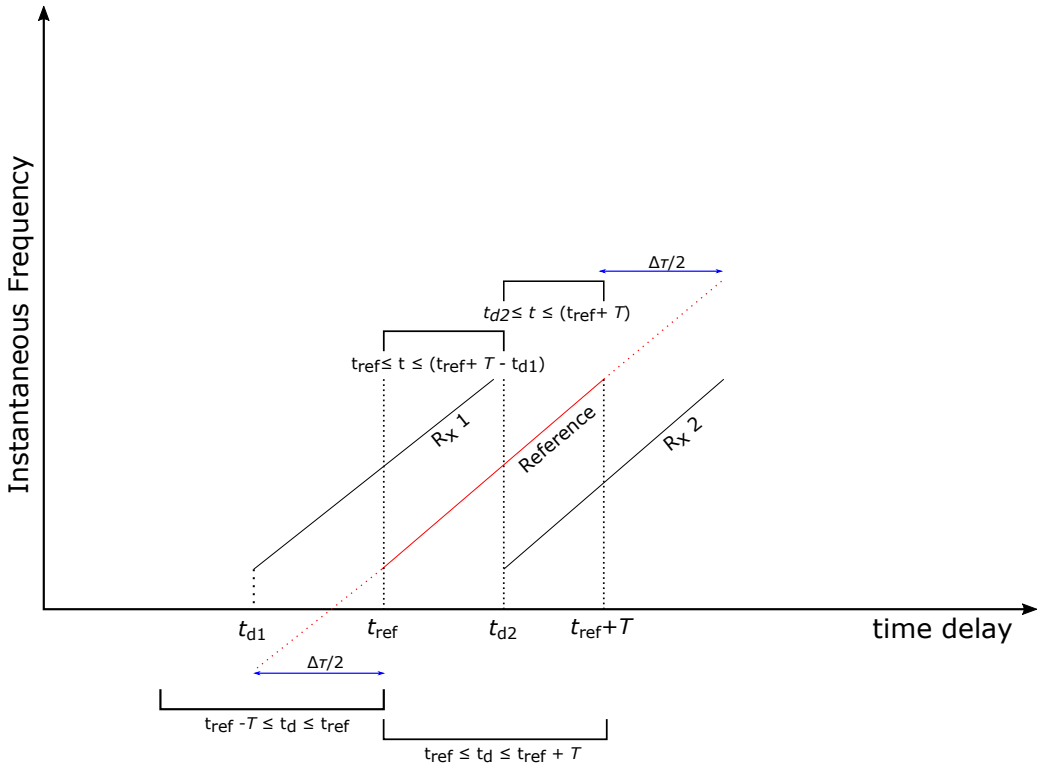

Figure 2.14: Illustration of the receive signal and reference signal timing. Also showing the lengthening of the reference waveform to maintain SNR and resolution

2.6.3.1 Transmit Waveform

Consider an LFM waveform that is centered at an intermediate frequency (IF), f_1,

$$s(t) = \cos\left(2\pi f_1 t + \pi \frac{B}{T}\left(t - \frac{T}{2}\right)^2 + \theta_1\right). \tag{2.38}$$

The LFM waveform must be mixed to an RF using an oscillator in order to transmit, and this is represented as

$$x_{\mathrm{LO},1} = cos(2\pi f_2 t + \theta_2) \qquad t \geq 0. \tag{2.39}$$

After the transmit waveform is mixed with the oscillator the resulting signal

$$s(t) = \cos\left(2\pi(f_1+f_2)t + \pi\frac{B}{T}\left(t-\frac{T}{2}\right)^2 + \theta_1 + \theta_2\right), \tag{2.40}$$

is now centered at frequency $f_{\mathrm{RF}} = f_1 + f_2$, where the lower sideband (a result of the mixing process) has already been removed via filtering. The waveform is now ready to be transmitted, and will propagate through the environment, be reflected by the targets and clutter present, and return to the receiver for receive processing.

2.6.3.2 Receiver

The mathematics detailed here follow a similar outline to the receive processing that is described in [24], and are shown to provide a baseline for comparing later modifications against. For illustration purposes, the return from a single point scatterer at a time delay t_d will be considered. Likewise, assume the use of a pulsed system, where the reference waveform coincides with the time delay t_{ref} which corresponds to the center of the range window. The return signal from the single point target is

$$\tilde{y}(t) = \cos[2\pi(f_1+f_2)(t-t_d) + \pi\frac{B}{T}((t-\frac{T}{2})-t_d)^2 + \theta_1 + \theta_2]. \tag{2.41}$$

On receive, the signal, $\tilde{y}(t)$, is mixed with a copy of the transmit modulation, denoted $s_{\mathrm{ref}}(t)$, the reference waveform. This mixing stage serves the dual purpose of both reducing the bandwidth and down-converting the signal to the intermediate frequency, f_1, where it can be bandpass filtered. The reference waveform is represented as

$$s_{\mathrm{ref}}(t) = \cos\left(2\pi f_2 t + \pi\frac{B}{T}\left((t-\frac{T}{2})-t_{\mathrm{ref}}\right)^2 + \theta_1 + \theta_2\right), \tag{2.42}$$

and this mixing process results in

$$y_{\mathrm{IF}}(t) = \cos\left(2\pi f_1(t-t_d) - 2\pi f_2 t_d + \pi\frac{B}{T}\left(-2\left(t-\frac{T}{2}\right)(t_d - t_{\mathrm{ref}}) + (t_d^2 - t_{\mathrm{ref}}^2)\right) + \theta_1\right) \quad (2.43)$$

where $t_{\mathrm{ref}} \leq t \leq (t_{\mathrm{ref}} + T - t_d)$ for a time delay that is less than or equal to the center of the receive window, and $t_d \leq t \leq (t_{\mathrm{ref}} + T)$ for a time delay greater than or equal to the center of the receive window. The upper sideband that results from the mixing process is filtered out, and the remaining signal is now centered at the intermediate frequency f_1. The amplitude of the return is dependent upon the radar and the RCS of the target, and will be ignored in this analysis for simplicity. It is also important to note at this point that the components of a stretch processor are all linear, therefore this analysis can be applied to a superposition of returns from multiple targets at different delays, and the use of single point target here is to simplify the process for illustration purposes.

The signal $y_{\mathrm{IF}}(t)$ is now mixed down to baseband, using another receive oscillator that has the form

$$s_{\mathrm{LO}}(t) = \cos(2\pi f_1 t + \theta_1), \qquad t \geq 0. \quad (2.44)$$

After this mixing stage, the resulting baseband signal is

$$y(t) = \cos(-2\pi(f_1 + f_2)t_{\mathrm{d}} + \pi\frac{B}{T}(-2(t-\frac{T}{2})(t_{\mathrm{d}} - t_{\mathrm{ref}}) + (t_{\mathrm{d}}^2 - t_{\mathrm{ref}}^2))) \quad (2.45)$$

where $t_{\mathrm{ref}} \leq t \leq (t_{\mathrm{ref}} + T - t_d)$ for $t_{\mathrm{ref}} - T \leq t_{\mathrm{d}} \leq t_{\mathrm{ref}}$ and $t_{\mathrm{d}} \leq t \leq t_{\mathrm{ref}} + T$ for $t_{\mathrm{ref}} \leq t_{\mathrm{d}} \leq t_{\mathrm{ref}} + T$

To simplify this expression some, let $\Delta t_{\mathrm{d}} = t_{\mathrm{d}} - t_{\mathrm{ref}}$ and $\varphi = \pi B/T(t_{\mathrm{d}}^2 - t_{\mathrm{ref}}^2)$, where φ is the residual video phase. A further simplification can be made by grouping the constant phase terms as $\theta = -2\pi(f_1 + f_2)t_{\mathrm{d}} + 2\pi B/2(\Delta t_{\mathrm{d}}) + \varphi$ which leaves

$$y(t) = \cos\left(2\pi\frac{B}{T}(\Delta t_{\mathrm{d}})t - \theta\right) \quad (2.46)$$

where $t_{\mathrm{ref}} \leq t \leq (t_{\mathrm{ref}} + T - t_{\mathrm{d}})$ for $(t_{\mathrm{ref}} - T) \leq t_{\mathrm{d}} \leq t_{\mathrm{ref}}$ and $t_{\mathrm{d}} \leq t \leq (t_{\mathrm{ref}} + T)$ for $t_{\mathrm{ref}} \leq t_{\mathrm{d}} \leq (t_{\mathrm{ref}} + T)$. Note that sign of the argument of the cosine can be changed due to the fact that cosine is an even

function.

The key to this mixing process is the resulting beat frequency $f_b = \frac{B}{T}(\Delta t_d)$, which is a result of the first mixing stage. It is important because its frequency value is the difference between the instantaneous frequency of the reference waveform and the received signal, which is related to the range of the target of interest as $R = \frac{ct_d}{2}$ where the time delay of the received signal will be related to the sampling frequency of the ADC. This relative time delay is related to both the sampling frequency and the digital frequency of the range compressed response.

The process of mixing the received signal down to baseband is used to have a way to distinguish returns that result from scatterers that are at time delays less than t_{ref} from those that are at time delays greater than t_{ref}. The baseband signal can be analytically represented as

$$y(t) = \exp\left(j\left(2\pi\frac{B}{T}(\Delta t_d)t - \theta\right)\right). \tag{2.47}$$

The range of possible beat frequencies (thus the range window size) is limited by the receiver's low pass filters, and the ADC must sample at a rate that is equal to or greater than the bandwidth of the filter. The digitized returns are then compressed in range through the application of a DFT (or an FFT), and if amplitude weighting is used it must occur prior to this range compression.

Another important thing to consider is the need for the reference waveform to be extended in order to avoid any loss in SNR or degradation in resolution. In order to make this happen, the reference waveform can be extended by $\Delta\tau/2$, where $\Delta\tau$ is the delay swath of the range window of interest (refer again to Fig. 2.14).

2.6.3.3 Mismatch Effects

For the purpose of this work, it is useful to examine the effects when there is not a perfect match between the chirp rates of the transmit waveform and the reference used to mix with on receive. As a first step in the examination of the result of this mismatch, we will first look at a situation where the transmit waveform having a single chirp rate deviates from that of the reference LFM

across the entire time extent. In the example shown in Fig. 2.15 three cases of varying degrees of mismatch are considered alongside the standard case of an LFM whose chirp rate matches the reference.

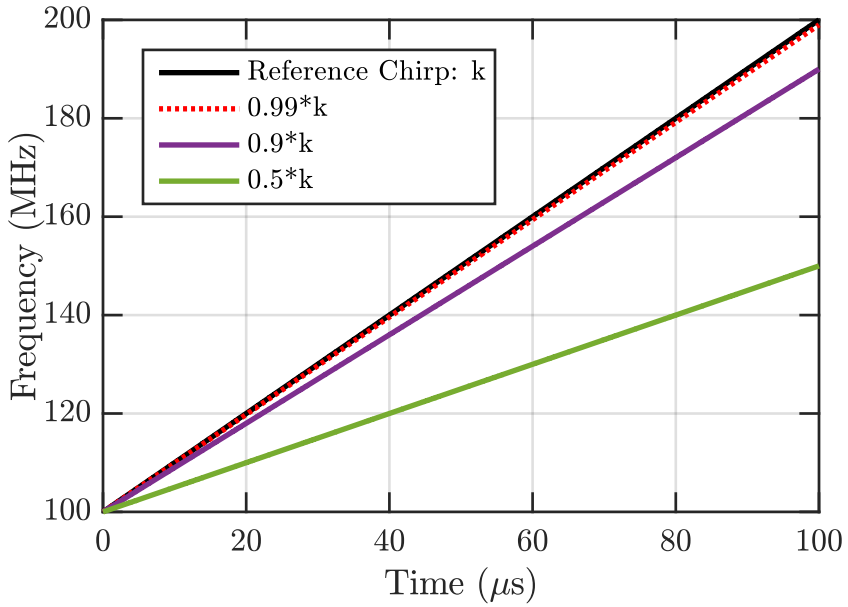

Figure 2.15: Comparison of chirp rates set relative to the reference value of $k = B/T$

2.6.3.4 Simulation Results

A simple simulation is used here to demonstrate several of the principles that have been discussed throughout this section. The bandwidth of the reference LFM is 100 MHz with a pulsewidth of 100 μs, hence the chirp rate, k, is 1MHz/μs (found from $k = \frac{100\text{MHz}}{100\mu\text{s}}$). The chirp rates of the LFM used to transmit are chosen to be 100% (a traditional matched chirp rate), 99%, 90%, and 50% of the reference chirp rate to examine the effects of different degrees of mismatch. The waveform spectra shown in Fig. 2.16 demonstrate how the modification of the chirp rates causes the bandwidth of each transmit waveform to become gradually narrower as the chirp rate is changed to smaller and smaller percentages of the reference chirp rate.

The results of applying stretch processing to each of these waveforms after they have been

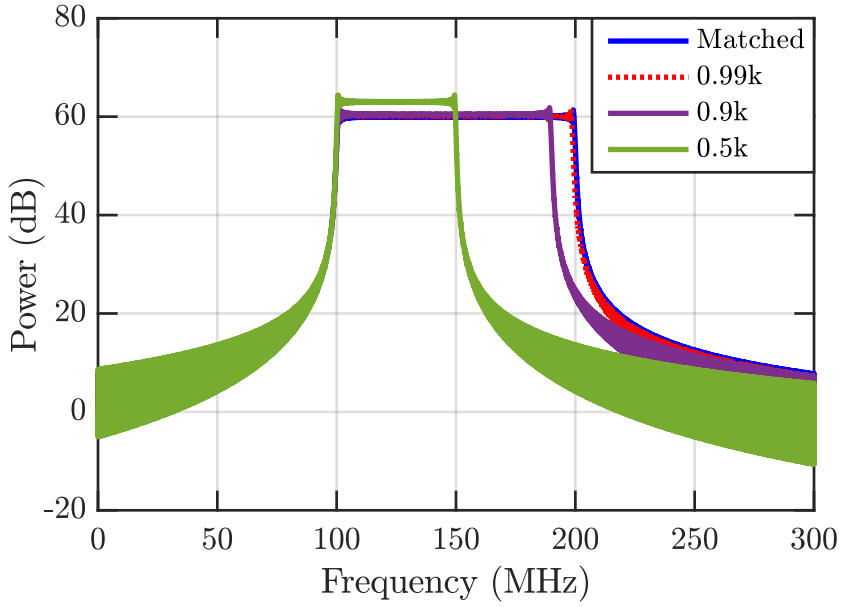

Figure 2.16: Comparison of the spectrums of the transmit waveforms given various mismatched chirp rates relative to the reference chirp rate

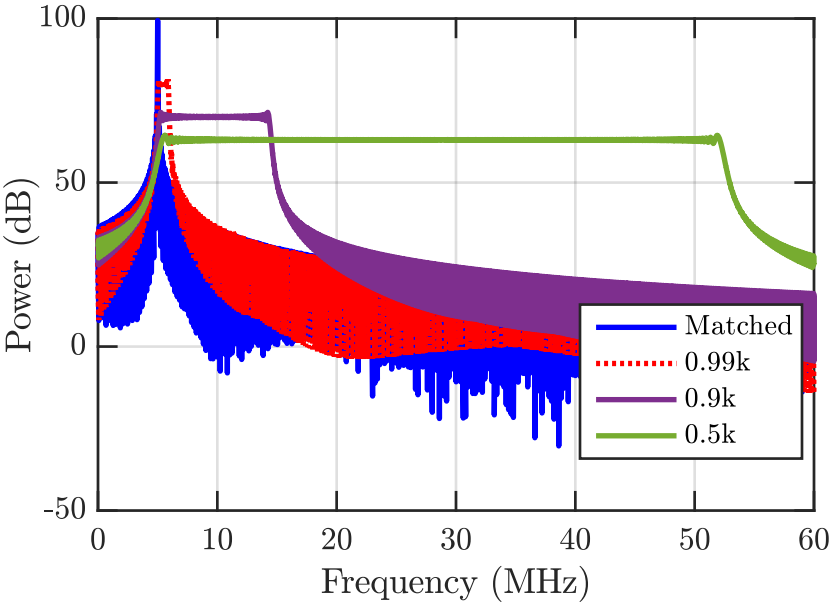

Figure 2.17: Comparison of the spectrum of the receive signal after stretch processing has been applied for various chirp rates

collected as returns from a single point target at a location corresponding to a 5 MHz frequency which can be related back to a specific range based on this frequency. As a quick reference, this calculation is done using $R = \frac{ct_{\mathrm{d}}}{2} = \frac{c}{2f_{\mathrm{b}}}$ where t_{d} and f_{b} are the time delay of the received waveform and the stretch processed beat frequency respectively. Examining these results in Figure 2.17 it is easily visible that when the transmit waveform's chirp rate is mismatched it becomes impossible to detect targets. Clearly this effect increases as the mismatch between the chirp rates of the transmit and reference waveforms increases, and the consequence is a loss in SNR that is dependent on this mismatch along with a smearing effect that causes the spectrum to be spread into the sidelobes.

2.7 Mismatched Filtering

A mismatched filter (MMF) is another technique that is used to obtain sidelobe suppression, and in many cases the sidelobes can be suppressed to levels much lower than a matched filter can hope to attain, although the amount of suppression is waveform dependent. Oftentimes this suppression can be achieved without incurring much mismatch loss (sometimes referred to as loss in processing gain), which is generally considered to be one of the metrics of how the "goodness" of a pulse compression receive filter. Other common metrics are peak sidelobe level (PSL) and integrated sidelobe level (ISL), where PSL is related to the largest sidelobe and PSL is related to the total energy contained in the sidelobes. These metrics are used to design MMFs, through either Least Squares (LS) minimization [25, 26] or using L_p norm minimization [27, 28], although this work will focus on the former method.

A general expression for the loss in SNR due to mismatched filtering of a received waveform is

$$\mathrm{SNR}_{\mathrm{loss,mismatch}} = -10\log_{10}\left(\frac{\mathrm{SNR}_{MMF}}{\mathrm{SNR}_{MF}}\right) \tag{2.48}$$

as in [1] where $\mathrm{SNR}_{\mathrm{MMF}}$ and $\mathrm{SNR}_{\mathrm{MF}}$ are defined at the mainlobe peaks of each filter response. If the filters are normalized such that the produce unity noise power gain then the noise power terms will cancel out such that the ratio falls between achievable signal powers after filtering.

To derive the LS MMF, assume a degree of over-sampling, denoted K, relative to the 3 dB bandwidth. The value K relates to the receive sampling period T_s and the pulsewidth T as

$$T = \frac{T}{K(BT)} = \frac{T}{N} \tag{2.49}$$

where B is the bandwidth and T is the pulse duration. Hence, the value N is the number of samples in a sampled version of the waveform. The LS MMF formulation is presented as

$$\mathbf{B}\mathbf{h}_{\text{LS,MMF}} = \mathbf{e}_m \tag{2.50}$$

where $\mathbf{e}_m$ is a length $(M+1)N-1$ elementary vector with a 1 placed in the m^{th} element and zeros elsewhere. The matrix $\mathbf{B}$ is defined following the formulation in [25] as

$$\mathbf{B} = \begin{bmatrix} s_1 & 0 & \cdots & 0 \\ \vdots & s_1 & & \vdots \\ s_N & \vdots & \ddots & 0 \\ 0 & s_N & & s_1 \\ \vdots & & \ddots & \vdots \\ 0 & \cdots & 0 & s_N \end{bmatrix}, \tag{2.51}$$

which is a Toeplitz matrix of size $((M+1)N-1) \times MN$, where M is a filter-length increase-factor. The columns of the matrix are formed using the discretized waveform vector $\mathbf{s} = [s_1\ s_2\ s_3\ \cdots\ s_N]^T$. Hence, when $K = 1$ (not over-sampled), the optimal mismatched filter in the least squares sense is

$$\mathbf{h}_{\text{LS,MMF}} = (\tilde{\mathbf{B}}^H \tilde{\mathbf{B}} + \delta \mathbf{I})^{-1} \tilde{\mathbf{B}}^H \mathbf{e}_m, \tag{2.52}$$

where δ is a diagonal loading factor and $\mathbf{I}$ is an $MN \times MN$ identity matrix that combined are considered a diagonal loading term that provides the ability to control the MMF performance. The difference between matrix $\mathbf{B}$ and matrix $\tilde{\mathbf{B}}$ is simply a beam-spoiling effect incorporated by

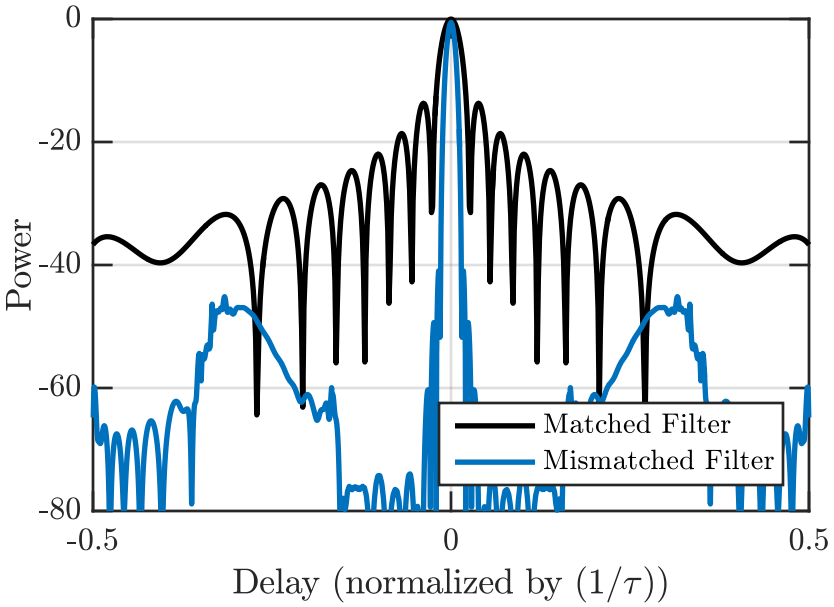

Figure 2.18: Comparison of the responses of the matched and mismatched filters

replacing rows above and below the m^{th} row with zeros. This is done to avoid creating a super-resolution condition that causes considerable mismatch loss despite producing a narrow mainlobe. The exact number of rows to zero in order to achieve the nominal resolution (resolution identical to the matched filter) filter is dependent on both the waveform and the value of K.

After determining the MMF, it can then be scaled to have $\| \mathbf{h}_{\text{LS,MMF}} \| = 1$ in order to produce a unity noise-power gain, which is useful to compare be able to compare the response with the matched filter response (see Fig. 2.18). This comparison was generated using a PCFM version of an LFM waveform, which results in greater sidelobe suppression than mismatched filtering applied to an LFM, and no diagonal loading or beam-spoiling has been included.

Chapter 3

Waveform-Diverse Stretch Processing

Traditionally, stretch processing has relied upon the use of linear frequency modulated (LFM) waveforms in order to reduce the bandwidth of a received signal prior to digitizing it. This reliance means that the ability to use waveform diversity in this kind of context is severely limited. However, when a modification is made to the final stage of stretch processing, it is still possible to detect targets using waveforms that are not strictly LFM.

As was mentioned in the introductory chapter, it has been analytically shown by [29] that stretch processing can only be used with LFM waveforms in its current state. The point was made that a pure tone can only be produced by the mixing of two LFM waveforms in order to use Fourier transform processing after sampling the receive signal. However, there are many examples of methods developed to address distortions caused by hardware to the structure of the transmit waveform (e.g. [30, 31, 32, 33]) These methods are essentially compensations for the deviations from the ideal LFM structure, and from this notion of compensation the term for the proposed modification is designated as a compensation matrix.

The use of nonlinear FM (NLFM) waveforms is proposed (e.g. [9, 10, 12, 13, 34, 35, 36, 37, 18]) in place of the typical LFM waveform, which, borrowing from the same idea as the aforementioned distortion compensating methods, involves a compensation to the traditional Fourier transform that is applied after sampling. Since the Fourier transform is essentially a matched filter bank for the collection of scaled sinusoids (whose delay shifts correspond to frequency shifts) produced by mixing the LFM receive waveform with the LFM reference, as is done in standard stretch processing, then it should be possible to generate similar filters matched to a different scenario of transmit waveform. This new set of matched filters, which is a compensated Fourier transform, will

have a collection of scaled responses that correspond to the mixed product of the NLFM waveform with the LFM reference for various delay shifts that still correspond to frequency shifts. The difference in the case of using a NLFM waveform, is that instead of having a collection of pure tones, this new realization involves a superposition of signals that each possess some small amount of bandwidth. This concept has been experimentally demonstrated in [38], and the procedure and results are also detailed in the following sections.

In order to ensure that the bandwidth-collapsing benefit of this mixer pre-processing stage it is important keep the bandwidth of the individual signals contained in the compensated Fourier transform matrix small. This means that the NLFM waveform used in this situation should still maintain chirp-like characteristics such that it is still sufficiently similar to the reference chirp. Specifically, the waveform and reference should both be up or down chirping, and the overall chirp-rate of the NLFM waveform should be similar to the chirp-rate of the reference LFM. There is no set limit on how similar the chirp-rates should be, but the limitations of a particular application will dictate how different the waveforms can be from one another (i.e. relatively small receive bandwidth on an RSA used to capture data).

3.1 Compensation Matrix

As was discussed previously in section 2.6, the final stage of standard stretch processing is an FFT, which is nothing more than an efficient implementation of a DFT, which itself is nothing more than a bank of matched filters for the different range responses. Here, we call this matched filter bank a compensation matrix, because it compensates for the deviations from the sinusoidal DFT structure. The response after application of of the compensation matrix can be visualized as shown in Figure 3.1, where the matrix is generated for the case of an LFM transmit waveform and an LFM reference. This figure shows multiple peaks, which are sinusoids of frequencies that correspond to various delays (these delays can then be related to the range of the scatterer). For comparison, the response after applying a compensation matrix of the scenario where the transmit waveform is no longer an LFM is shown in Figure 3.2. In this case, the mixed responses of the reference

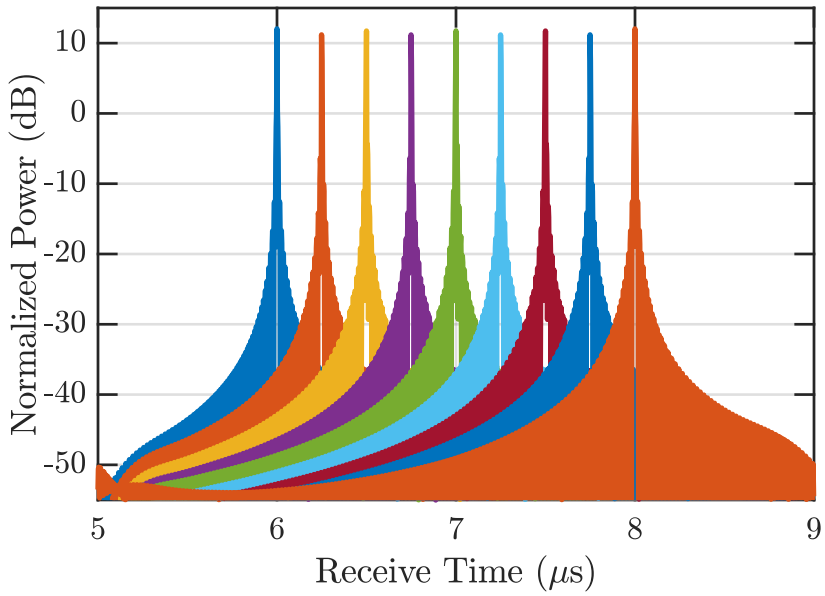

Figure 3.1: A visualization of the response after application of the compensation matrix for an LFM transmit waveform and LFM reference (in other words essentially the DFT matrix)

chirp and the transmit waveform are no longer pure tones. These images display columns of the compensation matrix plotted against the relative time delay (the columns are a collection of all of the potential receive signals for a given delay swath). Several arbitrary time delays were chosen for illustration purposes, which means that not all columns are plotted. In the following paragraphs an analytical explanation of the generation of these columns is detailed.

If we now consider the complex, baseband response of a waveform that has been reflected from a scatterer $p(t,R)$ (refer to section 2.6.2), and sample this response to realize the length L vector we are left with

$$\mathbf{p}(R) = [p(\tau_{\text{near}},R) \ \cdots \ p(\tau_{\text{near}}+(L-1)T_{\text{s}},R)]^T . \tag{3.1}$$

Here L is the sampled duration of the received signal, which is related to both the reference chirp duration and the receiver sampling period as

$$L = \frac{T_{\text{ref}}}{T_{\text{s}}}, \tag{3.2}$$

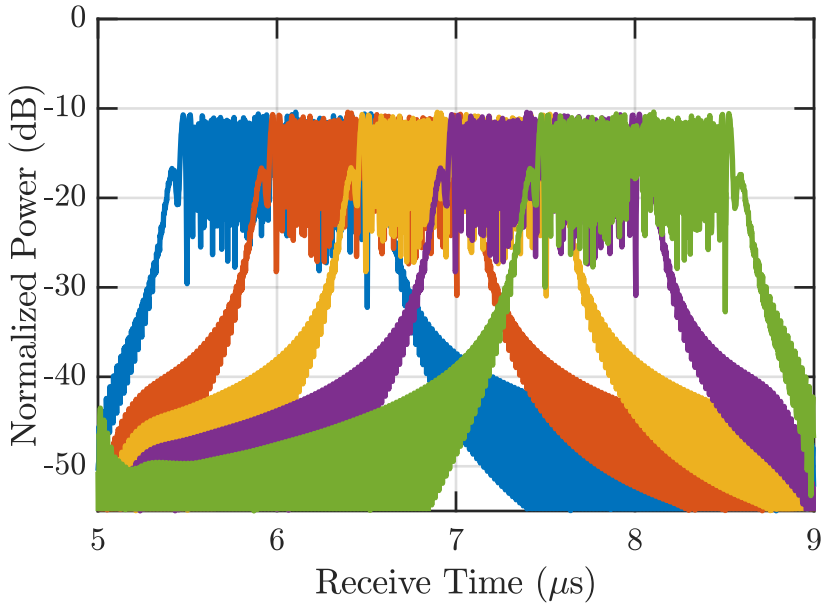

Figure 3.2: A visualization of the compensation matrix for an NLFM transmit waveform and LFM reference

with the restriction that $1/T_s$ must exceed the IF bandwidth for the observed interval of NLFM-LFM mixed products to avoid aliasing. This discretized response vector, after a normalization, is used to represent the R^{th} normalized matched filter as

$$\mathbf{w}(R) = \frac{1}{\|\mathbf{p}(R)\|_2}\mathbf{p}(R) \tag{3.3}$$

and the resultant matched filter estimate of the scattering at range R as

$$\hat{x}(R) = \mathbf{w}^H(R)\mathbf{y}. \tag{3.4}$$

When we consider the set of matched filters that are a result of mixed products of the NLFM and LFM waveforms, they can be collected into the $L \times N$ compensation matrix

$$\mathbf{W} = [\mathbf{w}(R_{\text{near}}) \quad \mathbf{w}(R_{\text{near}} + \delta R) \quad \cdots \quad \mathbf{w}(R_{\text{near}} + (N-1)\delta R)]. \tag{3.5}$$

where δR is the range sample spacing and $N = \frac{\Delta R}{\delta R}$ is the number of samples in the estimated range profile.

When $\mathbf{W}$ is constructed in this manner, it can be applied to the $L \times 1$ received data vector $\mathbf{y}$ to obtain the entire mixed NLFM-LFM matched filter estimate as

$$\hat{\mathbf{x}} = \mathbf{W}^H \mathbf{y}. \tag{3.6}$$

When the final FFT is considered from this filter bank perspective, it becomes clear that using an LFM to generate the complex baseband response to a range swath of interest, and the linear frequency modulated waveform that is traditionally used to generate this matched filter bank is simply a special case of a far broader set of possible waveforms. This realm of usable waveforms is limited by several factors that are discussed in the following sections.

3.1.1 Comparison of Compensation Matrix and Matched Filtering

A common metric that can be used for comparison of the effectiveness of this compensation matrix technique is the standard matched filter response. Since the compensation matrix is essentially a matched filter bank produced for a mismatched scenario, it is expected that it will perform with results similar to those produced by a matched filter. The two waveforms used in the following simulations are generated using the PCFM structure. A piecewise NLFM waveform is generated along with a chirp waveform that has a uniform chirp rate with a value identical to the reference chirp rate. A plot of these waveforms time-frequency characteristics is shown in Figure 3.3. A target is simulated at the range index 201, and after the echo from the scatterer has been mixed with the reference waveform on return each stretch processed signal is processed using either an FFT or the compensation matrix. In Fig3.4 a comparison is shown between the results of standard stretch processing and the use of the compensated receive processing for the use of a NLFM waveform. In this simulation, the compensation matrix yields the same range resolution and slightly lower sidelobe response. On the other hand, when both processing techniques are compared on the

NLFM waveform case, there is again a better sidelobe response and no effect on the resolution.

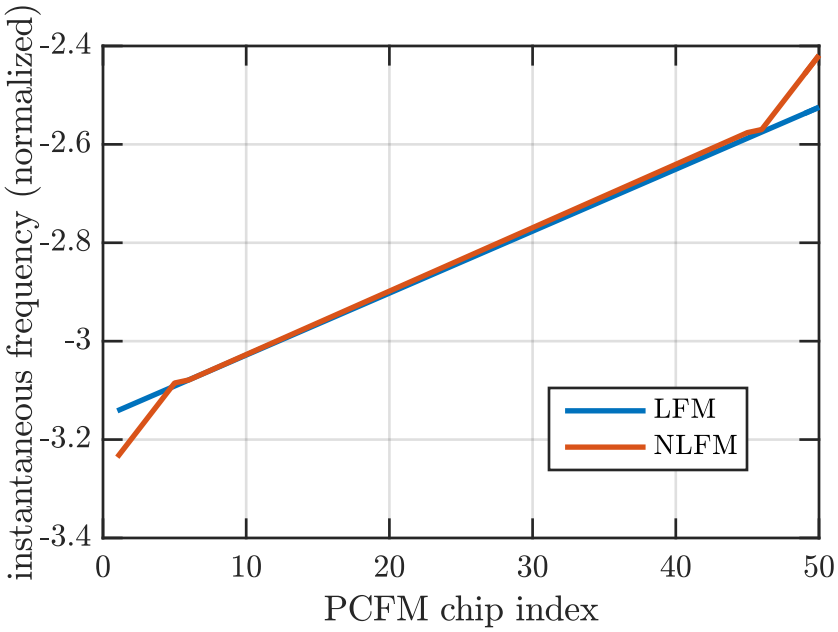

Figure 3.3: Transmit waveforms: Case 1

Obviously the deviation between the NLFM waveform and the reference waveform in Case 1 is not significantly large, which means that it will be useful to examine a case where the NLFM waveform deviates more drastically from the chirp rate of the reference waveform. To achieve this waveform, for Case 2, the chirp rate at either end of the waveform are increased and extend over a longer duration of the waveform, refer to Figure 3.5 to see this change in the NLFM transmit waveform. As the NLFM waveform differs more substantially, it becomes clear that the use of an FFT to pulse compress the range response is no longer a viable option. The NLFM-FFT response shown in Fig 3.6 exhibits higher sidelobe responses and a widening of the main lobe at the expected location of the scatterer. This would result in diminished ability to detect scatterers that are located closely in range to one another at dissimilar power levels. This consequence will become more severe as the NLFM chirp rates become less similar to the reference chirp. However, when the compensation matrix is used in lieu of the FFT, (see yellow trace in Fig. 3.6) the detrimental effects on the sidelobes and main lobe resolution are reduced.

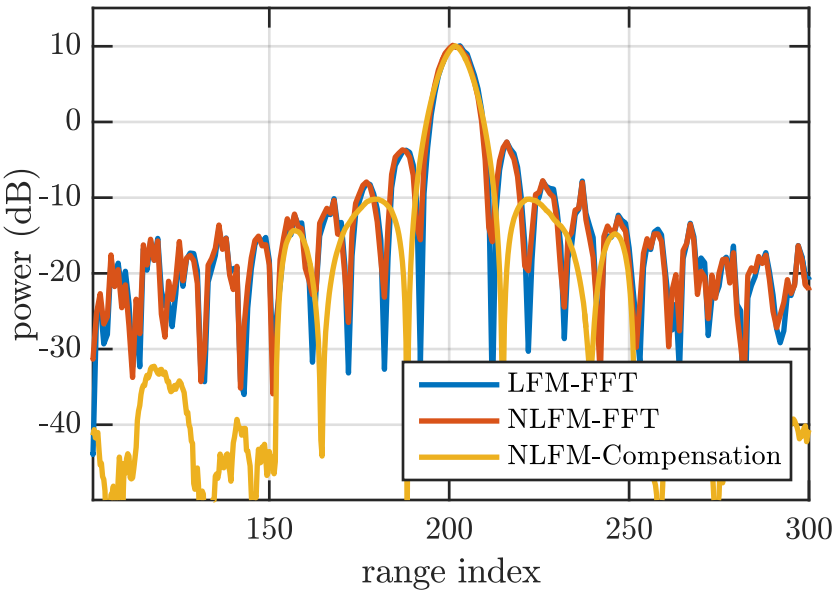

Figure 3.4: Here is a comparison between the application of an FFT or compensation matrix to the Case 1 transmit waveforms. The blue and red traces represent standard stretch processing applied to the LFM and NLFM respectively.The yellow trace shows the use of the compensation matrix in place of the FFT.

Now consider a final case, Case 3, where the transmit waveform is again an NLFM, but instead of having a piecewise, symmetrical design it has a single chirp rate that is slightly different from the reference. The transmit waveforms are shown in Figure 3.7, where the LFM is again used as a standard.

The use of an FFT in this case is not adequate as is obvious from the NLFM-FFT trace in Figure 3.8 where the peak of the scatterer has shifted to the right of where it should be. In contrast, the error that occurs as a result of traditional processing does not manifest itself after the use of the appropriate compensation matrix. The scatterer is found in the location that it is expected, and the sidelobe response has again been recovered to level that is similar to the matched filter response with no negative impact on the resolution achieved.

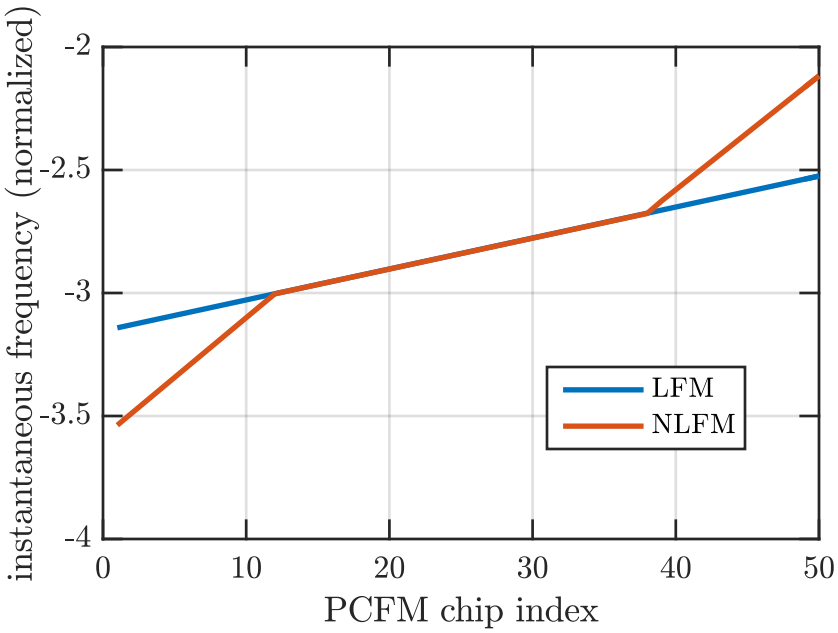

Figure 3.5: Transmit waveforms: Case 2

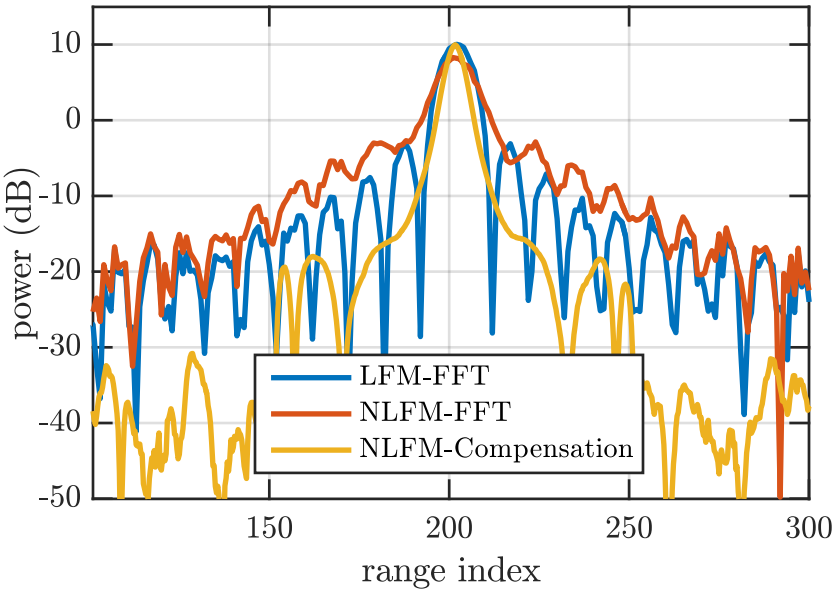

Figure 3.6: The range response of the Case 2 stretch processed waveforms. The blue trace is the standard for comparison (transmit waveform is an LFM and the receive processing is an FFT). The other two traces are both using the NLFM waveform using both receive processing techniques.

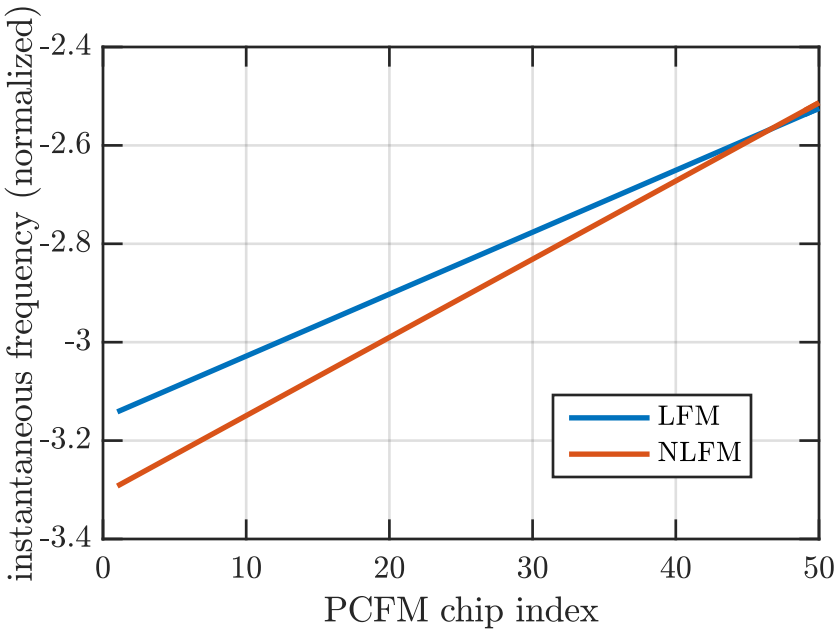

Figure 3.7: Transmit waveforms: Case 3

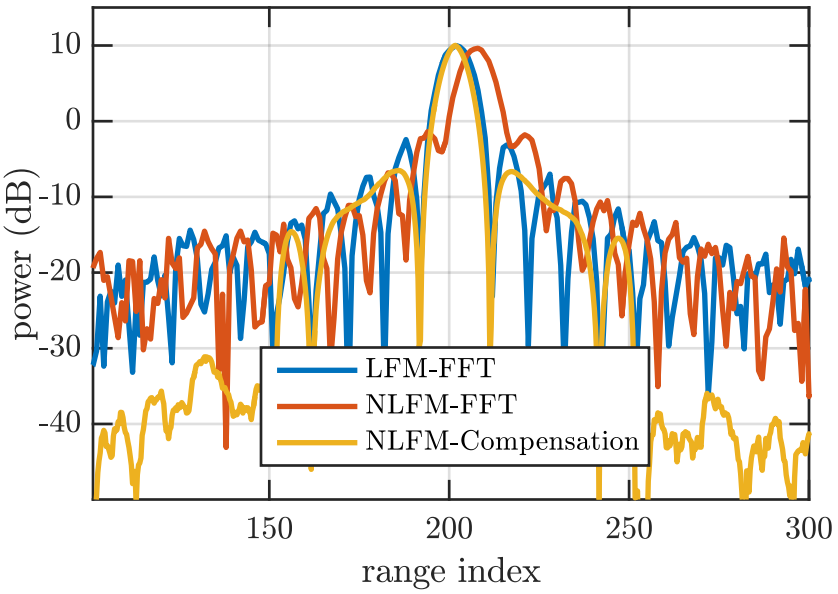

Figure 3.8: The range response of the Case 3 waveforms after stretch processing. The standard is shown in blue, and the application of both an FFT and a compensation matrix are also plotted.

3.2 Waveform Limitations

There is a general restriction of maintaining a "chirp-like" waveform to ensure the usefulness of this technique, which implies that the transmit waveform maintain similar attributes to an LFM. This restriction is necessary to be able to compensate for the new transmit waveform.

In order to determine what types of waveforms are feasible for this waveform-diverse stretch processing setup, it is necessary to consider the effects that are caused by a mismatch between the received waveform and the LFM reference. The most significant effect is the increase in bandwidth that results from the mismatched mixing of the LFM with the receive waveform when it is no longer an LFM.

3.2.1 Additional Sampling Bandwidth

For standard stretch processing, each column of the **W** matrix represents a complex sinusoid with a frequency that is dependent on the range. This implies that in the traditional case there is essentially no bandwidth contained by the mixed response in each column, because the mixed product is a single frequency. However, in the case of waveform-diverse stretch processing, it is necessary to consider the fact that the more a waveform deviates from the LFM reference, the more additional bandwidth is imparted to the individual sinusoids in the baseline **W** matrix. This concept of increased bandwidth was simulated in Section 2.6.3.4, where the frequency response of the signal after application of stretch processing had a bandwidth wider than that of the traditional case of using an LFM.

If we again start by first considering standard stretch processing, the sampling rate at the receiver is dictated by the receive bandwidth, B, corresponding to a desired range swath (ΔR). So, when there is a mixing of a chirp-like nonlinear FM waveform with the LFM reference, the additional bandwidth produced, denoted ΔB, necessitates an increased sampling bandwidth of $B + \Delta B$. Consequently, this is indicative of a trade-off between how different a NLFM waveform can be from the reference (in terms of instantaneous chirp-rate) and the acceptable additional sampling

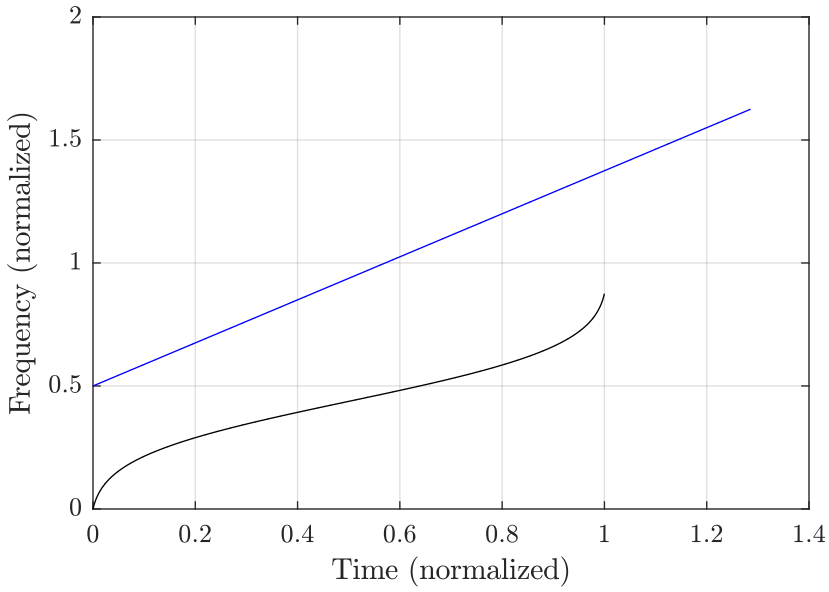

Figure 3.9: A plot of the instantaneous frequency of both the reference chirp (blue) and the NLFM transmit waveform (black)

bandwidth resulting from a mismatch.

A somewhat general expression to determine the additional bandwidth that is induced from the mixing of an arbitrary NLFM transmit waveform with the reference can be determined by examining the difference between the instantaneous frequency of the transmit waveform and the instantaneous frequency of the reference chirp, which will be denoted as $f_{\text{Tx}}(t)$ and $f_{\text{Ref}}(t)$ respectively. Recall that the instantaneous frequency of an LFM is $f_{\text{Ref}}(t) = f_0 \pm (\frac{B}{T})t$, where f_0 is the starting frequency, the $\pm$ determines whether it up-chirps or down-chirps, and $t \in [0, T]$. To provide a visual understanding of the process of calculating ΔB, refer to the reference chirp and NLFM waveform shown in Fig. 3.9, and the result of taking the difference of the transmit and reference instantaneous frequencies shown in Fig. 3.10. Using these waveforms, the difference in instantaneous frequencies, or $f_{\text{Tx}}(t) - f_{\text{Ref}}(t)$, which ultimately corresponds to the beat frequency f_b, is shown in Figure 3.10. The difference between an LFM waveform with a chirp rate that is identical to the reference chirp is also shown. For this case, the difference in instantaneous frequencies is a horizontal line, which is as expected based upon the analysis of traditional stretch

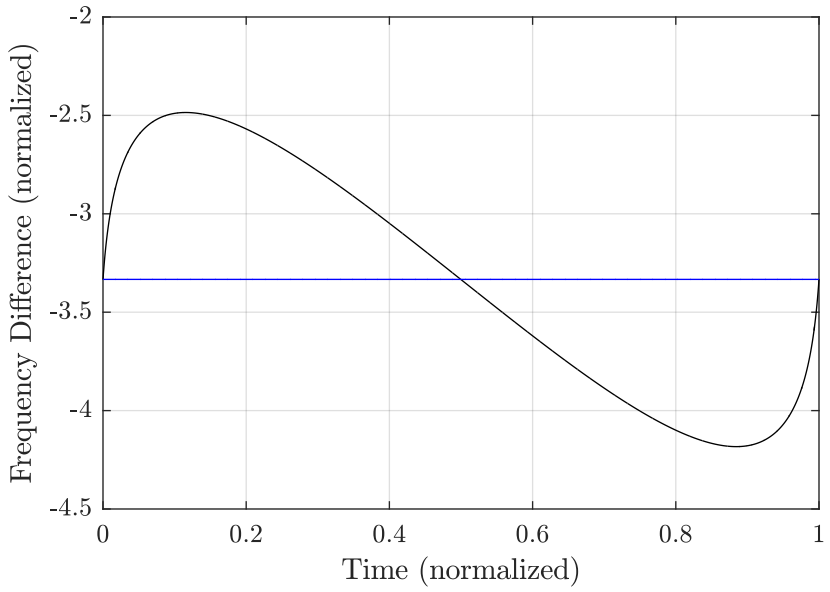

Figure 3.10: The black trace is the difference in instantaneous frequency of the reference waveform and the NLFM transmit waveform as a function of time. The horizontal (blue) line is the difference between the reference waveform and an LFM chirp having the same chirp rate.

processing where the result was a single beat frequency corresponding to the difference in frequencies between the reference and receive waveforms (which in this case happens to be zero). To determine the maximum deviation of an arbitrary transmit waveform from the reference we can use this type of calculation to discern the value of ΔB. In other words, in general the additional bandwidth incurred as a result of the mismatched mixing is defined as

$$\Delta B = \left| \max\left\{ f_{\mathrm{Tx}}(t) - f_{\mathrm{Ref}}(t) \right\} - \min\left\{ f_{\mathrm{Tx}}(t) - f_{\mathrm{Ref}}(t) \right\} \right|. \tag{3.7}$$

It is interesting to consider this particular limitation in terms of an opportunity to optimize the choice of a reference waveform based upon a desired transmit waveform. While all of the specifics for this process are not included in the scope of this work, a starting point for developing the framework is suggested.

Let us now instead refer to $f_{\mathrm{Tx}}(t)$ as $f(t)$ and let $f_{\mathrm{Ref}}(t)$ be $b(t) = kt + d$. The problem is then

formulated as solving 3.7 for $b(t)$ where $b(t)$ is constrained to the model $b(t) = kt + d$. The solution to this problem can be determined without analysis by using the Matlab minimax function, and will result in a reference waveform that is optimized to minimize the deviation between the transmit waveform and said reference. This in turn minimizes the additional bandwidth requirement as it is dependent on the deviation from the transmit waveform from the reference.

3.3 Waveform-Diverse Experimental Analysis: Piecewise NLFM

In order to evaluate this waveform-diverse stretch processing concept, it was evaluated in hardware via an open-air experiment. To be able to have a clear and concise mathematical outline the concept, a set of piecewise LFM waveforms are useful for the illustration of how the stretch processing setup is modified to compensate for the use of NLFM waveforms. The modification that is considered here is the construction and use of the appropriate compensation matrix. The experimental test setup and results will be discussed in the following sections, but the general structure of the waveforms implemented is discussed here. A standard LFM is used for a baseline to compare against, and the two cases of piecewise LFM are:

1. NLFM constructed from piecewise LFM and compacted to cover the same swept bandwidth as the baseline LFM (which means there is no similar chirp rate to the reference at any point in this waveform)

2. NLFM constructed using piecewise LFM, but with the same chirp rate as the baseline LFM. This waveform covers a wider swept bandwidth than the baseline LFM.

These waveforms are denoted as LFM, NLFM-1, and NLFM-2, respectively (see Fig. 3.11).

3.3.1 Experimental Setup

For experimental testing, the three transmit waveforms were all implemented at a center frequency of $f_c = 3.5$ GHz. The LFM reference signal is used on receive to mix the echoes from the range

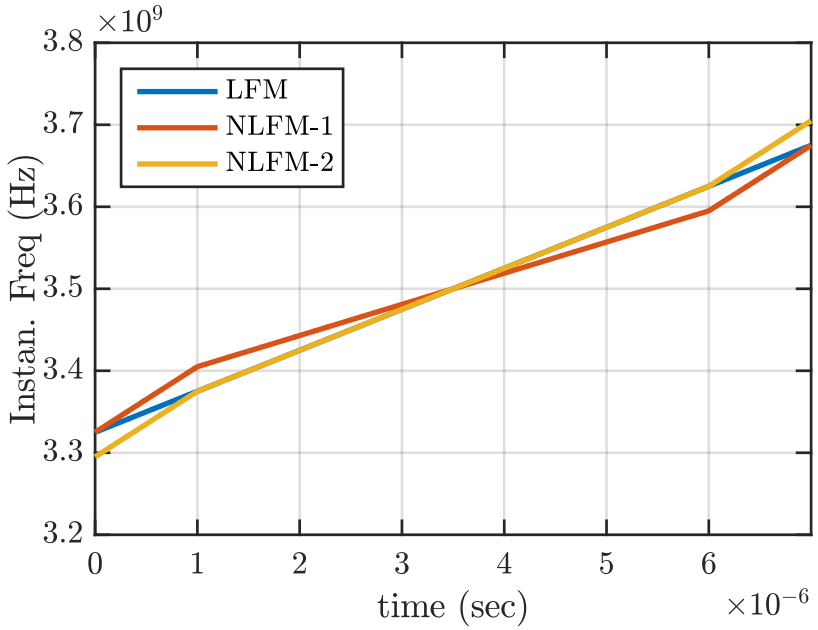

Figure 3.11: Time-frequency structure of the 3 transmitted waveforms

profile to an intermediate frequency of $f_{\text{IF}} = 500$ MHz. These mixed products are bandpass filtered, converted all the way to baseband, and IQ sampled using a Rohde & Schwarz real-time spectrum analyzer (RSA). This receive processing follows the traditional structure of a stretch processing setup, up until the final fast Fourier transform (FFT) stage.

The RSA used has a sampling rate of $f_s = 200$ MHz, and an analysis bandwidth of 160 MHz (due to the lowpass filters of the device). Because of this 160 MHz bandwidth, the desired range swath ΔR is set to correspond to a frequency of 100 MHz for the mixed products, so that the remaining 60 MHz of analysis bandwidth can be used to capture the additional frequency content that results from the mismatched mixing of the NLFM cases.

The range swath being considered for this setup is $\Delta R = 300$ m, and is set to have a range interval between $R_{\text{near}} = 900$ m and $R_{\text{far}} = 1200$ m. This range interval is illuminating the intersection at 23$^{\text{rd}}$ and Iowa in Lawrence, KS. The delay swath that corresponds to this range swath is $\Delta\tau = 2\mu$s, with a near delay $\tau_{\text{near}} = 6\mu$s and a far delay $\tau_{\text{far}} = 8\mu$s. This implies that the chirp rate, k, of both the LFM transmit waveform and the reference chirp are $50\frac{\text{MHz}}{\mu\text{s}}$. This chirp rate is set by the ratio of the receive frequency band and the delay swath

$$k = \frac{B_{\text{Rx}}}{\Delta\tau} = \frac{100\text{ MHz}}{2\ \mu\text{s}}. \tag{3.8}$$

In order to satisfy the 10% bandwidth requirement for the transmit waveforms to be considered wideband, they are set to have a bandwidth of at least 350 MHz. The LFM and NLFM-1 waveforms both have a 350 MHz bandwidth, while the NLFM-2 waveform has a bandwidth of 410 MHz. The resulting pulsewidth, calculated from the ratio of transmit bandwidth to chirp rate, is

$$T = \frac{350\text{ MHz}}{50\text{ MHz}/\mu\text{s}} = 7\ \mu s, \tag{3.9}$$

which means, according to 2.37 from Section 2.6.1, the duration of the reference LFM is

$$T_{ref} = T + \Delta\tau = 7\ \mu\text{s} + 2\ \mu\text{s} = 9\ \mu\text{s} \tag{3.10}$$

which coincides with the time interval [6 μs, 15 μs]. In order to mix the received responses from the range profile to the desired intermediate frequency ($f_{\text{IF}} = 500$ MHz), the reference signal must have a center frequency of $f_{\text{c,ref}} = 4$ GHz (determined from 3.5 GHz + 500 MHz).

Despite the different swept bandwidths of the two NLFM waveforms, each case still has a pulsewidth of 7 μs. The instantaneous time-frequency structure of the NLFM-2 waveform (as seen in Fig. 3.11) shows flared edges and a chirp rate through the center of the pulse that is identical to the reference. This causes the waveform to realize a 410 MHz swept bandwidth. Similarly, because the NLFM-1 waveform is compacted to the same 350 MHz swept bandwidth as the LFM waveform, this waveform has a lower center chirp rate relative to the reference. Additionally, because the flared edges have a faster transition they tend to contribute less to the overall bandwidth. In this way, NLFM-2 possesses roughly the same 3-dB bandwidth as the LFM, and NLFM-1 has a narrower 3-dB bandwidth. Therefore LFM and NLFM-2 realize essentially the same range resolution, while the resolution for NLFM-1 is slightly lower.

For this experiment, the chirp rates for the flared edges of both cases of NLFM waveform are set to 80 MHz/μs. When mixed with the chirp rate of the LFM reference (50 MHz/μs), a signal

with a bandwidth of 60 MHz is produced. Thus, combined with the 100 MHz receive frequency band that realizes the 300 m range swath, the mixed products caused by the NLFM waveforms completely fill the analysis bandwidth of the RSA.

3.3.2 Simulation Results

The mixed frequency responses for all three waveforms for a hypothetical scatterer in the middle of the range swath are shown in Figure 3.12. The IF center frequency of 500 MHz corresponds to a range of 1050 m. It is useful to note that the LFM frequency response is the same as the LFM matched filter response, therefore it results in the highest peak. There is significant SNR loss for both cases of NLFM waveform, as well as a smearing effect on the sidelobes. In these circumstances, the NLFM-2 waveform performs somewhat better than the NLFM-1 waveform, due to the fact that it has an identical center chirp-rate to the LFM reference. Hence its mixing still produces a peak, but this peak is lower than the LFM case because of the mismatch at the flared edges. In contrast, there is no peak at all for the NLFM-1 case since its chirp-rates do not match the reference.

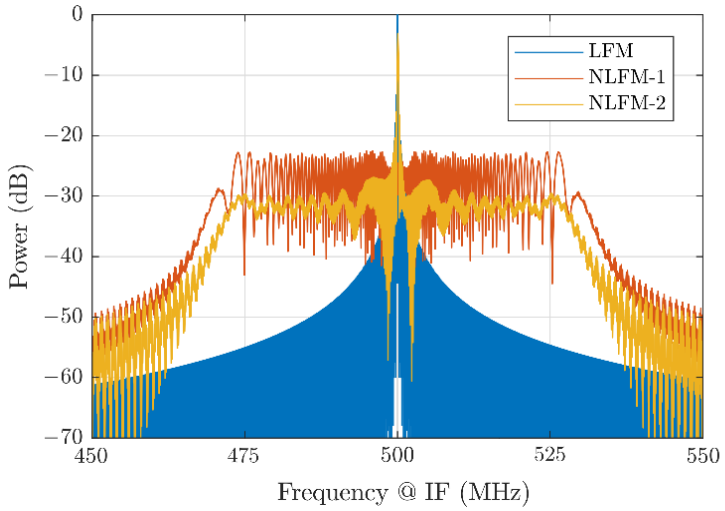

Figure 3.12: Mixed frequency responses for the three waveforms to a hypothetical scatterer at range 1050 m with application of the FFT (standard stretch processing).

However, when the appropriate compensation matrices are applied to the NLFM-1 and NLFM-2 waveforms instead of the FFT, the responses shown in Figure 3.13 are realized. Observing this result, it is important to again note that these NLFM waveforms were not selected for their sidelobe performance, which is slightly better than the LFM case close to the mainlobe, but with a slower roll-off further out (see Fig. 3.13 inset). Nevertheless, the important part about this result is that using chirp-like NLFM waveforms in combination with their appropriate compensation matrices enables the use of stretch processing. This capability is demonstrated experimentally using open-air measurements in the following section.

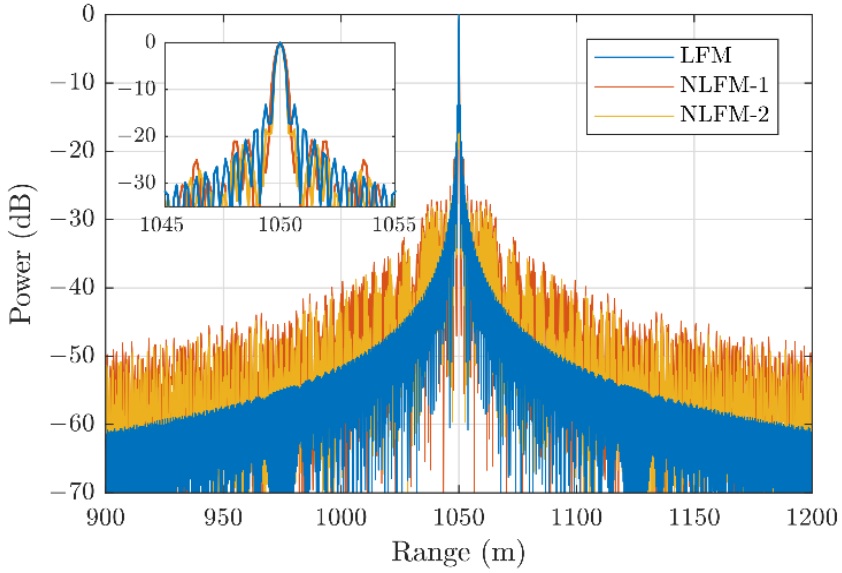

Figure 3.13: Mixed transform responses (frequency and compensation) for the three waveforms to a hypothetical scatterer at range 1050 meters

3.3.3 Experimental Results

The three waveforms, RF receive chain, and associated processing described in the previous sections are now considered in open-air measurements collected from the rooftop of Nichols Hall on the University of Kansas campus. 1000 pulses are coherently combined after stretch processing of

each waveform response (using either the FFT or compensation matrix as appropriate) for these results. The field of view and hardware instrumentation setup are depicted in Figures 3.14 & 3.15.

Figure 3.14: Field of view for open-air measurements with 12.3° antenna beam

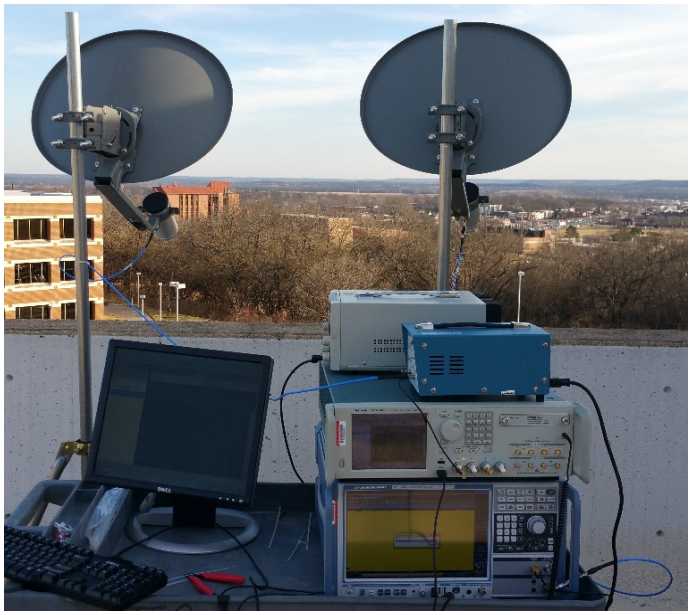

Figure 3.15: Hardware instrumentation setup for open-air measurements

The field of view contains the 300 m range swath centered at the intersection of 23rd street and Iowa street in Lawrence, KS, where there is a consistent flow of traffic. Two identical dish antennas with 12° beamwidth were used for separate transmit and receive as shown in Fig. 3.15.

Now, examining the zero-Doppler response for each waveform, Figures 3.16-3.18 represent the responses to the LFM, NLFM-1, and NLFM-2 waveforms, respectively. In Fig. 3.16, the baseline LFM case, there are multiple scatterers that can be observed. The dominant scatterer, near the

range 1050 m is believed to be from the building in the northwest corner of the intersection being illuminated. Similarly, figures 3.17(a) and 3.18(a) show the result of applying standard stretch processing, with an FFT as the final stage, to the NLFM waveforms. In the case of NLFM-1 (Fig. 3.17), there are no scatterers visible due to the complete lack of similar chirp rate. This follows from the results of the simulation (Fig. 3.12), where there was no visible peak as a result of mismatch. Conversely, for the NLFM-2 case in Fig. 3.18, the illuminated scatterers are visible, although there is a loss in SNR of approximately 2 dB due to the chirp-rate mismatch at the flared edges of the waveform.

On the other hand, Figs. 3.17(b) and 3.18(b) display the zero-Doppler response to the NLFM waveforms when their corresponding compensation matrices are applied. In both cases, all scatterers are clearly visible since the NLFM-LFM mixed products are actually being matched filtered. For the zero-Doppler responses, these results involving the compensated version of stretch processing for NLFM waveforms are qualitatively no different from the baseline LFM version.

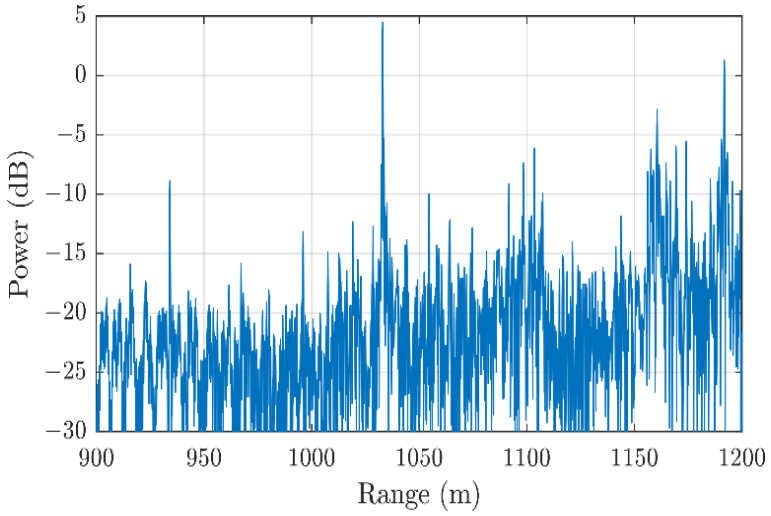

Figure 3.16: Zero-Doppler range profile for LFM using FFT processing

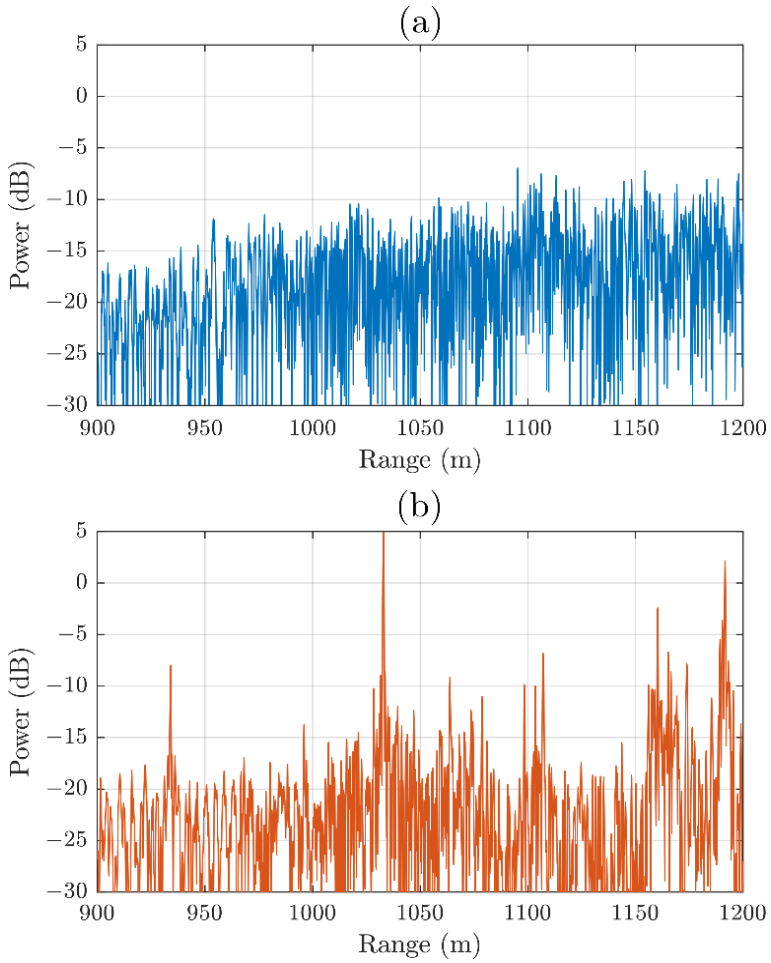

Figure 3.17: Zero-Doppler range profile for NLFM-1 using (a) FFT processing and (b) compensation matrix

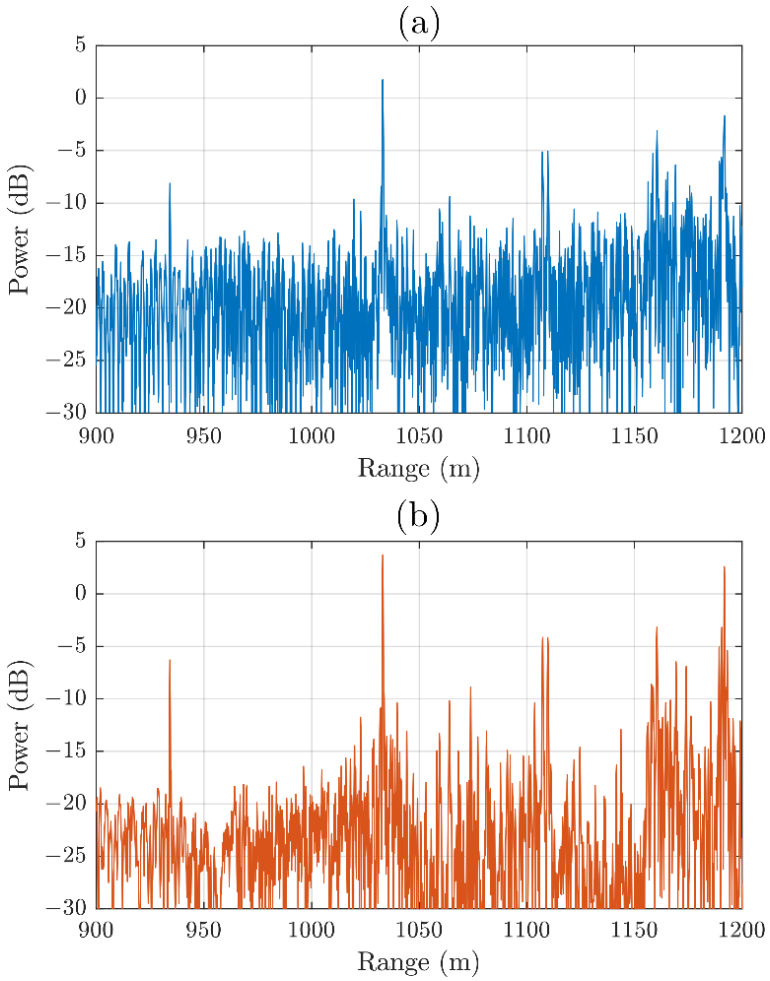

Figure 3.18: Zero-Doppler range profile for NLFM-2 using (a) FFT processing and (b) compensation matrix

Considering now the Doppler processing and clutter cancellation with the three waveforms, it is first necessary to note that separate waveform CPIs could not capture the exact same moving target scene. Clutter cancellation was performed using a simple zero-Doppler projection as a result of the instrumentation being stationary. The LFM is again used for a baseline to compare the results of both cases of NLFM against. The results of using standard stretch processing with an LFM are shown in Fig. 3.19. In this image, multiple vehicles are observed entering and leaving the intersection. The problem with trying to use standard FFT-based stretch processing is again illustrated in figures 3.20 and 3.21. The application of an FFT to both cases of NLFM yields SNR loss and smeared responses, that, again, depend on the degree to which the Fourier transform

provides a peak as shown in Fig. 3.12. However, the application of the appropriate compensation matrices to both NLFM-1 and NLFM-1 results in revealing the collections of moving targets in the scene. The usefulness of this approach has been verified experimentally, and points towards the potential for using a much wider array of waveforms for wideband radar applications. In the following sections, the use of an optimized waveform will be examined with the goal of achieving improved sidelobe responses.

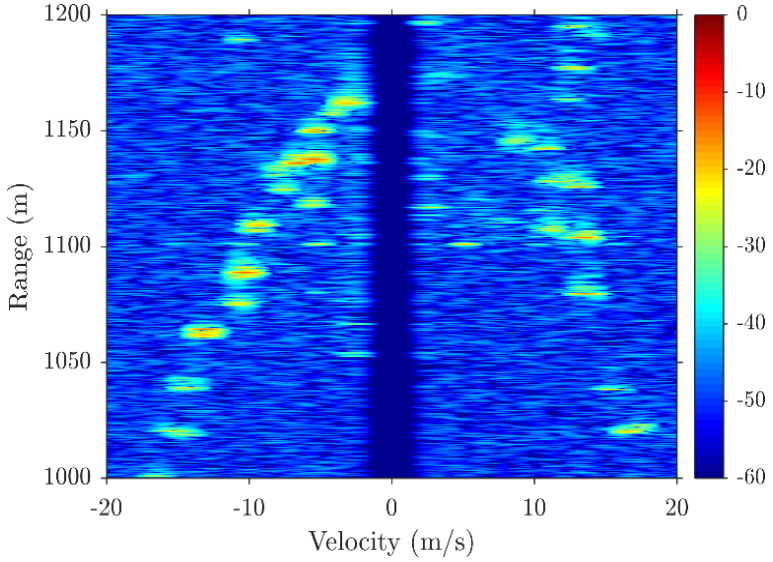

Figure 3.19: Range-Doppler response for LFM using FFT processing

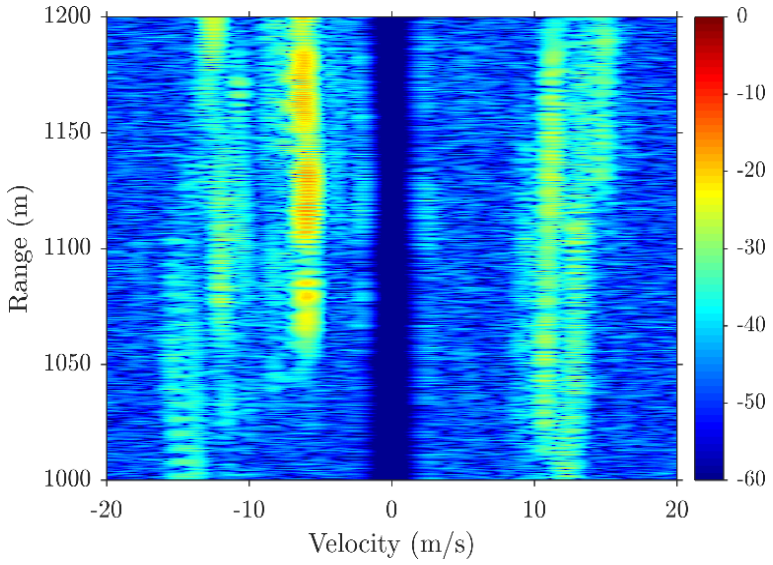

Figure 3.20: Range-Doppler response for NLFM-1 using FFT processing

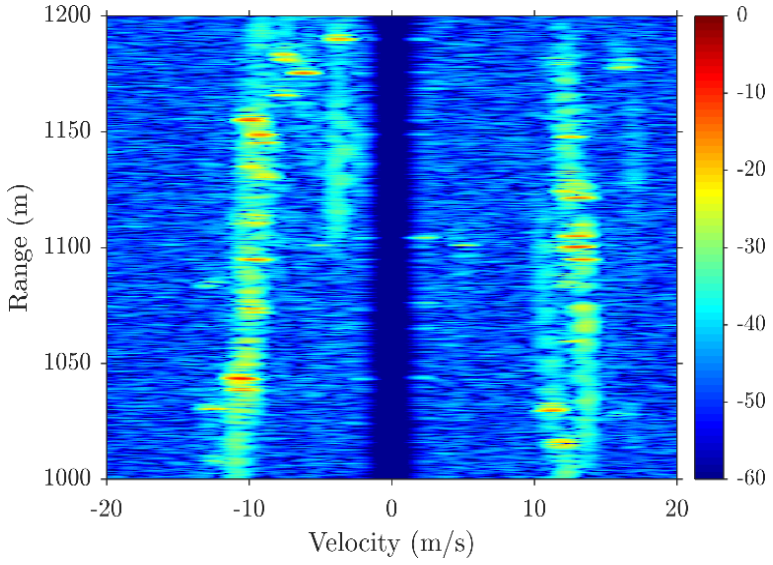

Figure 3.21: Range-Doppler response for NLFM-2 using FFT processing

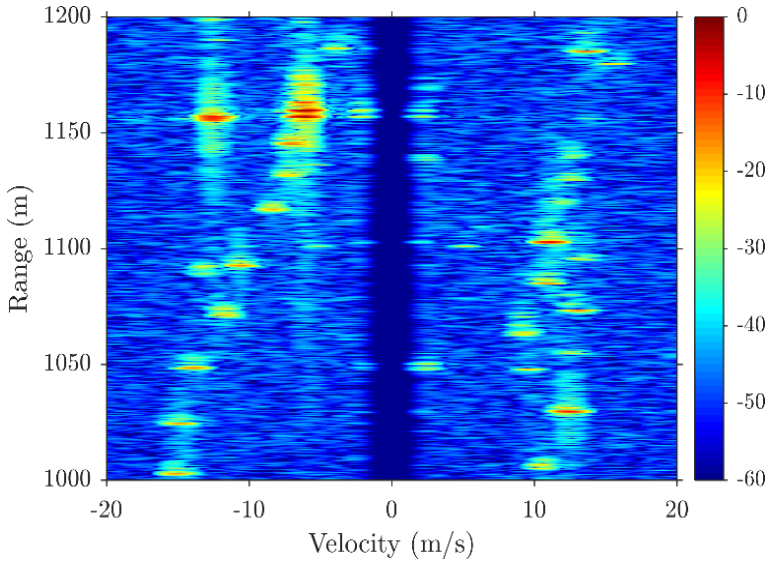

Figure 3.22: Range-Doppler response for NLFM-1 using the compensation matrix (same data as Fig. 3.20)

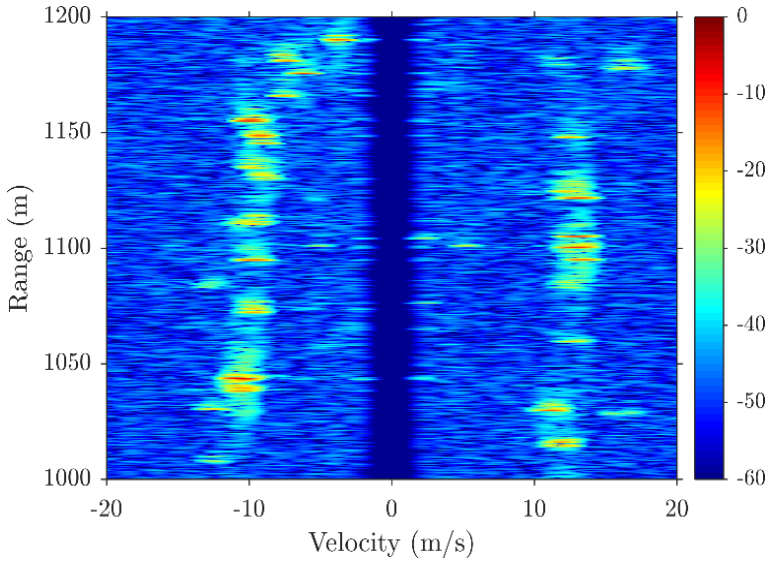

Figure 3.23: Range-Doppler response for NLFM-2 using the compensation matrix (same data as Fig. 3.21)

3.4 Waveform-Diverse Experimental Analysis: S-NLFM

As was seen in the comparison of the results from the use of piecewise NLFM with the achievable results using a matched filter, there is a need to optimize the waveform in order to obtain reduced sidelobes in the autocorrelation response. One common technique for reducing the sidelobes, that was discussed in detail in Section 2.3.1.1, is to use an S-NLFM for transmit because it is known to

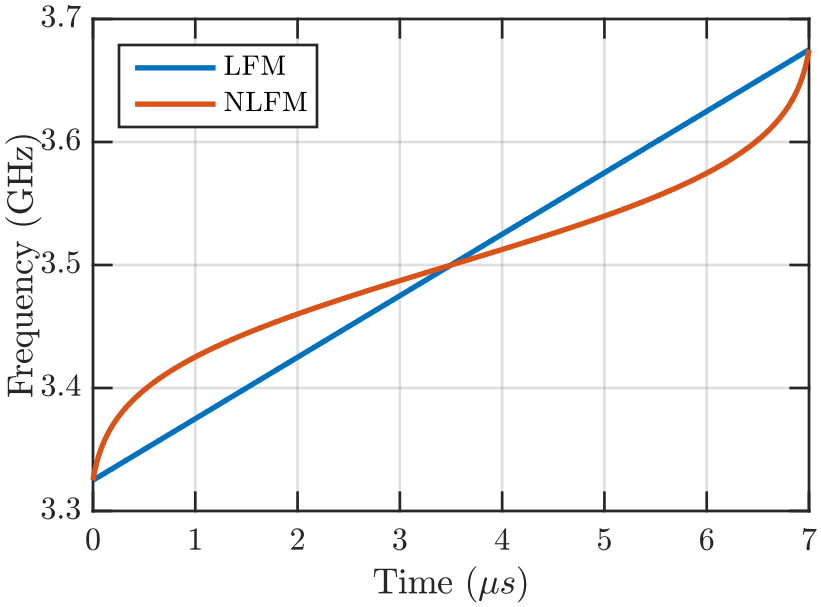

Figure 3.24: Time-Frequency structure of the two transmitted waveforms

have the capability to suppress sidelobes without significant loss in SNR or resolution.

The S-curve NLFM waveform that is used here is constructed using the Principle of Stationary Phase that was previously discussed, and is designed to traverse the same bandwidth as the LFM waveform that is used for a baseline. The pulsewidth of both waveforms is likewise the same, and the time-frequency relationship of these waveforms can be seen in Figure 3.24.

3.4.1 Experimental Setup

In this scenario, the transmit waveform has the same 350 MHz bandwidth as was previously used, and the pulse duration is also again 7μs. This time however, the waveform is an S-curve NLFM designed using the procedure outlined in Section 2.3.1.1. The time envelope is constant modulus (chosen to be able to operate amplifiers in saturation), and the frequency template that is used is a Gaussian (because ideally this produces zero sidelobe response). This frequency template, and the resulting spectral content are shown in Figure 3.25 Using these moduli to determine the phase responses results in an "S" shaped instantaneous frequency over the time duration of the waveform

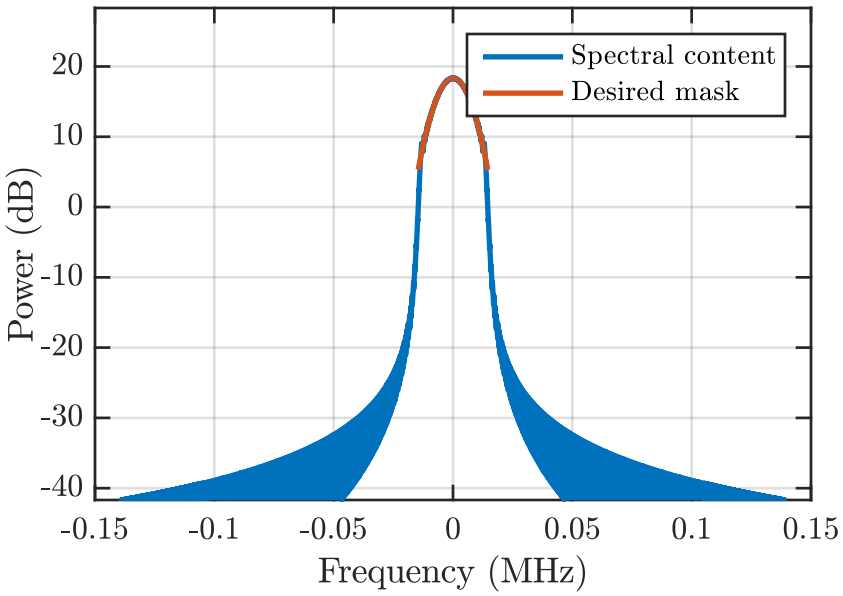

Figure 3.25: The spectral content of the S-NLFM waveform compared with the frequency template that was used to create it

(see to Fig. 3.24). A standard LFM transmit waveform will also be used to compare the results against, and the parameters of this waveform are identical to those used to gather the previous experimental data. The reference waveform in this scenario is the same as before, which means that the receive signal will be mixed down to an intermediate frequency of $f_{IF} = 500$ MHz. As before, the mixed products will be bandpass filtered, mixed down to baseband, and IQ sampled using an RSA. The receive processing will consist of applying both an FFT and the compensation matrix in order to compare the effectiveness in the new transmit waveform scenario. All other parameters of the test setup remain the same, and are summarized in Table 3.1.

ΔR	300 m	R_{near}	900 m	R_{far}	1200 m
$\Delta\tau$	2 μs	τ_{near}	6 μs	τ_{far}	8 μs
$f_{c,LFM}$	3.5 GHz	k_{LFM}	$50\frac{\text{MHz}}{\mu\text{s}}$	T_{LFM}	7μs
$f_{c,ref}$	4 GHz	k_{ref}	$50\frac{\text{MHz}}{\mu\text{s}}$	T_{ref}	9μs

Table 3.1: Table of relevant parameters of waveforms

The RSA has an analysis bandwidth of 160 MHz, however 100 MHz of that is still required for the receive frequency band of the downconverted receive signal. The mismatched mixing of the LFM reference (50 MHz/μs chirp rate) with the new NLFM waveform results in an additional bandwidth that is still small enough to be processed within this bandwidth.

3.4.2 Simulation Results

The following simulation is useful to demonstrate the ability of this compensation transform to provide detectability of targets, and to compare it against the results of applying standard FFT processing to a NLFM waveform used for stretch processing. In this simulation two different cases of transmit waveform and receive processing are implemented: an LFM waveform and an s-NLFM waveform are processed using both an FFT and a compensation transform. Both waveforms have a bandwidth of 350 MHz and pulse durations of 7 μs, and are convolved with a scene having multiple scatterers at a range of different powers. The resulting received signals (one from the LFM and another from the s-NLMF) are mixed with a reference chirp with a bandwidth of 450 MHz and pulse duration 9 μs. This reference chirp has a chirp rate that is identical to the LFM transmit waveform, specifically 50 MHz/μs.

The simulated range profiles shown in Figures 3.26 and 3.27 both contain the same 13 scatterers that are randomly distributed in range with reflected powers that are assigned at random from a uniform distribution on $[-40\text{dB},\ 0\text{dB}]$. The application of FFT processing after stretch processing of both received waveforms results in an inability to detect any of the scatterers in the case of the s-NLFM waveform, as shown in Fig. 3.26. If the compensation matrix is instead applied to each waveform (recall that the compensation matrix for an LFM is the FFT) these scatterers become visible in the case of the s-NLFM waveform, and are in fact more easily distinguishable because of the improved sidelobe suppression that is characteristic of the s-NLFM waveform structure.

In order to provide a theoretical baseline for the compensation that will occur in the open-air experimental results section that follows, the frequency responses after the first mixing stage of the receive processing chain are shown in Figure 3.28. This result assumes a hypothetical scatterer

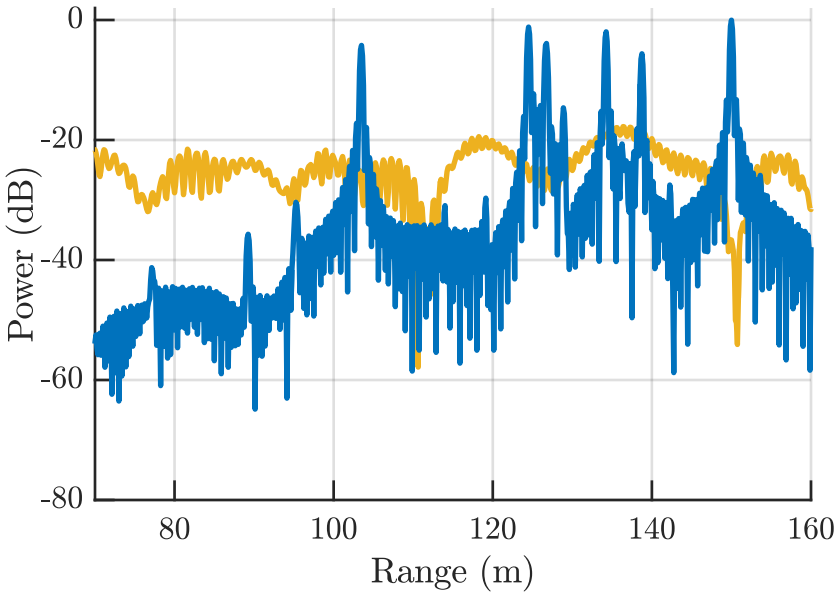

Figure 3.26: Simulated range profile for standard stretch processing of an LFM (blue) and an s-NLFM (yellow)

in the center of the range swath. Due to the identical setup of this simulation to the simulation that was shown in Section 3.3.2, the received signals are likewise mixed down to the intermediate frequency of 500 MHz, which corresponds to a range of 1050 m.

As in the previous NLFM waveform simulation (for the piecewise NLFM waveforms), the LFM frequency response is the same as the LFM matched filter response, meaning it results in the highest peak. For the NLFM waveform, there is significant loss in SNR, and the smearing effect on the sidelobes is again evident as a result of the fact that the DFT matrix is not a matched filter bank for stretch processed receive waveform. As expected, there is no peak for this case of NLFM waveform due to the lack of chirp rate match between the receive waveform and the LFM reference.

Yet, when the compensation matrix is generated for and applied in place of the DFT matrix, the smearing effect on the sidelobes of the NLFM response is diminished.

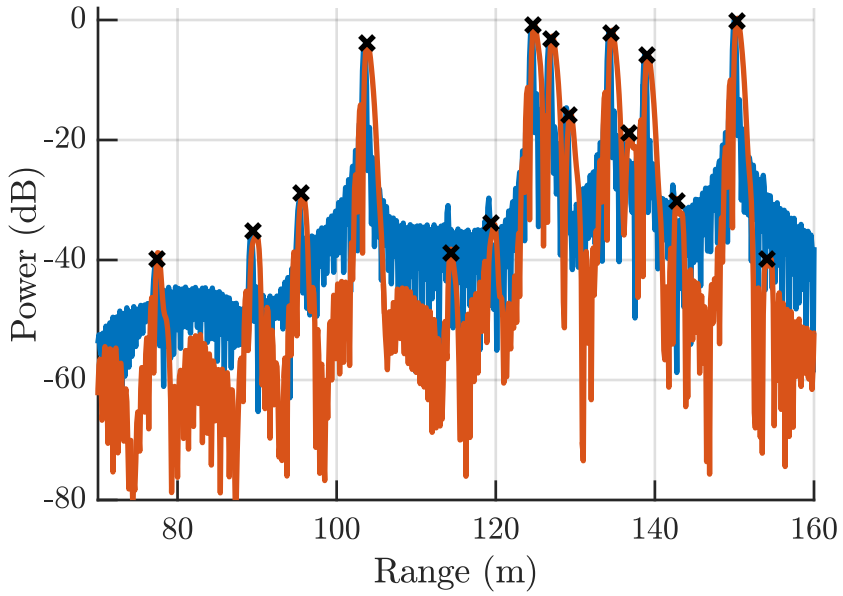

Figure 3.27: Simulated range profile for the use of a compensation matrix stretch processing framework of an LFM (blue) and an s-NLFM (yellow)

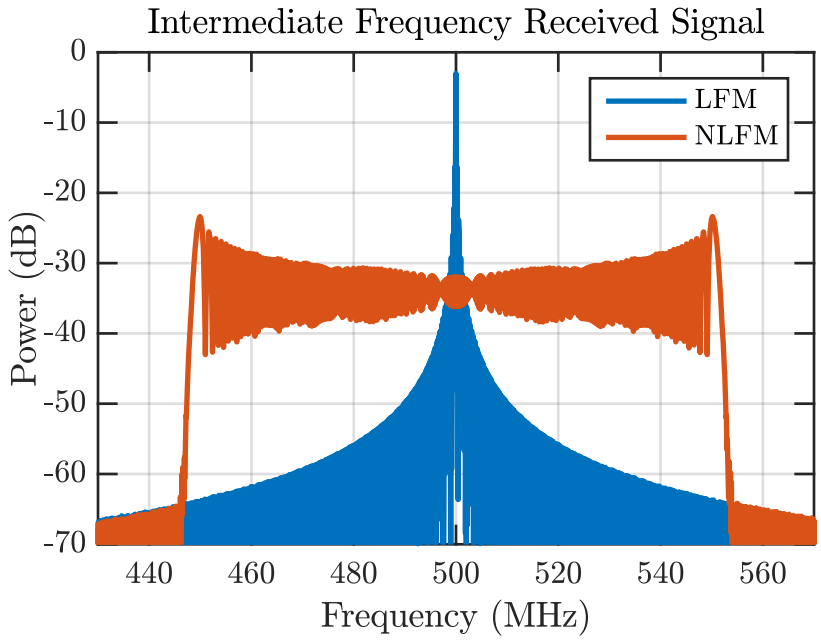

Figure 3.28: Mixed frequency responses for an LFM and S-curve NLFM waveform to a hypothetical scatterer at range 1050 m using an FFT for receive processing (standard stretch processing).

3.4.3 Experimental Results

The new waveform detailed in the previous section and the associated RF receive chain and processing described in earlier sections are used again here for open-air measurements (collected from the rooftop of Nichols hall). 1000 pulses are coherently combined after stretch processing of the waveform using either the traditional FFT processing or the compensation matrix for the results that are discussed here. The field of view and hardware can be seen in Figures 3.14 & 3.15 in Section 3.3.

The same 12° dish antennas are used for transmit and receive. The waveforms are sent out to collect returns from the 23rd street intersection mentioned in the previous experimental results section. The field of view being illuminated has a 300 m range swath which corresponds to a 2 μs delay swath.

The zero-Doppler responses for the s-NLFM waveform is shown in Figures 3.29 and 3.30. The result of applying the FFT matrix is seen in Fig. 3.29, and it is clear that the application of the FFT in this case does not apply the appropriate bank of matched filters to the received waveform, thus causing significant enough loss in SNR as to make the targets in the scene undetectable. This case of transmit waveform is similar to the NLFM-1 waveform used in the previous section in that its chirp rate does not match the reference chirp rate at any point. However when the compensation matrix is used in place of the FFT the scatterers present in the range swath being illuminated become visible as a result of properly match filtering the NLFM-LFM mixer products, as depicted in Fig. 3.30. The dominant scatterer in this scene is believed to be from a building in the northwest corner of the intersection.

Because the illuminated scene consisted of an intersection, data collection intervals could be timed to coincide with green lights in the North-South direction of traffic in order to be able to obtain the movement of the cars for Doppler processing. These range-Doppler results are also processed using both an FFT and a compensation matrix, and can be seen in Figures 3.31 and 3.32. The FFT processing in this case of transmit waveform results in the same smearing effect across the range sidelobes as was seen in both cases of piecewise NLFM waveform. The targets

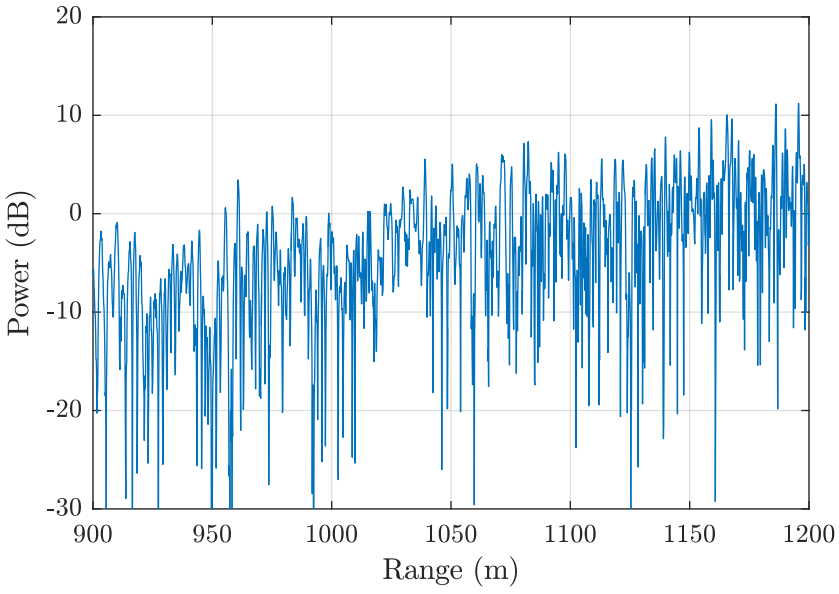

Figure 3.29: Zero-Doppler range profile for s-NLFM waveform using traditional FFT processing

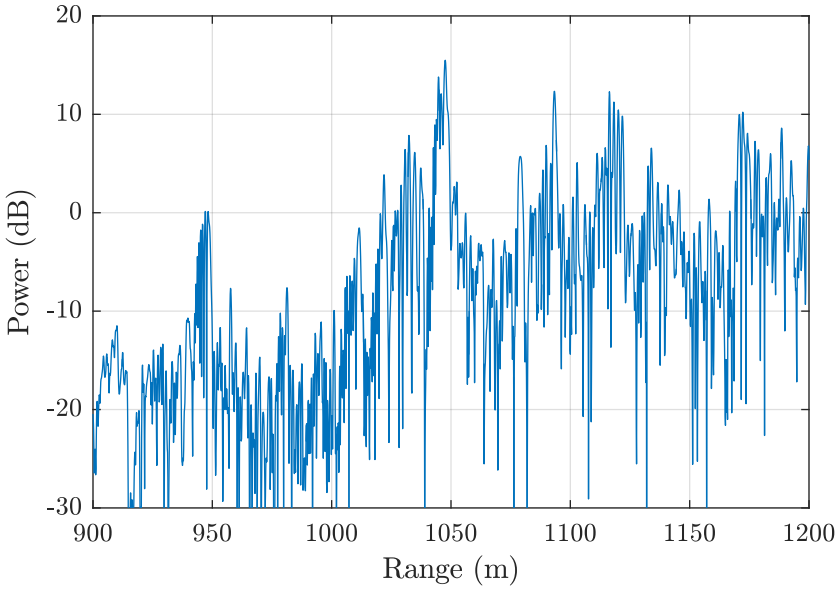

Figure 3.30: Zero-Doppler range profile for s-NLFM waveform using the compensation matrix in place of an FFT

in Fig. 3.31 are undetectable due in part to this effect as well as the SNR loss that results. Once the compensation matrix has been applied in place of the FFT the targets become clearly visible because the mismatch effect of FFT-processing has been addressed. In this case, the expected advantage of the s-NLFM waveform is apparent in the amount of sidelobe suppression that is apparent in this range-Doppler map. The targets in this test setup are easily distinguishable when a compensation matrix is used for pulse compression of the stretch processed data.

When considering the Doppler processing and clutter cancellation using these two waveforms it is important to again note that clutter cancellation was performed using a simple zero-Doppler projection. This type of cancellation can be used due to the fact that the instrumentation is stationary.

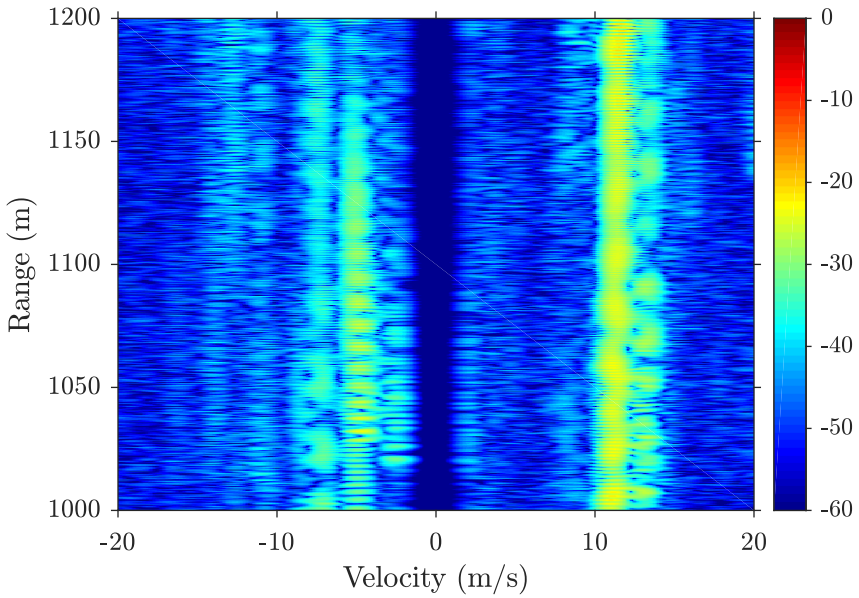

Figure 3.31: Range-Doppler response for the s-NLFM waveform using FFT processing

Because the motivation behind the use of this waveform was to achieve improved sidelobe suppression relative to what is achievable by a matched filter, it is important to examine these results by comparing them with what was achieved using the piecewise NLFM waveforms from Section 3.3. Comparison of the range-Doppler responses post application of an appropriate compensation

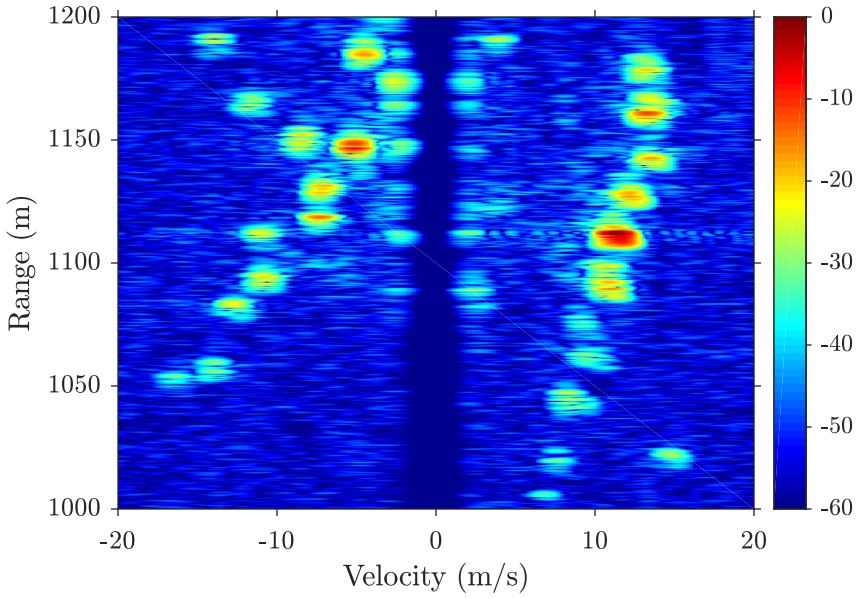

Figure 3.32: Range-Doppler response for the s-NLFM waveform using the compensation matrix

matrix exhibits the advantage that is inherent in the structure of the s-NLFM waveform. It proves to be a more optimal choice of waveform under the goal of achieving suppressed range sidelobes. The targets in Fig. 3.32 are much more separated from one another than are those of the piecewise NLFM waveforms in Figs. 3.22 & 3.23.

Chapter 4

Stretch Processing Mismatch Filtering

As was discussed in section 2.7, stretch processing traditionally performs matched filtering using a matched filter bank for the LFM transmit waveform mixed with an LFM reference. Here we consider the concept of replacing this matched filter bank approach with a least-squares based mismatched filtering technique that can be used in place of the Fourier transform (that is the conventional final step of a stretch processing setup). The reason for using this type of filter is that it has the advantage of minimizing both peak and integrated sidelobes. Though there is a trade off for this in the form of a degree of mainlobe mismatch loss. As a first step towards developing this technique, the optimal mismatch filter will be employed for the traditional case of stretch processing: an LFM transmit waveform with an identical chirp rate to the reference (as in [26]). This technique, while discussed here with experimental results, has been verified in [39]. After the technique has been established for the conventional transmit waveform, the results of modifying the transmit waveform will be explored. The modifications that will be made to the waveform are identical to those discussed in Chapter 3.

4.1 Derivation

The least-squares (LS) mismatch filter was proposed in [25] for phase-coded waveforms, and recently it has been extended to apply to arbitrary FM waveforms ([26, 40, 41]). To be applied to arbitrary FM waveforms, there is a requirement for the waveform to be over-sampled relative to the waveform's 3-dB bandwidth. This ensures that the model mismatch effects are minimized because they would otherwise limit the sidelobe suppression and create range straddling effects. However,

it is important to be careful to not impose a range super-resolution condition [42] because this will cause increased sidelobes as a trade-off for the improved resolution. To correct for this effect it is possible to "spoil" the mainlobe such that it results in the nominal resolution of the matched filter. When these factors are considered for, the mismatched filter yields significant sidelobe suppression with minimal mismatch loss (a fraction of a dB). Another advantage of this filter is that the resolution is not degraded as a result of its use.

The analog receive model in 2.30 is sampled just as before and represented as the vector in 2.35 ($\mathbf{y} = [y(\tau_{\text{near}}) \quad y(\tau_{\text{near}} + T_{\text{s}}) \quad \cdots \quad y(\tau_{\text{near}} + (L-1)T_{\text{s}})]^T$), which can also be represented using the $L \times N$ compensation matrix $\mathbf{W}$ as it was defined in section 3.1. The columns of this matrix represent the structure of the expected signals within the range interval and are modeled as

$$\mathbf{y} = \mathbf{W}\mathbf{x} + \mathbf{u} \tag{4.1}$$

where $\mathbf{x}$ is the same previously mentioned vector of the scattering between R_{near} and R_{far}, and $\mathbf{u}$ is a length L vector of additive noise at the output of the ADC. Both $\mathbf{W}$ and $\mathbf{x}$ are over-sampled by a factor of K relative to the nominal range resolution that is associated with the bandwidth of the transmit LFM. Using these, we can now define the $N \times N$ matrix $\mathbf{D}$ as

$$\mathbf{D} = \left(\mathbf{W}^H \mathbf{W}\right) \odot \mathbf{E} \tag{4.2}$$

with $\mathbf{E}$ an $N \times N$ banded Toeplitz matrix that has ones along the main diagonal as well as the $K-1$

diagonals above and below the main diagonal, and zeros everywhere else, as shown in 4.3.

$$\mathbf{E} = \begin{bmatrix} E_{1,1} & \cdots & E_{1,K-1} & 0 & \cdots & \cdots & 0 \\ \vdots & E_{2,2} & & \ddots & 0 & & \vdots \\ E_{K-1,1} & & \ddots & & \ddots & 0 & \vdots \\ 0 & \ddots & & \ddots & & \ddots & 0 \\ \vdots & 0 & \ddots & & \ddots & & E_{N-K+1,N} \\ \vdots & & 0 & \ddots & & \ddots & \vdots \\ 0 & \cdots & \cdots & 0 & E_{N,N-K+1} & \cdots & E_{N,N} \end{bmatrix}. \tag{4.3}$$

The matrix $\mathbf{D}$ results in $2K-1$ non-zero valued diagonals which represent the entire mainlobe response. Because of the over-sampling that has been applied, a super-resolution effect will be avoided.

Equation 4.2 can be used to obtain the $L \times N$ mismatched filter bank by solving the least-squares cost function

$$J_{\mathrm{LS}} = \left\| \mathbf{W}_{\mathrm{MMF}}^{H} \mathbf{W} - \mathbf{D} \right\|_{F}^{2} \tag{4.4}$$

where $\|\bullet\|_F$ is the Frobenius norm. This cost function can be rewritten as

$$\left\| \mathbf{W}_{\mathrm{MMF}}^{H} \mathbf{W} - \mathbf{D} \right\|_{F}^{2} = \mathrm{Tr}\left\{ \mathbf{W}_{\mathrm{MMF}}^{H} \mathbf{W} \mathbf{W}^{H} \mathbf{W}_{\mathrm{MMF}} \right\} - \mathrm{Tr}\left\{ \mathbf{W}_{\mathrm{MMF}}^{H} \mathbf{W} \mathbf{D}^{H} \right\} - \mathrm{Tr}\left\{ \mathbf{D} \mathbf{W}_{\mathrm{MMF}} \mathbf{W}^{H} \right\} + \mathrm{Tr}\left\{ \mathbf{D} \mathbf{D}^{H} \right\}, \tag{4.5}$$

where $\mathrm{Tr}\{\bullet\}$ is the trace of a matrix. Thus, the result of taking the gradient of this cost function is

$$\nabla_{\mathbf{W}_{\mathrm{MMF}}^{*}} J_{\mathrm{LS}} = \mathbf{W} \mathbf{W}^{H} \mathbf{W}_{\mathrm{MMF}} - \mathbf{W} \mathbf{D}^{H}. \tag{4.6}$$

The mismatch filter bank can now be determined by setting 4.6 equal to $\mathbf{0}_{L \times N}$ and solving for $\mathbf{W}_{\mathrm{MMF}}$. The solution of which is

$$\mathbf{W}_{\mathrm{MMF}} = \left(\mathbf{W} \mathbf{W}^{H} \right)^{-1} \mathbf{W} \mathbf{D}^{H}. \tag{4.7}$$

The mismatched filter bank can be diagonally loaded to avoid any potential ill-conditioning effects, resulting in

$$\mathbf{W}_{\text{MMF}} = \left(\mathbf{W}\mathbf{W}^H + \delta \mathbf{I}_{L\times L}\right)^{-1} \mathbf{W}\mathbf{D}^H \tag{4.8}$$

where δ is a positive scalar value and $\mathbf{I}_{L\times L}$ is a square identity matrix.

Now that the mismatched filter bank has been derived, it can be applied to the received data vector $\mathbf{y}$ (2.35) as

$$\hat{\mathbf{x}}_{\text{MMF}} = \mathbf{W}_{\text{MMF}}^H \mathbf{y} = \mathbf{D}\mathbf{W}^H \left(\mathbf{W}\mathbf{W}^H + \delta \mathbf{I}_{L\times L}\right)^{-1} \mathbf{y}, \tag{4.9}$$

which is the desired mismatched filter estimate of the range profile of interest. This range profile estimate will have range sidelobes which are significantly suppressed relative to those of the matched filter estimate, but will preserve the range resolution and only induce a small amount of mismatch loss.

4.2 Simulation Results

The effectiveness of the mismatched filter will be compared against the standard matched filter as it is a useful metric to compare against for any receive processing techniques due to its well known performance in terms of sidelobe responses and SNR. It will also be compared with the compensation matrix technique to determine whether there are any additional benefits or disadvantages to using one or the other. The waveforms that are used in the following simulations are identical to those in Sect. 3.1.1, but the transmit waveforms are shown again here for ease of reference.

4.2.1 Comparison of Mismatched Filter with other techniques

The simulations discussed here are useful to examine how effective these processing techniques are as the transmit waveform deviates by varying degrees from an LFM waveform. The comparison between various alternative techniques for stretch processing that was discussed in Section 3.1.1 will be explored here, but now with the addition of the results of applying a mismatched filter in

place of the previously examined receive processing techniques. The following results will include the use of matched filtering, application of a compensation matrix, and mismatched filtering for three cases of transmit waveforms. An LFM chirp is used to show the baseline to analyze the effectiveness of each technique.

The first case of transmit waveform is the piecewise NLFM, which is shown again here in Figure 4.1(a) for convenience. The results of the three different processing techniques applied to this waveform are shown in Fig. 4.1(b). The blue trace is the baseline case (LFM-FFT) and the orange trace is the matched filter applied to the NLFM waveform. As before, there is not much distinction between the NLFM and LFM waveform responses using the matched filter because the deviation in the NLFM waveform from a standard LFM waveform is not large. As expected, the sidelobes of the NLFM-MMF response are significantly lower (approximately 20 dB) than the matched filter response, and approximately 15 dB lower than the compensation matrix response. This result is not surprising due to the fact that mismatched filters are well known to provide these levels of sidelobe reduction. It is also important to note that there is a negligible effect from the mismatch loss on the resolution of the mainlobe.

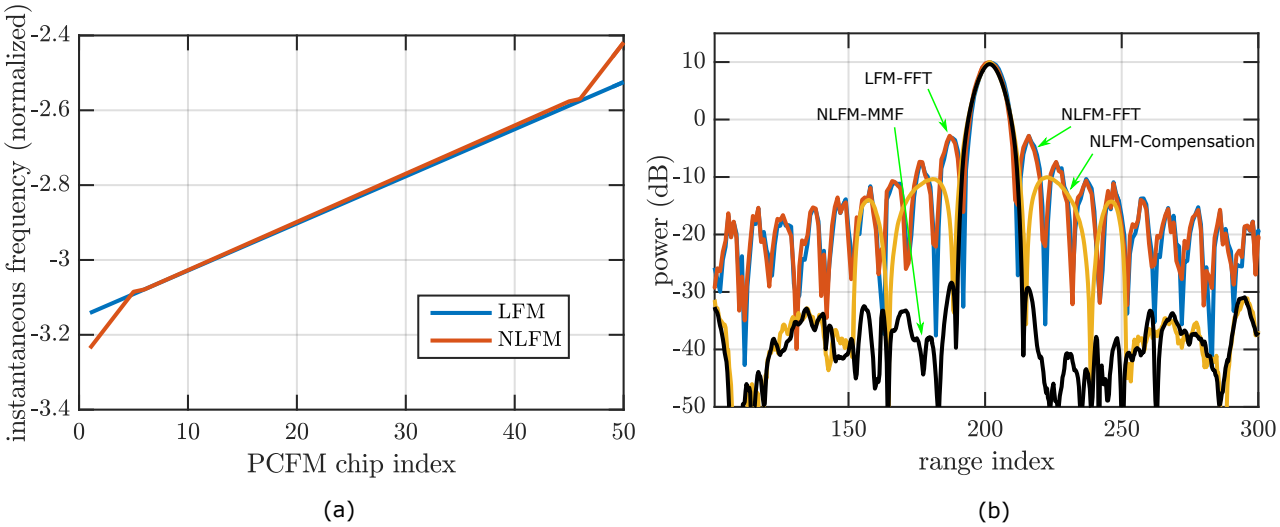

Figure 4.1: Comparison of MF, compensation matrix, and MMF

For the second case to examine, another piecewise NLFM waveform is used; however this time

with more significant variation in its chirp rates relative to the reference. The transmit waveforms are shown in Figure 4.2, along with the range responses after stretch processing and receive filtering are completed. These results provide information on how the effectiveness of these techniques changes as the transmit waveform deviates farther from an LFM. It is clear that as the transmit waveform becomes less similar to an LFM the MF and compensation matrix are not as robust as the MMF.

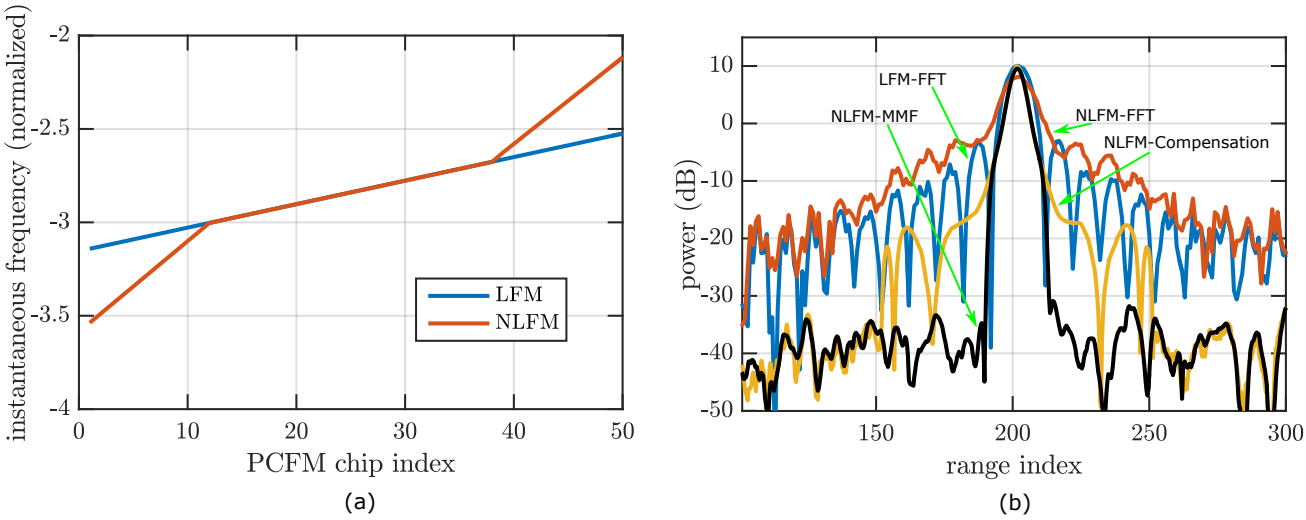

Figure 4.2: Comparison of MF, compensation matrix, and MMF

For the third case in this comparison of the usefulness of a mismatched filter versus other techniques developed, the NLFM transmit waveform is now an LFM that has a chirp rate that is mismatched to the reference waveform (see Fig. 4.3(a)). As was already seen, this case causes an inability to accurately detect the range of a scatterer when the receive processing consists of a matched filter. However, because the mismatched filter is derived using the compensation matrix, the inaccuracy in detection of range is corrected for and the target is detectable after applying the MMF. This is due to the fact that a bank of matched filters relative to the new transmit waveform and the known delay swath being observed can be formed. Once more, the sidelobes of the MMF response are more than 20 dB below what is achievable using either the matched filter or compensation matrix, and there is negligible effect on the mainlobe as a result of the mismatch loss that is

induced in applying the MMF.

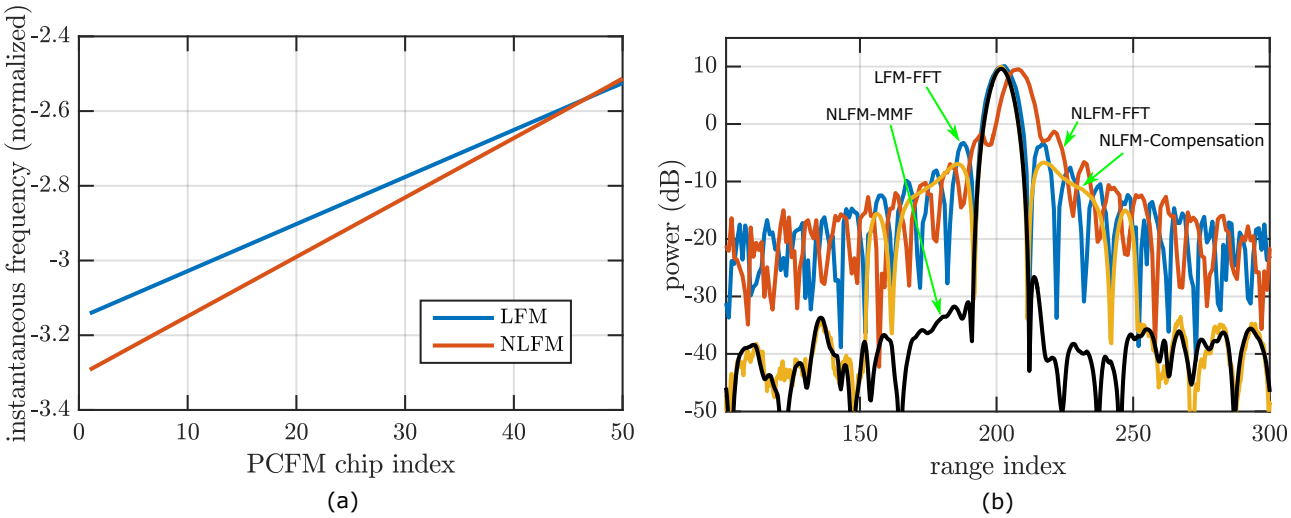

Figure 4.3: Comparison of MF, compensation matrix, and MMF

4.3 Experimental Results: Transmit LFM

Open-air measurements were conducted using parameters identical to those that are outlined in detail in Section 3.3.1. The same LFM and reference waveform are used in the following results, as well as an identical hardware setup and range swath of interest. This is done in order to make straightforward comparisons between the performance of the mismatched filter against previous metrics. The results of this test setup can be seen in Figure 4.4, where a comparison between the matched filter response is plotted along with the results of instead applying the MMF.

The mismatched filter provides about 10-15 dB of sidelobe suppression, which can more easily be seen when the peaks are looked at over smaller range intervals (as in the inset of Fig. 4.4). There is only a small fraction of a dB of mismatch loss suffered in this case, which has a negligible effect on the resolution.

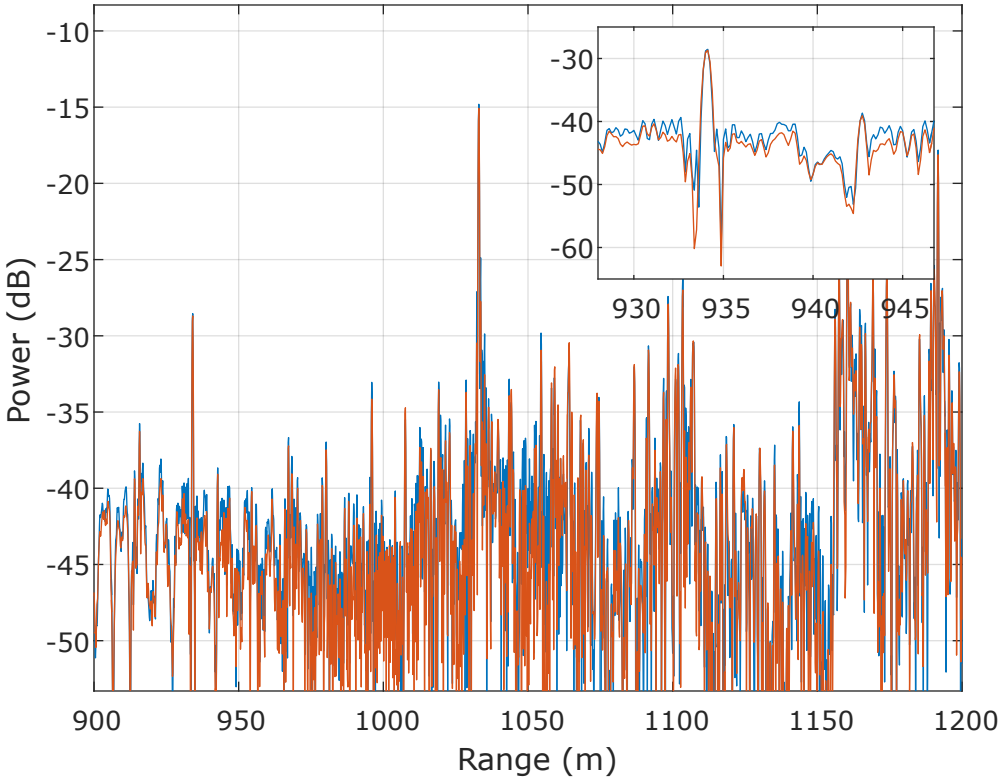

Figure 4.4: Zero-Doppler range profile comparison for an LFM transmit waveform using a matched filter (blue) and a mismatched filter (orange). The inset displays a magnification around the peak near 1030 m in range

4.4 Experimental Results: Transmit NLFM

When the mismatched filters are generated from the corresponding compensation matrices (which are essentially matched filter banks) for each piecwise NLFM waveform and applied to the received data, the outcome is similar to what was shown in the previous section regarding the traditional LFM waveform. For specific waveform parameters refer to Sect. 3.3. In this instance, there is also a reduction in the levels of the sidelobes while suffering only minimal effects on the resolution as a result of mismatch loss. The resulting range profile after application of the filter banks (matched and mismatched) to the case using the NLFM-1 waveform are shown in Figure 4.5. The range profile for the case using the NLFM-2 waveform can be seen in Figure 4.6.

When these results are compared with the results in Fig.4.4 it is clear that the mismatched filter

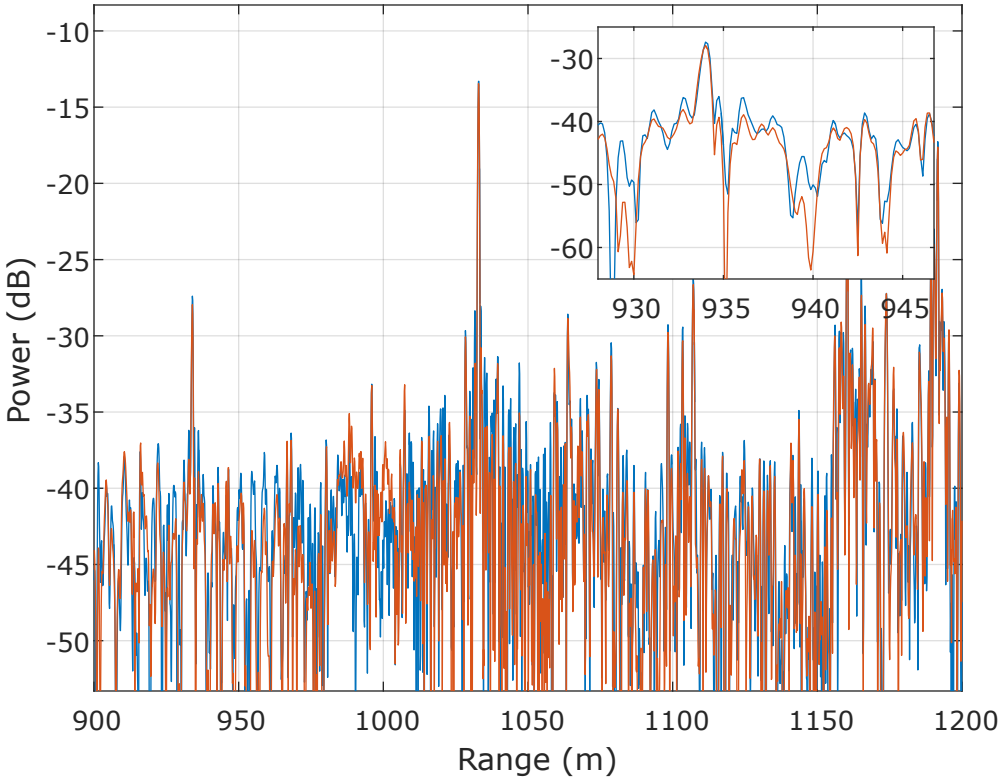

Figure 4.5: Zero-Doppler range profile comparison for the NLFM-1 transmit waveform using a matched filter (blue) and a mismatched filter (orange)

performs well in terms of range resolution, and is able to account for waveforms other than an LFM. Likewise, this filter is still able to provide greater sidelobe suppression than the matched filter, even using NLFM waveforms that introduce a mismatch effect requiring compensation.

While the results of these cases of transmit waveform already surpass the sidelobe suppression that is achievable using matched filtering, it is useful to investigate whether this could be increased. Thus, the mismatched filtering technique will be applied to a waveform that is well-known for its ability to produce low range sidelobes: the s-NLFM waveform. A similar test setup is used for this final case of transmit waveform, and the resulting range profile can be seen in Figure 4.7.

Based on the zero-Doppler plots, there does not appear to be a significant advantage in using the mismatched filter in place of the matched filter with the s-NLFM waveform. Examination of the range-Doppler map leads to the same conclusion, although While the results are not easily

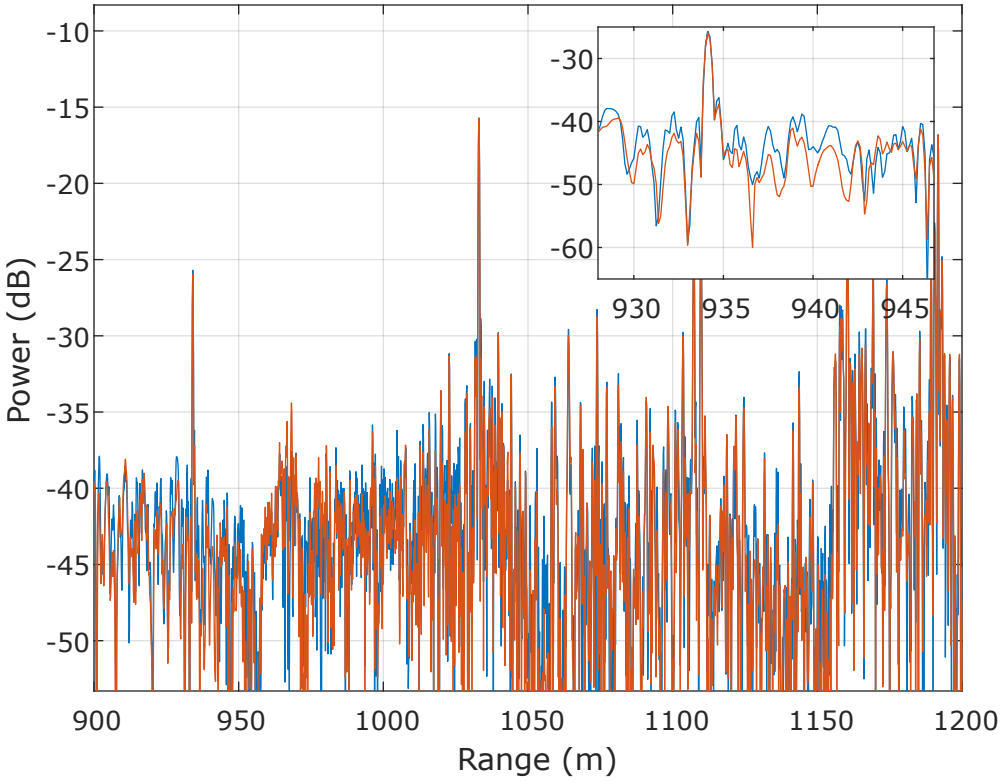

Figure 4.6: Zero-Doppler range profile comparison for the NLFM-2 transmit waveform using a matched filter (blue) and a mismatched filter (orange)

discernible in either of these figures, there is a small amount of improvement in the range-Doppler plot (fig. 4.8) using the MMF. However, the amount of additional sidelobe suppression in this case is not significant enough to argue that the use of an s-NLFM waveform combined with MMF receive processing is useful.

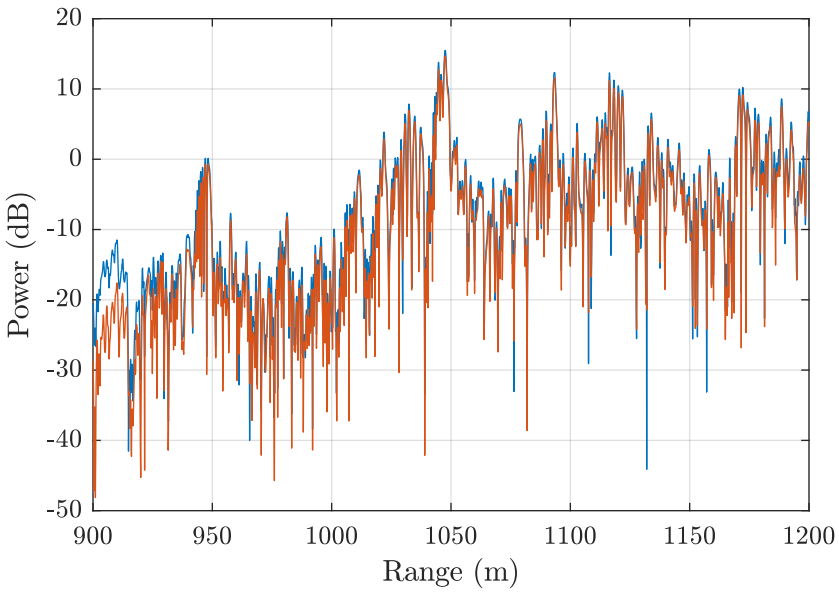

Figure 4.7: Zero-Doppler range profile comparison for the s-NLFM transmit waveform using a matched filter (blue) and a mismatched filter (orange)

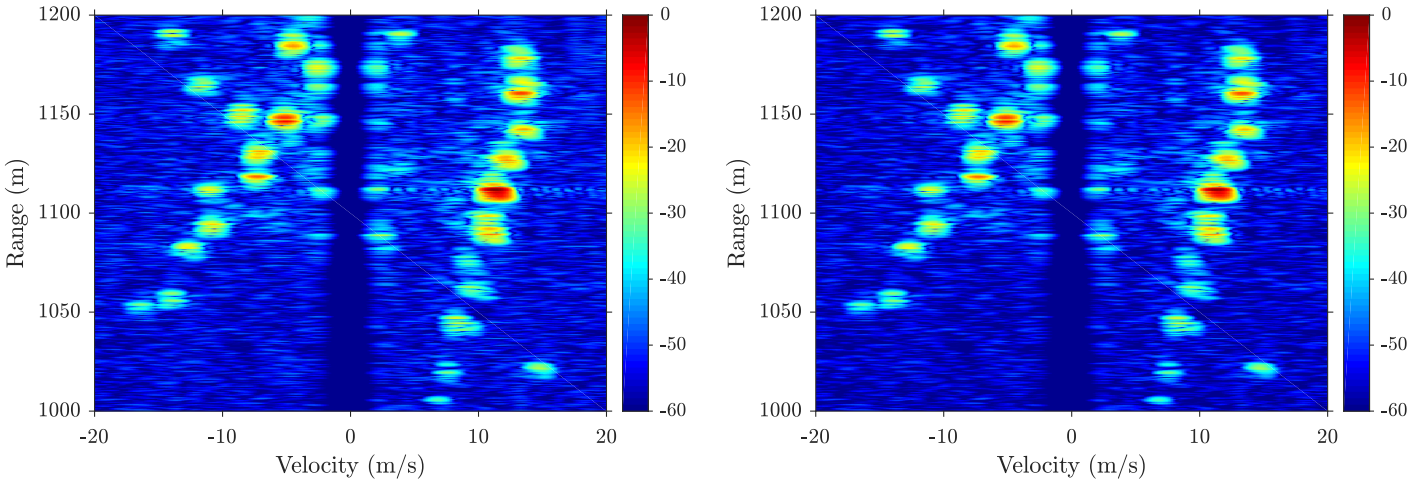

Figure 4.8: The left figure is the range-Doppler map using the compensation matrix for reference. The image on the right is the range-Doppler map resulting from the use of the MMF

Chapter 5

Conclusions

Chirp-like nonlinear FM waveforms can be used with stretch processing, with the requirement that a compensation matrix be used to realize the appropriate matched filter bank in place of the FFT that has been the standard previously. This new matched filter bank is similar to the DFT (from which the FFT is derived) with the difference that the matched filters are now generated for the NLFM-LFM mixed products as opposed to LFM-LFM products. Therefore the matrix still has a frequency-shifted structure across the columns. It is also necessary to consider the additional sampling bandwidth that results from the mismatched mixing of a nonlinear waveform and the reference LFM on receive. This additional bandwidth requirement is based on the maximum difference in instantaneous chirp rate between the NLFM waveform and the reference chirp, so it is application dependent as to whether it remains a useful option with the additional bandwidth that is incurred as a result of this. This technique of generating a compensation matrix based upon an NLFM transmit waveform has been experimentally demonstrated, and thus enables the use of optimized and/or diverse, wideband NLFM waveforms such as the s-curve NLFM waveform. The use of this type of waveform was also experimentally demonstrated and achieved the expected improvement in sidelobe suppression that this type of waveform is known to offer without incurring a loss in SNR or degradation in resolution.

Further, the generalization to chirp-like NLFM waveforms facilitates the development of an optimal mismatch filter bank derived from a least-squares based formulation. This filter bank, when generated using the compensation matrix, provides another alternate processing technique, and provides more sidelobe suppression than the compensation matrix alone. Moreover, there is negligible impact on the achievable resolution, nor is there a significant amount of mismatch loss

incurred as a result of mismatched filtering.

This new category of waveforms, in combination with the proposed filtering schemes, opens up new avenues of research for wideband waveform diversity that could be applicable to legacy radar systems that already rely on stretch processing. Furthermore, the addition of this compensation technique also provides greater design freedom for applications relying on wideband radar systems to achieve fine range resolution. There is also the potential for optimizing the reference waveform such that the additional bandwidth requirement is minimized, and further research into that topic can enhance the benefits already provided through this technique. The inherent consequence of modifying the transmit waveform is higher receive processing bandwidths, but if the reference waveform can be optimized based on a desired transmit waveform then the necessary additional bandwidth can be minimized.

The usefulness of these proposed changes to stretch processing in its original form is application dependent as to whether this bandwidth increase is tolerable. The need for an alternative waveform and/or higher levels of sidelobe suppression will have to be weighed against the ability to handle wider bandwidths in the receive processing architecture.

Appendix A

Waveform Diverse Stretch Processing Analysis

This section will provide a mathematical baseline of the waveform diverse stretch processing procedure by walking through the implementation in mathematical detail. As in the analysis that is contained in Section 2.6.3, a heterodyne (two mixing stages) representation of a receiver is used in this analysis.

A.0.1 Transmit Waveform

For this mathematical analysis, we will consider an NLFM waveform that is defined by its mismatched chirp rate, denoted $\tilde{B}$, relative to the reference waveform with a chirp rate B. The first few stages of this process are nearly identical to standard stretch processing; the waveform, centered at intermediate frequency f_1, is mixed up to RF with the only difference in this case being the chirp rate $\tilde{B}$ appearing in the expression for the transmit signal at IF. The expression for the new transmit waveform at IF is

$$s_{\text{NLFM}}(t) = \cos\left(2\pi f_1 t + \pi\frac{\tilde{B}}{T}\left(t-\frac{T}{2}\right)^2 + \theta_1\right), \tag{A.1}$$

where $\tilde{B}$ is any arbitrary chirp rate such that $\tilde{B} \neq B$. The NLFM transmit waveform is mixed up to RF using $x_{\text{LO},1} = \cos(2\pi f_2 t + \theta_2), t \geq 0$, at which point it can be represented as

$$s_{\text{NLFM}}(t) = \cos\left(2\pi(f_1+f_2)t + \pi\frac{\tilde{B}}{T}\left(t-\frac{T}{2}\right)^2 + \theta_1 + \theta_2\right), \tag{A.2}$$

where the waveform is again centered at the RF frequency $f_{\text{RF}} = f_1 + f_2$. This transmit signal is sent out to propagate through space where it is reflected off of scatterers in the environment and

these echoes are returned to the receiver to be processed.

A.0.2 Receiver

The signal that is received from the environment, assuming a single point target at a delay t_{d} and the use of a pulsed system, is represented as

$$\tilde{y}(t) = \cos\left[2\pi(f_1+f_2)(t-t_{\mathrm{d}}) + \pi\frac{\tilde{B}}{T}\Big((t-\frac{T}{2})-t_{\mathrm{d}}\Big)^2 + \theta_1 + \theta_2\right]. \tag{A.3}$$

The receive signal $\tilde{y}(t)$ is mixed down to IF using a reference waveform with a chirp rate that is not the same as what was used to generate the transmit waveform, and thus ultimately that of the received waveform. Instead, as mentioned previously, the reference waveform has a different chirp rate, denoted B. The reference waveform is expressed as

$$s_{\mathrm{ref}}(t) = \cos\left(2\pi f_2 t + \pi\frac{B}{T}\left((t-\frac{T}{2})-t_{\mathrm{ref}}\right)^2 + \theta_1 + \theta_2\right), \tag{A.4}$$

and in a normal stretch processing framework this initial mixing stage serves the dual purpose of reducing the bandwidth of the received signal while also down-converting it to an IF. However, in this case, while there is still a bandwidth reduction, it is limited by the deviation between the transmit waveform and the reference LFM. Refer to section 3.2.1 for the details on this additional bandwidth requirement. The result of this mixing stage is

$$\begin{aligned} y_{\mathrm{IF}}(t) = \cos\Bigg[&2\pi f_1(t-t_{\mathrm{d}}) - 2\pi f_2 t_{\mathrm{d}} + \pi\Big(\frac{\tilde{B}}{T}-\frac{B}{T}\Big)t^2 + \pi\Big(\frac{B}{T}-\frac{\tilde{B}}{T}\Big)tT \\ &+\pi\Big(\frac{\tilde{B}}{T}-\frac{B}{T}\Big)\frac{T^2}{4} - \frac{2\pi\tilde{B}}{T}\Big(t-\frac{T}{2}\Big)\Big(t_{\mathrm{d}}-\frac{B}{\tilde{B}}t_{\mathrm{ref}}\Big) \\ &+\pi\Big(\frac{\tilde{B}}{T}t_{\mathrm{d}}^2 - \frac{B}{T}t_{\mathrm{ref}}^2\Big) + \theta_1\Bigg]. \end{aligned} \tag{A.5}$$

where $t_{\mathrm{ref}} \leq t \leq (t_{\mathrm{ref}} + T - t_{\mathrm{d}})$ for a time delay that is less than or equal to the center of the receive window, and $t_{\mathrm{d}} \leq t \leq (t_{\mathrm{ref}} + T)$ for a time delay greater than or equal to the center of the receive

window. The higher frequency components that result from this mixing process are filtered out, and the signal is now centered at the intermediate frequency f_1. For simplicity, the amplitude of the return will be ignored. Now the signal will be mixed down to baseband using another receive oscillator having the form

$$s_{\mathrm{LO}}(t) = \cos(2\pi f_1 t + \theta_1), \qquad t \geq 0, \tag{A.6}$$

the resulting baseband signal is

$$\begin{aligned} y_{\mathrm{NLFM}}(t) = \cos\Bigg[&-2\pi(f_1+f_2)t_{\mathrm{d}} + \pi t^2\Big(\frac{\tilde{B}}{T}-\frac{B}{T}\Big) + \pi t T\Big(\frac{B}{T}-\frac{\tilde{B}}{T}\Big) + \pi\frac{T^2}{4}\Big(\frac{\tilde{B}}{T}-\frac{B}{T}\Big) \\ &-\frac{2\pi\tilde{B}}{T}\Big(t-\frac{T}{2}\Big)\Big(t_{\mathrm{d}}-\frac{B}{\tilde{B}}t_{\mathrm{ref}}\Big) + \pi\Big(\frac{\tilde{B}}{T}t_{\mathrm{d}}^2 - \frac{B}{T}t_{\mathrm{ref}}^2\Big)\Bigg]. \end{aligned} \tag{A.7}$$

In order to simplify this expression let $\Delta t_{\mathrm{d}} = t_{\mathrm{d}} - \frac{\tilde{B}}{T}t_{\mathrm{ref}}$ and $\varphi = \pi\Big(\frac{\tilde{B}}{T}t_{\mathrm{d}}^2 - \frac{B}{T}t_{\mathrm{ref}}^2\Big)$ where φ again is the residual video phase. Likewise, let $\Delta k = \frac{B}{T} - \frac{\tilde{B}}{T}$ and we are left with the following expression for the baseband receive signal

$$y_{\mathrm{NLFM}}(t) = \cos\left(-\frac{2\pi B}{T}\Big(t-\frac{T}{2}\Big)(\Delta t_{\mathrm{d}}) - 2\pi(f_1+f_2)t_{\mathrm{d}} + \varphi + \pi(\Delta k)t^2 - \pi(\Delta k)tT + \pi(\Delta k)\frac{T^2}{4}\right). \tag{A.8}$$

To further simplify this expression the constant phase terms can be grouped as $\theta = \frac{2\pi B}{T}\frac{T}{2}(\Delta t_{\mathrm{d}}) - 2\pi(f_1+f_2)t_{\mathrm{d}} + \varphi + \pi(\Delta k)\frac{T^2}{4}$, and by using the fact that cosine is an even function we are left with

$$y_{\mathrm{NLFM}}(t) = \cos\left(\frac{2\pi B}{T}t(\Delta t_{\mathrm{d}}) - \pi(\Delta k)t^2 - \pi(\Delta k)tT + \theta\right). \tag{A.9}$$

At this point we can compare this expression for $y_{\mathrm{NLFM}}(t)$ to the outcome of standard stretch processing which was derived earlier, but shown again here for reference

$$y(t) = \cos\left(2\pi\frac{B}{T}(\Delta t_{\mathrm{d}})t - \theta\right). \tag{A.10}$$

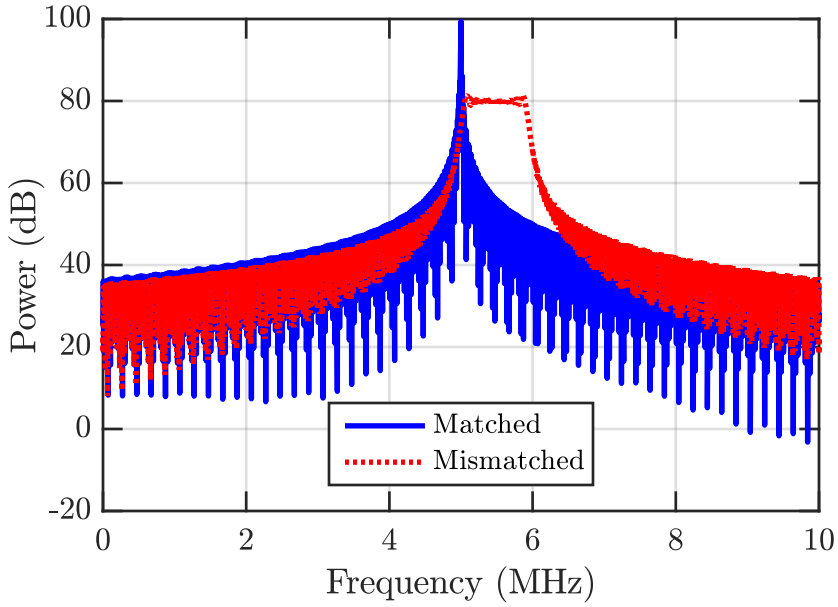

Figure A.1: A comparison of stretch processing applied to an LFM with an identical chirp rate and an LFM with a mismatched chirp rate (chirp rates relative to the reference LFM)

Examining Equations A.9 and A.10 it is evident that when an NLFM waveform is used, the mixed product is no longer simply a sinusoid; it instead contains remnants of a chirp structure which are evident from the quadratic terms in Eq. A.9. This is supported by the simulation results shown in Figure A.1, where the case of the mismatched transmit LFM after the mixing stage yields what looks like the frequency spectrum of an LFM instead of the single frequency that is expected.

Looking at these residual terms in more detail, we can represent $y_{\text{NLFM}}(t)$ in the following way

$$\begin{aligned} y_{\text{NLFM}}(t) = \pi\left(\frac{B}{T}-\frac{\tilde{B}}{T}\right)t^2 + \pi\left(\frac{\tilde{B}}{T}-\frac{B}{T}\right)tT + \pi\left(\frac{B}{T}-\frac{\tilde{B}}{T}\right)\frac{T^2}{4} \\ -\frac{2\pi B}{T}\left(t-\frac{T}{2}\right)\left(t_{\text{d}}-\frac{\tilde{B}}{B}t_{\text{ref}}\right) + \pi\left(\frac{B}{T}t_{\text{d}}^2-\frac{\tilde{B}}{T}t_{\text{ref}}^2\right) \end{aligned} \tag{A.11}$$

and observe that the first four terms (shown on the first line of the equation) would normally cancel out in stretch processing using the traditional waveforms. If we combine these first few terms we are left with the following

$$y_{\text{NLFM}}(t) = \pi\frac{B-\tilde{B}}{T}\left(t-\frac{T}{2}\right)^2 + \cdots \tag{A.12}$$

where $(\cdots)$ is the rest of the expression that is not of interest at the moment. At this point it is easy to recognize this term as a portion of the expression for an LFM recalling that the rest of the terms were combined into the variable θ. It is useful to note that the chirp rate for this LFM is now related to the difference in chirp rates of the reference chirp and transmit waveform.

As is detailed in Chapter 3, these extra terms can be accounted for through the use of a compensation transform in place of the standard FFT. This compensation transform serves to redress these terms because the receive waveform will essentially be match filtered across the entire range swath using an expression that likewise has these "extra" leftover terms.

References

[1] S. D. Blunt and E. L. Mokole, "Overview of radar waveform diversity," *IEEE Aerospace and Electronic Systems Magazine*, vol. 31, no. 11, pp. 2–42, November 2016.

[2] M. Wicks, E. Mokole, and S. Blunt, *Principles of Waveform Diversity and Design*, V. Amuso and Schneible, Eds. SciTech Publishing, 2010.

[3] S. Pillai, K. Li, I. Selesnick, and B. Himed, *Waveform Diversity: Theory & Applications: Theory & Application*. McGraw-Hill Education, 2011.

[4] F. Gini, A. De Maio, and L. Patton, *Waveform Design and Diversity for Advanced Radar Systems*, ser. Electromagnetics and Radar Series. IET Press, 01 2012.

[5] M. A. Richards, J. A. Scheer, and W. A. Holm, *Principles of Modern Radar, Volume I - Basic Principles*. SciTech Publishing, 2010.

[6] J. R. Klauder, A. C. Price, S. Darlington, and W. J. Albersheim, "The theory and design of chirp radars," *The Bell System Technical Journal*, vol. 39, no. 4, pp. 745–808, July 1960.

[7] C. Cook and M. Bernfeld, *Radar Signals: An Introduction to Theory and Application*, ser. Electrical Science Series. Academic Press, 1967.

[8] N. Levanon and E. Mozeson, *Radar Signals*. Wiley-IEEE Press, 2004.

[9] C. Cook, "A class of nonlinear fm pulse compression signals," *Proceedings of the IEEE*, vol. 52, pp. 1369 – 1371, December 1964.

[10] E. Fowle, "The design of fm pulse compression signals," *IEEE Transactions on Information Theory*, vol. 10, no. 1, pp. 61–67, Jan 1964.

[11] M. Labitt, "Obtaining low sidelobes using non-linear fm pulse compression," Citeseer, Tech. Rep., 1994.

[12] I. Gladkova, "Design of frequency modulated waveforms via the zak transform," *IEEE Transactions on Aerospace and Electronic Systems*, vol. 40, no. 1, pp. 355–359, Jan 2004.

[13] A. Doerry, "Generating nonlinear fm chirp waveforms for radar," Sandia Report, Tech. Rep., 09 2006.

[14] R. Frank, "Polyphase codes with good nonperiodic correlation properties," *IEEE Transactions on Information Theory*, vol. 9, no. 1, pp. 43–45, January 1963.

[15] B. L. Lewis and F. F. Kretschmer, "A new class of polyphase pulse compression codes and techniques," *IEEE Transactions on Aerospace and Electronic Systems*, vol. AES-17, no. 3, pp. 364–372, May 1981.

[16] B. Lewis and F. Kretschmer, "Linear frequency modulation derived polyphase pulse compression codes," *IEEE Transactions on Aerospace and Electronic Systems*, vol. AES-18, no. 5, pp. 637–641, Sept 1982.

[17] C. J. Nunn and G. E. Coxson, "Polyphase pulse compression codes with optimal peak and integrated sidelobes," *IEEE Transactions on Aerospace and Electronic Systems*, vol. 45, no. 2, pp. 775–781, April 2009.

[18] P. S. Tan, J. Jakabosky, J. M. Stiles, and S. D. Blunt, "On higher-order representations of polyphase-coded fm radar waveforms," in *2015 IEEE Radar Conference (RadarCon)*, May 2015, pp. 0467–0472.

[19] D. North, "An analysis of the factors which determine singal/noise discrimination in pulsed-carrier systems," *Proceedings of the IEEE*, vol. 51, no. 7, July 1963.

[20] W. J. J. Caputi, "Stretch: A time-transformation technique," *IEEE Trans. Aerospace & Electronic Systems*, vol. AES-7, no. 2, pp. 269–278, March 1971.

[21] M. Skolnik, *Radar Handbook, Third Edition*, ser. Electronics electrical engineering. McGraw-Hill Education, 2008.

[22] G. Stimson, H. Griffiths, C. Baker, and D. Adamy, *Introduction to Airborne Radar, Third Edition*, ser. Aerospace & Radar Systems. SciTech Pub., 2014.

[23] J. Curlander and R. McDonough, *Synthetic Aperture Radar: Systems and Signal Processing*, ser. Wiley Series in Remote Sensing and Image Processing. Wiley, 1991.

[24] W. Melvin, J. Scheer, and eds., *Principles of Modern Radar, Vol. II: Advanced Techniques*. Edison, NJ: SciTech Publishing, 2013.

[25] M. H. Ackroyd and F. Ghani, "Optimum mismatched filters for sidelobe suppression," *IEEE Transactions on Aerospace and Electronic Systems*, vol. AES-9, no. 2, pp. 214–218, March 1973.

[26] D. Henke, P. McCormick, S. D. Blunt, and T. Higgins, "Practical aspects of optimal mismatch filtering and adaptive pulse compression for fm waveforms," in *2015 IEEE Radar Conference (RadarCon)*, May 2015, pp. 1149–1155.

[27] J. E. Cilliers and J. C. Smit, "Pulse compression sidelobe reduction by minimization of lp-norms," *IEEE Transactions on Aerospace and Electronic Systems*, vol. 43, no. 3, pp. 1238–1247, July 2007.

[28] A. D. Maio, Y. Huang, M. Piezzo, S. Zhang, and A. Farina, "Design of radar receive filters optimized according to l_p-norm based criteria," *IEEE Transactions on Signal Processing*, vol. 59, no. 8, pp. 4023–4029, Aug 2011.

[29] L. Yeh, K. Wong, and H. Mir, "Viable/inviable polynomial-phase modulations for 'stretch-processing'," *IEEE Trans. Aerospace and Electronic Systems*, vol. 48, no. 1, pp. 923–926, January 2012.

[30] H. D. Griffiths, "The effect of phase and amplitude errors in fm radar," in *IEEE Colloquium on High Time-Bandwidth Product Waveforms in Radar and Sonar*, May 1991, pp. 9/1–9/5.

[31] D. J. Rabideau, "Adaptive waveform distortion compensation," in *Conference Record of the Thirty-Ninth Asilomar Conference on Signals, Systems and Computers, 2005.*, Oct 2005, pp. 788–792.

[32] H. Krichene, E. Brawley, K. Lauritzen, A. Wu, and S. Talisa, "Time sidelobe correction of hardware errors in stretch processing," *IEEE Transactions on Aerospace and Electronic Systems*, vol. 48, no. 1, pp. 637–647, Jan 2012.

[33] Y. X. Zhang, R. J. Hong, P. P. Pan, Z. M. Deng, and Q. F. Liu, "Frequency-domain range sidelobe correction in stretch processing for wideband lfm radars," *IEEE Transactions on Aerospace and Electronic Systems*, vol. 53, no. 1, pp. 111–121, Feb 2017.

[34] J. Jakabosky, P. Anglin, M. R. Cook, S. D. Blunt, and J. Stiles, "Non-linear fm waveform design using marginal fisher's information within the cpm framework," in *2011 IEEE RadarCon (RADAR)*, May 2011, pp. 513–518.

[35] J. Jakabosky, S. D. Blunt, M. R. Cook, J. Stiles, and S. A. Seguin, "Transmitter-in-the-loop optimization of physical radar emissions," in *2012 IEEE Radar Conference*, May 2012, pp. 0874–0879.

[36] S. D. Blunt, J. Jakabosky, M. Cook, J. Stiles, S. Seguin, and E. L. Mokole, "Polyphase-coded fm (pcfm) radar waveforms, part ii: optimization," *IEEE Transactions on Aerospace and Electronic Systems*, vol. 50, no. 3, pp. 2230–2241, July 2014.

[37] J. Jakabosky, S. D. Blunt, and B. Himed, "Optimization of 'over-coded' radar waveforms," in *2014 IEEE Radar Conference*, May 2014, pp. 1460–1465.

[38] D. M. Hemmingsen, P. M. McCormick, S. D. Blunt, C. Allen, A. Martone, K. Sherbondy, and D. Wikner, "Waveform-diverse stretch processing," in *2018 IEEE Radar Conference (RadarConf18)*, April 2018, pp. 0963–0968.

[39] L. Harnett, D. Hemmingsen, P. M. McCormick, S. D. Blunt, C. Allen, A. Martone, K. Sherbondy, and D. Wikner, "Optimal and adaptive mismatch filtering for stretch processing," in *2018 IEEE Radar Conference (RadarConf18)*, April 2018, pp. 0682–0686.

[40] S. Blunt, M. Cook, E. Perrins, and J. de Graaf, "Cpm-based radar waveforms for efficiently bandlimiting a transmitted spectrum," in *2009 IEEE Radar Conference*, May 2009, pp. 1–6.

[41] S. D. Blunt, M. Cook, J. Jakabosky, J. D. Graaf, and E. Perrins, "Polyphase-coded fm (pcfm) radar waveforms, part i: implementation," *IEEE Transactions on Aerospace and Electronic Systems*, vol. 50, no. 3, pp. 2218–2229, July 2014.

[42] S. D. Blunt, K. Gerlach, and T. Higgins, "Aspects of radar range super-resolution," in *2007 IEEE Radar Conference*, April 2007, pp. 683–687.